

**MICROFLUIDIC TOOLKIT FOR SCALABLE LIVE IMAGING,  
DEVELOPMENTAL AND LIFESPAN DYNAMIC STUDIES OF *C.  
ELEGANS* WITH SINGLE ANIMAL RESOLUTION**

A Dissertation

Presented to

The Academic Faculty

by

Jan Krajniak

In Partial Fulfillment

of the Requirements for the Degree

Doctor of Philosophy in the

School of Chemical & Biomolecular Engineering

Georgia Institute of Technology

August 2013

Copyright © 2013 by Jan Krajniak

**MICROFLUIDIC TOOLKIT FOR SCALABLE LIVE IMAGING,  
DEVELOPMENTAL AND LIFESPAN DYNAMIC STUDIES OF *C.  
ELEGANS* WITH SINGLE ANIMAL RESOLUTION**

Approved by:

Dr. Hang Lu, Advisor

School of Chemical & Biomolecular  
Engineering

*Georgia Institute of Technology*

Dr. Daniel Goldman

School of Physics

*Georgia Institute of Technology*

Dr. Sven Behrens

School of Chemical & Biomolecular  
Engineering

*Georgia Institute of Technology*

Dr. Lakeshia Taite

School of Chemical & Biomolecular  
Engineering

*Georgia Institute of Technology*

Dr. Victor Breedveld

School of Chemical & Biomolecular  
Engineering

*Georgia Institute of Technology*

Date Approved: June 24<sup>th</sup>, 2013

To my Family and Friends who are Family

## **ACKNOWLEDGMENTS**

I wish to thank my labmates for making this process interesting by providing intellectually stimulating discussion and an open mind when discussing my projects and ideas. I'd especially like to thank Matt Crane, Jeffrey Stirman, Kwanghun Chung, Ed Park, Mei Zhan and Loice Chinghoza for providing not only valuable input but also making my time in the lab entertaining. I'd like to thank my advisor, Dr. Hang Lu, for providing me with guidance and support while allowing me to freely explore my ideas and pursue avenues of research as I saw fit, as one would do with a colleague. I would also like to thank my committee for valuable feedback and helping me structure my thoughts.

I especially want to thank my family and my friends who are family. I would like to thank my Mutulka, Apukam, Martinko, Mike and Kristel, for being patient with my ups and downs, for helping me keep my focus and my head straight, and for always being there to listen and help me see what I needed to see.



## TABLE OF CONTENTS

ACKNOWLEDGMENTS .....	IV
LIST OF TABLES .....	IX
LIST OF FIGURES .....	X
LIST OF SYMBOLS AND ABBREVIATIONS .....	XIV
SUMMARY .....	XV
CHAPTER 1      INTRODUCTION .....	1
1.1 <i>C. elegans</i> as a Model Organism .....	1
1.2    Advances in Imaging and Manipulating <i>C. elegans</i> Physiology .....	2
1.3    Biological and Neuroscience Research of <i>C. elegans</i> : Static and Dynamic Studies.....	5
1.3.1    Static Studies.....	5
1.3.2    Dynamic Studies .....	7
1.3.3    Inherent Difficulties of Dynamic Studies .....	9
1.4    Standard Methods of <i>C. elegans</i> Imaging and Handling .....	11
1.5    The Field of Microfluidics and Its Application in <i>C. elegans</i> Studies.....	13
1.5.1    General Microfluidic System Features and Principles.....	15
1.5.2    Microfluidic Systems for Improved Handling of <i>C. elegans</i> .....	16
1.6    Thesis Objectives .....	24
CHAPTER 2      MICROFLUIDIC SYSTEM FOR LONG TERM CULTURE OF <i>C. ELEGANS</i> WITH HIGH-RESOLUTION IMAGING FOR DEVELOPMENTAL STUDIES .....	26
2.1    Overview of the System.....	26
2.2    System Design Process .....	28
2.2.1    Exploration of Animal Tracking and Immobilization Methods .....	28
2.2.2    Pluronic F127 as an Immobilization Agent .....	31
2.2.3    Compatibility of Pluronic F128 with <i>C. elegans</i> Physiology .....	33
2.3    Final System Design .....	35
2.3.1    Hybrid Platform Design.....	36
2.4    Materials and Methods.....	38

2.4.1	Device Fabrication .....	38
2.4.2	Solutions and Materials.....	39
2.4.3	Animal culture, assay and microscopy .....	40
2.5	Results.....	41
2.5.1	Immobilization Cycle for Imaging.....	41
2.5.2	Image Quality with Pluronic F127 as Immobilization Agent.....	43
2.5.3	Extent of Immobilization with Pluronic F127 Solution.....	44
2.5.4	Long-Term Culture Inside Microfluidic Device for Early Stages of Development .....	46
2.6	Conclusions.....	47
CHAPTER 3 MICROFLUIDIC TRAP ARRAY FOR CHEMICAL AND THERMAL MANIPULATION OF <i>C. ELEGANS</i> EMBRYOS .....		49
3.1	Introduction.....	49
3.2	General System Overview .....	50
3.3	System Design .....	52
3.3.1	Microfluidic Component.....	52
3.3.2	Temperature Control on Device.....	55
3.4	Final Design .....	59
3.4.1	Passive Trapping Principles .....	61
3.4.2	Temperature Control Mechanism .....	67
3.5	Methods.....	70
3.5.1	Fabrication .....	70
3.5.2	Culture of <i>C. elegans</i> and Extraction of Embryos .....	72
3.5.3	Solutions .....	73
3.5.4	Experimental Methods .....	73
3.5.5	Auxiliary Hardware .....	74
3.6	Results.....	75
3.6.1	Embryo Trap Efficiency .....	75
3.6.2	Temperature Control on Device.....	76
3.6.3	Rapid Fluid Exchange.....	79
3.6.4	Culture of <i>C. elegans</i> on Device .....	81
3.6.5	Observing Developmental Events on Device .....	83

3.7	Conclusions.....	84
CHAPTER 4 C.L.I.P – CONTINUOUS LIVE IMAGING PLATFORM FOR DIRECT OBSERVATION OF <i>C. ELEGANS</i> PHYSIOLOGICAL PROCESSES.....		
4.1	System Design Process .....	85
4.2	Final System Design .....	87
4.2.1	System Design Principles and Operation.....	89
4.3	Materials and Methods.....	92
4.3.1	Device Fabrication and Setup .....	92
4.3.2	Materials .....	94
4.3.3	<i>C. elegans</i> Culture, Experimental Procedure, and Microscopy .....	94
4.4	Results.....	95
4.4.1	Loading and Analysis of Gel Behavior.....	95
4.4.2	Temperature Characterization.....	98
4.4.3	Characterization of Nutrient Delivery and Animal Feeding.....	99
4.4.4	Immobilization of the Animal Body to Facilitate Long-term Imaging.....	102
4.5	Conclusions.....	105
CHAPTER 5 <i>C. ELEGANS</i> LIFE-SPAN ON CHIP WITH INTEGRATED TEMPERATURE CONTROL AND HIGH CONTENT STUDIES.....		
5.1	General System Overview .....	108
5.2	Adaptation of Existing Designs for Life-Span on Chip.....	109
5.3	Final Design .....	112
5.3.1	Microfluidic Device .....	112
5.3.2	Fluid Delivery System .....	114
5.3.3	Bench-Top Temperature Control.....	115
5.3.4	Imaging of Animals on Chip.....	115
5.4	Methods.....	117
5.4.1	Fabrication .....	117
5.4.2	Solutions .....	117
5.4.3	<i>C. elegans</i> Culture, Experimental Procedure, and Image Processing.....	117
5.5	Results.....	119
5.5.1	Microfluidic Device .....	119
5.5.2	Temperature Control.....	122

5.5.3	Fluid Delivery .....	126
5.5.4	Life-Span On Chip .....	127
5.6	Conclusions .....	130
THESIS CONTRIBUTIONS AND FUTURE DIRECTIONS.....		131
5.7	Thesis Contributions .....	131
5.8	Future Directions .....	134
APPENDIX.....		138
A.1.	Publications and Other Scientific Activity .....	138
A.1.1.	Journal and Book Publications.....	138
A.1.2.	Conference Talks .....	138
A.1.3.	Poster Presentations .....	139
A.2.	Image Reuse Permissions and Licenses.....	139
REFERENCES .....		141

## LIST OF TABLES

Table 3.1 List of available low-melting/fusible alloys available from RotoMetals (rotometals.com).....	56
Table 4.1 Description of the various features of the different designs tested.....	87
Table 5.2 Results of flow rate measurement through devices connected to the peristaltic fluid delivery system.....	127

## LIST OF FIGURES

Figure 1.1 Body of the nematode <i>C. elegans</i> and the major features of the body.....	2
Figure 1.2 Modes of <i>C. elegans</i> physiology visualization.....	3
Figure 1.3 Examples of static studies. ....	6
Figure 1.4 Examples of results obtained from dynamic studies. ....	9
Figure 1.5 Standard method of agarose pad preparation and <i>C. elegans</i> imaging. ....	12
Figure 1.6 Examples of microfluidic immobilization systems. ....	17
Figure 1.7 Examples of behavior analysis systems. ....	20
Figure 1.8 Time-lapse imaging system with peltier cooler based immobilization for imaging. ....	22
Figure 1.9 WormFarm device. An array of large chambers designed to perform lifespan experiments on groups of animals. ....	23
Figure 2.1 System overview. ....	27
Figure 2.2 Early design concepts. ....	29
Figure 2.3 Example of animals trapper in droplets for segregation and long term developmental culture on device. ....	30
Figure 2.4 Physical properties of Pluronic F127. ....	32
Figure 2.5 Examination of biocompatibility of Pluronic F127 with <i>C. elegans</i> physiology. .....	34
Figure 2.6 Two-layer microfluidic device used by our hybrid platform. ....	37
Figure 2.7 Device fabrication method. ....	38
Figure 2.8 Temperature measurement of heating liquid at inlet of microfluidic device. .	40
Figure 2.9 Immobilization cycle. ....	42
Figure 2.10 Comparison of image quality between standard procedures (on agarose pads with anaesthetics) (a,b) and using PF127 gel in microfluidic devices (c,d). ....	44

Figure 2.11 Verifications of the extent of immobilization by the PF127 gel inside the microfluidic device by imaging animals.....	45
Figure 2.12 Long-term culture on chip.....	47
Figure 3.1 Schematic of the system operation and components.....	51
Figure 3.2 Early microfluidic device designs.....	54
Figure 3.3 Concept of electrodes molded in PDMS.....	57
Figure 3.4 COMSOL Simulation results.....	58
Figure 3.5 Final design.....	60
Figure 3.7 Opening of the narrow channel of the embryo trap.....	62
Figure 3.8 Time lapse of embryo trapping.....	63
Figure 3.9 Microfluidic chamber design for passive holding of animals. a) 3D rendering of the chamber features and dimensions. b) Flow velocity across a chamber. The high velocity in the inlet helps prevent animals from escaping. In the bulk of the chamber the flow velocity significantly decreases, leading to lower shear rates and higher bacterial residence time. c) Close-up view of the flow velocity profile through an embryo trap.....	64
Figure 3.10 Flow routing principles in trap array.....	65
Figure 3.11 Transparent electrode heaters.....	68
Figure 3.12 Non-uniform electrode resistance due to substrate un-evenness.....	69
Figure 3.13 Uniform electrode resistance despite substrate un-evenness.....	70
Figure 3.14 Device and electrode slide alignment procedure.....	72
Figure 3.15 Loading efficiency of embryos into chambers in the microfluidic array.....	75
Figure 3.16 Experimentally determined relationship between the applied current and chamber temperature in a device with flowing PF127 solution.....	77
Figure 3.17 COMSOL Simulation of device temperature profile from heating a single chamber.....	78

Figure 3.18 Time-lapse of <i>C. elegans</i> immobilization for imaging via Pluronic F127, showing the animal becoming fully immobilized after a heat pulse. The immobilization occurs via the sol-gel transition of the solution of PF127 triggered via heating from the transparent ITO electrodes.....	79
Figure 3.19 Average fluorescent intensity inside culture chambers after a pulse of dye solution (grey). The exchange of fluids is rapid following the introduction of a dye pulse of 40, 20 and 10 seconds. ....	80
Figure 3.20 Hatching of trapped embryo and subsequent development of the hatched animal inside the culture chamber of the microfluidic array. ....	81
Figure 3.21 Comparison of biofilm formation between untreated devices and devices treated with 1% solution of Pluronic F127. ....	82
Figure 3.22 Synaptic rearrangement of DD motor neuron synapses from the dorsal to the ventral side. Arrows point to synapses. ....	83
Figure 4.1 Early long term developmental study testing design, which was used as a technical inspiration for the C.L.I.P platform. ....	86
Figure 4.2 Microfluidic device component of the platform.....	88
Figure 4.3 Simple loading procedure.....	90
Figure 4.4 High feature fidelity of the SU-8 master (a) and corresponding PDMS mold (b) could only be achieved using a chrome mask over a conventional transparency printed mask used for rapid prototyping. ....	93
Figure 4.5 Device functional characterization.....	96
Figure 4.6 Sample gel behavior of the sodium alginate/gelatin mixtures.....	97
Figure 4.7 The temperature of Pluronic F127 solution as measured at the inlet to trapping channels using a fluorescent intensity measurement technique.....	99
Figure 4.8 COMSOL model of the velocity field surrounding the muzzle area.....	100
Figure 4.9 Characterization of animals' environment and feeding on device. ....	101
Figure 4.10 Dynamic studies of <i>C. elegans</i> using C.L.I.P.....	103



Figure 4.11 Statistical analysis of dynamic changes. ....	104
Figure 5.2 Design iterations for efficient loading and trapping of L4 <i>C. elegans</i> larvae. .....	111
Figure 5.4 Step-by-step preparation, loading, and re-connection procedure. ....	113
Figure 5.5 The simple fluid delivery system used to provide even flow rates to multiple devices running in parallel. ....	114
Figure 5.6 Schematic of the bench-top temperature controller for microfluidic devices. .....	116
Figure 5.7 Life-span on chip loading efficiency. ....	120
Figure 5.8 Trapping efficiency on chip. ....	121
Figure 5.9 Average number of inlets remaining unblocked during an experiment. ....	122
Figure 5.10 Results of the temperature distribution simulation. ....	124
Figure 5.11 Summary of simulation results. ....	125
Figure 5.12 Results of temperature measurement of devices placed on bench-top temperature controller. ....	126
Figure 5.13 Comparison of life-span data for wild type N2 animals obtained experimentally on the life-span chip to previously reported data from Houthoofd <i>et</i> <i>al</i> , <i>Experimental Gerontology</i> , 2003 [179] (Resuse permission license: 3161501375891). ....	128
Figure 5.14 Measurement of pharyngeal pumping rate of <i>C. elegans</i> on device. The rate is lowest immediate after loading, but returns to the range of normal values 24 and 48 hours after loading. ....	129
Figure 5.15 Incidence of reversals and head-tail touches before, during, and after exposure to the repellent 2-nonanone. ....	130

## LIST OF SYMBOLS AND ABBREVIATIONS

$\text{Ca}^{2+}$	Calcium cation (2+ charge)
<i>C. elegans</i>	<i>Caenorhabditis elegans</i>
COMSOL	Physics simulation software
<i>I</i>	Current
CFP	Cyan fluorescent protein
GFP	Green fluorescent protein
GCaMP	Green fluorescent protein-Calmodulin-M13 protein
$\rho$	Density
<i>D</i>	Diffusivity
<i>F</i>	Fluid driving force in COMSOL simulation
<i>E. coli</i>	<i>Escherichia coli</i>
EO	Ethylene oxide
FRET	Fluorescent resonant energy transfer
FUdR	Fluoruridine deoxyribose
GABA	Gamma-aminobutyric acid
GUI	Graphic user interface
ITO	Indium Tin Oxide
<i>Q</i>	Resistive heating power
HC	Hydrocortisone
<i>L</i>	Length scale
NGM	Nematode growth media
NSF	N-ethylmaleimide sensitive fusion proteins
<i>n</i>	Normal vector in COMSOL simulation
PDMS	Poly(dimethylsiloxane)
<i>Pe</i>	Peclet number
PEO	Poly(ethylene oxide)
PPO	Poly(propylene oxide)
<i>R</i>	Electrical resistance
<i>Re</i>	Reynolds number
RNA	Ribonucleic acid
RNAi	Interference ribonucleic acid
SNB-1	Synaptobrevin, integral membrane protein of secretory vehicles
SNARE	Soluble NSF Attachment Protein Receptor
<i>k</i>	Thermal conductivity
<i>V</i>	Velocity
$\mu$	Viscosity
YFP	Yellow fluorescent protein

## SUMMARY

The nematode *Caenorhabditis elegans* has served as one of the primary model organisms in biology and neuroscience. Significant genetic homology and many important conserved biological mechanisms between the nematode and higher model organisms and humans has helped accelerate understanding of gene function, the role of genes in generating behaviors, the function of nervous networks and metabolic pathways, and many other processes. As *C. elegans* research became more specific, so have the biological tools for manipulating *C. elegans* improved and opened possibilities for new studies. Additionally, in several avenues of research, technologies have been developed to manipulate the animals in very efficient and quantitative ways. Laser micro-surgery and ablation, high-throughput screening, and behavioral response tracking systems are examples of such technologies. However, dynamic studies have remained without significant technological support, lacking tools to repeatedly image animals over time or to continuously image animals at benign conditions. With such tools available, studies could focus on processes occurring over time and span a range of time-scales of i) minutes to hours such as analysis of changes in genetic expression, which require continuous imaging for accurate observation, ii) hours to days such as study of synaptic re-arrangement during development, which require periodic imaging of the same animal, and iii) days to weeks such as life-span experiments requiring daily monitoring. Because of a lack of suitable tools and technologies to perform such studies, researchers have to either resort to standard biological methods with very limited usefulness for dynamic studies, or perform these studies without the full set of desired conditions, such as leaving out feeding during continuous imaging.

To address these problems, this thesis aims to create a comprehensive microfluidic toolkit for dynamic studies. I developed a novel method for reversible and repeatable immobilization at benign conditions. The method uses the thermo-reversible sol-gel

transition of the solution of Pluronic F127 to temporarily immobilize animals. The method works in tandem with a microfluidic system for isolated culture of *C. elegans* with integrated temperature control. This is the first technology capable of following development of a single animal with high-resolution repeated imaging. The system thus makes a broad range of previously impossible dynamic developmental studies with single animal resolution possible.

The next system is capable of efficiently loading and trapping *C. elegans* embryos in a high-throughput and scalable fashion for embryonic stimulation with subsequent study of development. The system works passively via design of features and flow dynamics and facilitates precise chemical and thermal stimulation at the embryonic stage (and during development as well). The embryos hatch on device and the system allows for studying the effect of stimulation on their development. The integrated thermal stimulation electrodes may also be used for immobilization via PF127. This design enables a broad range of studies such as following the distribution of P granules and of the heat shock protein after stimulation into development, or the effect of drug exposure on normal physiological functions.

The next system is capable of selective immobilization of animals' bodies, while simultaneously facilitating feeding and normal physiological function. This functionality is critical for live imaging without affecting the observed processes. Dynamic change in size of lipid droplets in time was observed, which is of interest in studying genetic regulation of lipid storage mechanisms with implications in healthcare. Additionally, the chip can be used for a range of applications from observing synaptic vesicle transport, through axonal regeneration, to maintenance of germ cells.

The last system is capable of culturing animals over their life-span with efficient animal handling, environmental control, and high data-content experimentation. The system integrates a microfluidic device for loading, trapping, culturing and potentially chemically stimulating animals with a bench-top temperature controller and a peristaltic

pump fluid delivery system. The temperature controller eliminates the need for incubators and the fluid delivery systems allows connecting multiple devices to nutrient solution flow at will without affecting flow to other connected devices. Together, the system facilitates highly scalable parallel life-span experimentation with per-animal tracking and the ability to perform additional studies while observing life-span. One such example is to perform analysis of behavioral response to various stimulants or repellants, such as the example shown in this thesis using 2-nonanone. This system overall enables high-throughput life-span experiments with control of dietary restriction conditions and temperature, with per-animal tracking, and high data-content analysis.

As a whole, the work in this thesis enables dynamic studies over the large range of time scales applicable to *C. elegans* research. The biological applications range from dynamically studying lipid droplet morphology, through observing the dynamics of synaptic re-arrangement during development, to performing high-content life-span experiments. Additionally, these systems can be directly applied to research on other nematode model organisms (*C. briggsae*) without the need for modification and the design principles can be applied to systems for manipulation of zebra fish embryos, single cells or embryoid bodies. By simplifying peripheral equipment and unifying peripheral control into one interface and thereby improving robustness, these systems will be more readily distributable to biological laboratories and applied to relevant biological problems.

# CHAPTER 1 INTRODUCTION

This document presents the work of creating microfluidic-based systems for performing previously very challenging or impossible studies of the neuroscience model organism *C. elegans*. This chapter introduces the model organism itself and familiarizes the reader with the significance of *C. elegans* for neuroscience research. Additionally, it describes the methods for manipulating and visualizing *C. elegans* physiology as well as the two principal approaches to studying physiological processes; static and dynamic studies. The differences between the requirements and outputs of static and dynamic studies are explained and where the bottlenecks lie for performing dynamic individual-animal based studies with standard biological techniques. The chapter also introduces the field of microfluidics and several microfluidic systems already used for *C. elegans* research with a discussion on the advantages and disadvantages of these sample systems. Lastly, the chapter presents an argument for creating a toolkit for dynamic per-animal studies of *C. elegans* and describes the systems which would be necessary to cover a broad range of dynamic processes based on their time scales. The creation of these systems are the goals and the body of work of this thesis.

## 1.1 *C. elegans* as a Model Organism

*C. elegans* was introduced to the scientific community in the 1950s and became increasingly popular as a model organism following the work of Sydney Brenner. [1-4] This small soil dwelling nematode has subsequently become prominent in the biology, genetics, and neuroscience communities because of its favorable properties. The organism is transparent, a hermaphrodite, and has a generation cycle of only three days. In 1998 [5] *C. elegans* became the first multicellular organism with a fully sequenced genome. Despite its small size and superficial simplicity, *C. elegans* has approximately 20,000 genes, of which about 60-80% have human homologues. [6, 7] Additionally,

many systemic, molecular and genetic mechanisms are conserved between the nematode and human. [5, 8-10]. Further, the nematode has a nervous system capable of processing external and internal cues to produce complex behavior and regulate internal mechanisms. In each hermaphrodite, this nervous system consists of 302 neurons of which the physical connections have been fully mapped out. [3, 4, 11-13]. In combination, these features make it the ideal model organism for understanding the function and genetic regulation of the nervous and other systems in the human body. Since its introduction, research into *C. elegans* has yielded significant advances for science. As a testament to the utility of the nematode, three Nobel prize awards for work based on *C. elegans* research for i)programmed cell death [14], ii)interference RNA [15], and iii) the use of green fluorescent protein [16] have been awarded over the last decade.

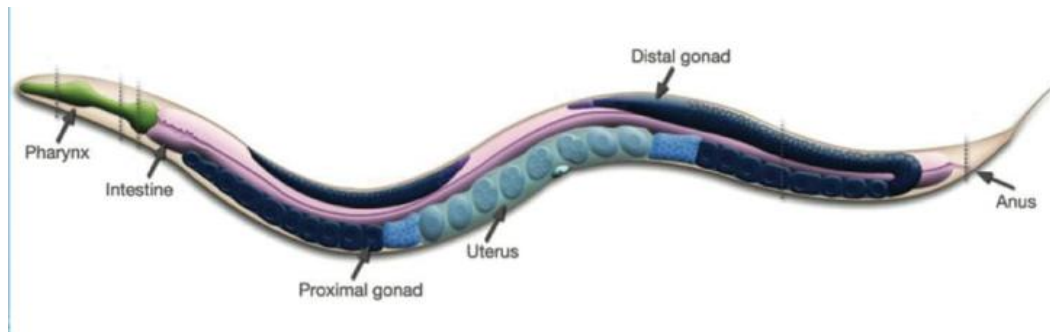


**Figure 1.1** Body of the nematode *C. elegans* and the major features of the body. (image: wormatlas.org [17]. General re-use permission granted).

## 1.2 Advances in Imaging and Manipulating *C. elegans* Physiology

After the introduction by Sydney Brenner, the dissection of the nervous system in *C. elegans* began via electron microscopy and cryo-sectioning.[18] Bodies of neurons, the location of neuronal process and synapses all of the neurons in the network have been mapped out by combining serial sections of the nematode body.[3, 12, 13] Next began the investigation of function of the networks of neurons in the nervous system. This was achieved by laser ablating individual neurons. [19-22] By removing these single nodes in the circuit and observing the changes in function, adaptation, or inability to adapt, the

specific role of the ablated neuron could be inferred. This method has greatly contributed to the field of behavioral science and to dissecting the signal integration and behavioral output generation of between sensory, inter and motor neurons.

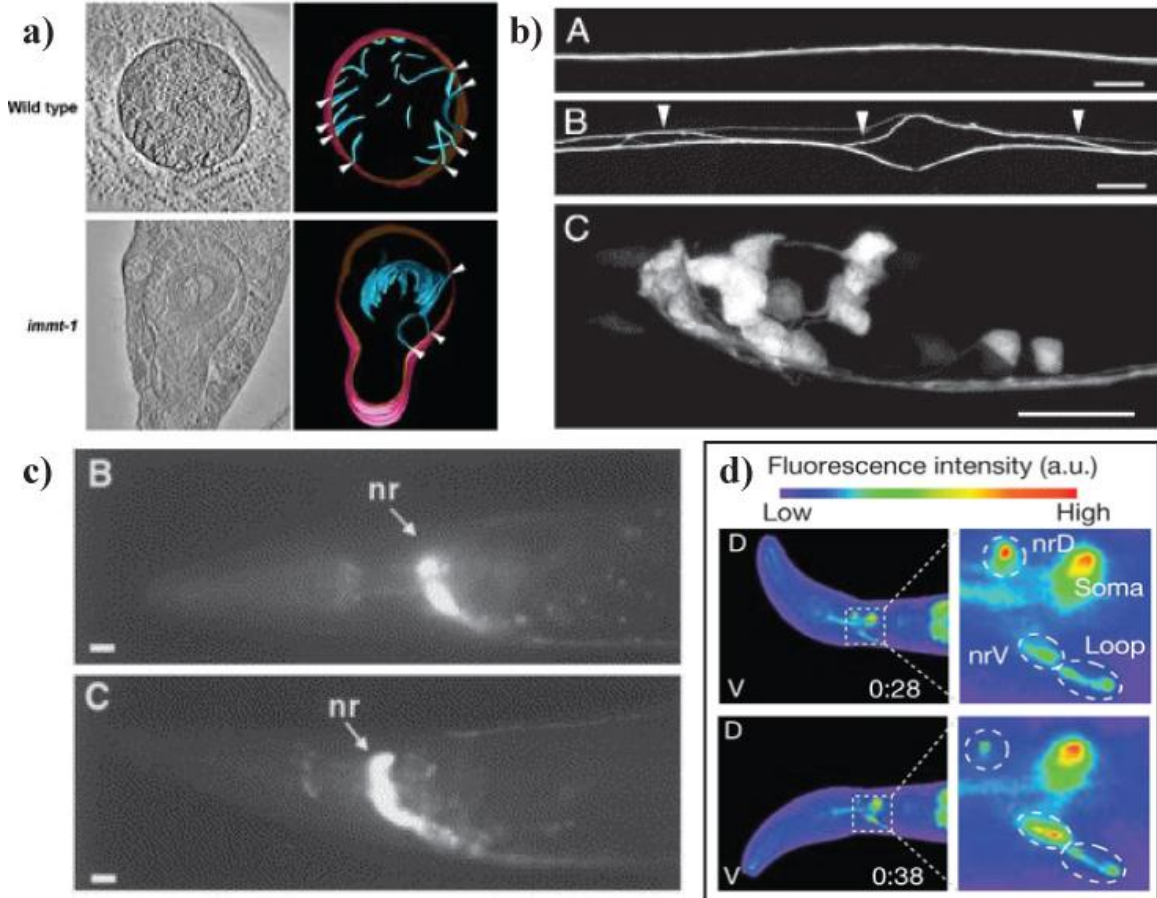


**Figure 1.2** Modes of *C. elegans* physiology visualization. a) EM cross section of the *C. elegans* mitochondria cristae and the corresponding 3D reconstruction (image: Mun *et al.*, Journal of Cellular Physiology, 2010 [23], Reuse license number: 3161420755282). b) *C. elegans* expressing *glr-1::GFP* for labeling of ventral nerve cord to detect defects. (image: Hutter *et al.*, Developmental Biology, 2005 [24], Reuse license number: 3161430923941). c) *SNB-1::GFP* fusion protein expression in *C. elegans* labeling the nerve ring and synapses on the nerve cords. (image: Nonet, Journal of Neuroscience Methods, 1999 [25], Reuse license number: 3161430466403). d) Fluorescent intensity measurement of the RIA neuron and its functional subdomains using GCaMP. (image: Hendricks *et al.*, Nature, 2012 [26], Reuse license number: 31614331163024)

With the discovery of the green fluorescent protein (GFP), visualization of the *C. elegans* physiology in a very detailed fashion became possible without the need for electron microscopy. Since the *C. elegans* body is transparent, visualization of gross (cell bodies)



and extremely fine (synapses, individual proteins) features are equally possible with sufficiently high magnification on compound fluorescent or confocal microscopes. By using specific gene promoter sequences upstream of the DNA sequence encoding GFP, it is possible to achieve cell specific GFP expression and also to determine when particular genes are turned on. Furthermore, combining the sequence for functional proteins with the sequence of GFP allows for visualizing the location of those proteins on a sub-cellular level and determine the function of such proteins. The proteins contributing to the formation and structure of synapses and the transport of transmitters to the synapse have been determined in such a fashion for example.

Other fluorescent markers allow for extracting additional features and details of the *C. elegans* nervous system. For example, GCaMP, a fusion of the green fluorescent protein, calmodulin, and M13, is a genetically encoded calcium indicator.[27-30] Since neuronal activity in *C. elegans* is mediated by action potentials, which trigger a change in cytoplasmic free  $\text{Ca}^{2+}$  ions concentration (such as the activation of glutamate receptors during synaptic transmission), GCaMP can be used to measure said activity in real time via fluorescent intensity measurements. Another real time activity measurement tool is FRET (fluorescence resonance energy transfer).[31-34] In the FRET class fusion protein markers, fluorescent proteins with two different excitation and emission spectra are combined. In absence of  $\text{Ca}^{2+}$  ions, excitation of one of the fluorophores, such as CFP, leads primarily to CFP emission, with lesser energy transfer to the other fluorophore such as YFP and low YFP emission. Upon an increase in  $\text{Ca}^{2+}$  ions, the resulting binding of the ions to calmodulin, and physical attraction of M13 in the complex, both fluorophores are brought into a closer position. In this position, excitation of CFP will lead to energy transfer to YFP and primarily YFP emission. This change in emission wavelength can be used to ratiometrically determine neuronal activity.

One of the most recent advances, channelrhodopsin has been introduced as an optogenetic tool for visualizing physiological interconnectedness of networks and for

stimulating tissue. This light-gated ion channel can be expressed cell-specifically by using the appropriate promoter sequences. When exposed to blue light, the channel allows passage of cations, including  $\text{Ca}^{2+}$ . This can be used to induce signaling from specific neurons for example via targeted exposure to blue light. Thus, by either exciting or silencing specific cells, the interconnectedness and functionality of entire nervous system networks can be analyzed. [35, 36]

### **1.3 Biological and Neuroscience Research of *C. elegans*: Static and Dynamic Studies**

The over-arching principle of the majority of research using *C. elegans* has been to establish the connection between the genome and gene expression and development, function of the major systems, interpretation of external cues, generation of behavior, or making survival based decision. In studying this connection, several methods have been established, which take advantage of the tools for visualizing animals' physiology. These methods or study approaches can be grouped into two classes; static and dynamic studies.

#### **1.3.1 Static Studies**

Static studies are performed by observing a single animal at only one time point. Mutagenesis with the purpose of observing changes to a stereotypical phenotype is one example. First, animals expressing GFP driven by a specific promoter or fused to a protein are mutagenized. If after mutagenesis a change to the original GFP expression pattern is observed, the animal's genome can be sequenced and the mutation localized to a specific gene. By analyzing the type of phenotypical change, the role of the mutated gene can be inferred. In this case, each animal only need be observed once at a single time point to ascertain whether its phenotype has changed. Using this approach, several major genetic players involved in synaptogenesis and synaptic function have been identified. [37-42]. Elimination of gene function or cells has been applied to other

developmental processes where a single snapshot is sufficient as well, such as formation of the pharynx, guidance of axons, or cell fate of specific interneurons. [43-46]

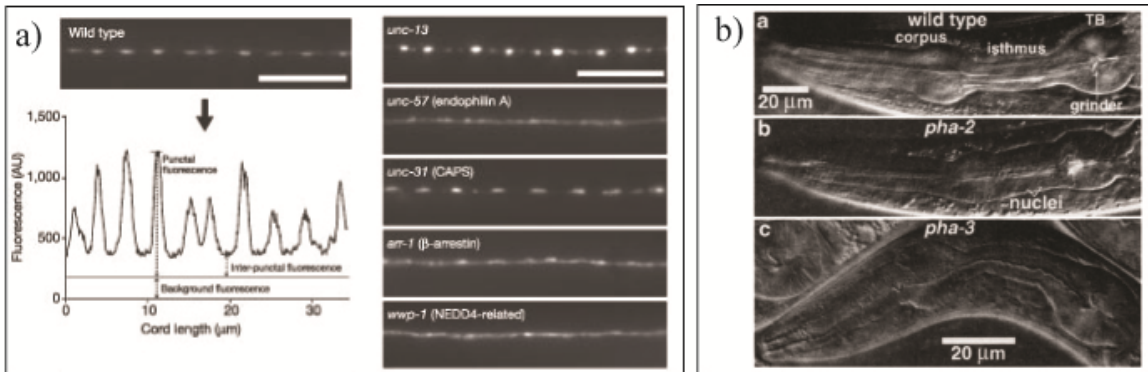


**Figure 1.3** Examples of static studies. The roles of genes in development and formation of structures such as synapses or the pharynx can be inferred by mutagenizing individual genes and observing changes compared to the wild type phenotype. a) Comparison of expression of SNB-1:GFP, a fusion of synaptobrevin and GFP. SNB-1 is a part of the SNARE complex in synapses and involved in docking of vesicles. As such it localizes to synapses. Changes in the wild type phenotypical expression may indicate involvement of the mutated genes in formation or function of synapses. (image: Sieburth *et al.*, Nature, 2010 [41] Reuse license number: 3157751282241) b) The role of genes on development of gross features such as the structure of a synapse can also be analyzed using static studies. Once animals have developed, the changes in the pharyngeal muscle structure and in the presence of specific features can be used to determine the specific roles of genes such as *pha-2* and *pha-3* (Avery, Genetics, 1993 [44] Reuse license number: Written permission received).

Another type of static studies are classical behavior studies, such as chemotaxis assays. In these, animals are placed in a scoring arena, with a source of attractant or repellent and a neutral smell. At the end of the assays, the animals' proximity to either source is scored and their propensity to like or dislike said chemicals is inferred. Additionally, specific neurons can be ablated and the assay repeated to determine the individual node's role in processing smells or generating chemical specific behaviors. This same elimination approach can be applied to genes via mutagenesis, as well as to other types of sensing behaviors such as mechano- and thermo-sensation. [47-56].

### 1.3.2 Dynamic Studies

Dynamic studies involve continuous or repeated observation of a single animal over a period of time while a developmental or physiological event of interest is occurring. Because of the direct observation of a process in question, dynamic studies can provide a more detailed picture of the event itself as well as record the minute differences between two different animals. This is critical as *C. elegans* are being studied in ever greater depth and complexity. The time scales of processes of interest can be used to classify the types of dynamic studies into three categories.

Processes occurring over several seconds or minutes, which require continuous live or very frequent imaging fall into the live dynamic studies category. For example, the function of synapses is affected by its structure but also by the morphology, docking ability and amount of the synaptic vesicles containing neurotransmitters. Additionally, these vesicles have to be transported from the soma to the synapses and are also shuttled back and forth between synapses. A single snapshot in time only provides the information on sites of vesicle accumulation (as in section 1.3.1). Dynamic observation can provide information on the rates of transport, ratios of retrograde to anterograde transport, and the time vesicles spend at specific synapses. [57].

Those processes occurring over a period of hours to days, which require periodic imaging at different time points fall into the dynamic developmental studies category. For example, in *C. elegans*, a class of motor neurons (DD) innervates ventral body wall muscles, while they receive synaptic inputs on the dorsal side. Once a second class of motor neurons develops (VD), the original DD neurons' synapses restructure. The DD neurons then begin to innervate dorsal body wall muscles. This process occurs during the transition between the two earliest larval stages, L1 and L2. From snapshots taken after the process is complete, one could determine changes in morphology and location of these synapses after mutagenesis. However, by dynamically observing the process, one can observe the specific timing of this event and how individual genes may affect this

timing. [58] Such observations are critical for understanding the full scope of roles of genes in development and function.

A dynamic approach to behavior analysis can also yield a wealth of additional information. In comparison to an end-point read out odor assay as described in section 1.3.1, dynamic observation of animals' behavior during the experiment provided a much more complete picture of behavior. [59] First, different types of body postures could be associated with specific behavior; omega turns become more frequent when animals seek to leave a specific area. Next, stereotypical responses of animals' after entrance into or exit from an odorant area could be established and the differences between animals with different mutations could be determined. Additionally, the average residence time of animals near the odorant could be established, with animals moving in and out of the area periodically. Combined, the dynamic approach provides a much more complete picture of behavioral responses to chemical odor stimuli and of the genes involved in generating those responses.

Processes occurring over the life-span of animals or which affect the life-span fall into the dynamic life-span studies category. A typical lifespan assay involves monitoring a population of animals over time to count the number of animals still alive to determine the role of various genes on aging. [60-62] This is done periodically, most commonly on a daily basis. However, animals in these assays are rarely tracked on an individual basis. Without individual tracking, it is impossible to increase the depth of data gathering. For example, it is impossible to record the change in behavioral response of individual animals to stimuli as they age to determine a possible correlation. Also, discovery of early lifespan predictors, such as the number of progeny, cannot be achieved without being able to match individual animals' progeny count to the specific animals' life spans. In short, full investigation of biological and environmental cues on lifespan and the effects of aging on the organism require the application of the dynamic studies principles.

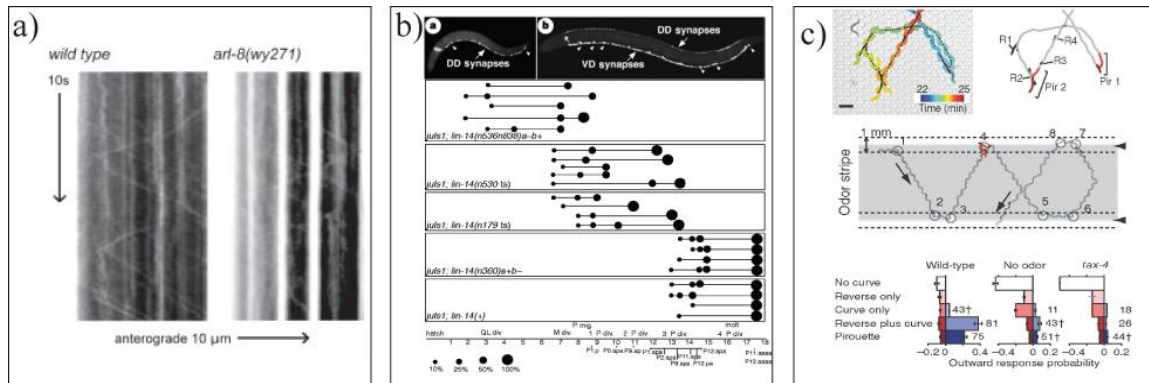


**Figure 1.4** Examples of results obtained from dynamic studies. a) Chimographs depicting the position of vesicles in time of wild type and mutant animals. The diagonal paths represent vesicles moving along the axons and bright vertical bands indicate accumulation of vesicles. Via dynamic observation, it is possible to see rates of vesicle transport, average travel and pause duration, and ratios of antero- to retrograde transport (image: Klassen *et al.*, Neuron, 2010 [57] Reuse license number: 3157760787685). b) Analysis of the timing of synaptic re-arrangement after the development of VD motor neurons. By observing the developmental process over time, it is possible to discern the role of various genes on the timing of this process. This data was obtained via a population composite. This is because of the inherent difficulties of dynamic developmental studies (image: Hallam *et al.*, Nature, 1998 [58] Reuse license number: 3157760958706). c) Dynamic observation of animal behavior in a chemosensory assay. Observing animals over time made it possible to determine typical behavior patterns and postures and behavior after entering and exiting odorant areas, in addition to the final animal distribution. (Albrecht *et al.*, Nature, 2011 [59] Reuse license number: 3157761282059).

### 1.3.3 Inherent Difficulties of Dynamic Studies

With the additional information on physiological and development process that dynamic studies can provide and the large number of available biological tools for manipulating and visualizing *C. elegans* physiology, it would seem the obvious choice for any experiment would be the dynamic approach. However, in practice, this is not the case. The reason is the number of requirements and the combination of requirements in handling animals and practically implementing live or dynamic observation of *C. elegans*.

First, imaging of cellular and sub-cellular objects requires high-magnification imaging. This is the case because of the very small size of objects such as synapses, clusters of

receptors, or neuronal processes. However, because of the small size, the exposure time needed to collect enough light from the sample is large. A single image may require exposures of up to hundreds of milliseconds. Additionally, at times, multiple images at different depths need to be acquired either for building a three dimensional composite or to project the stack onto one plane to collect as much light as possible. These stacks can take up to several seconds to acquire. Therefore, while animals are being imaged, they have to remain perfectly immobilized. Otherwise, the acquired images would be distorted and smeared and data acquisition would be impossible.

Next, the immobilization method has to be benign and cannot affect physiology. Whether the immobilization is continuous for live observation, or frequently repeated for developmental and long-term studies, normal physiological functions such as feeding or proper development cannot be affected. Otherwise, observation itself would alter the process and invalidate the experiment. For this reason, live imaging requires immobilization while i) animals are allowed to feed as they normally would, ii) they remain within their physiological temperature range of 15-25 °C, and iii) their physiological processes are not otherwise affected. For long term or developmental studies, very short term intermittent imaging and immobilization has to be used. Therefore, animals' normal development and function has to be facilitated between imaging cycles. Then, during imaging, animals i) have to be immobilized without affecting physiology and development and ii) the immobilization has to be easily reversible.

Additionally, dynamic long-term studies require tracking of individual animals throughout the experiment. This may be required for a period of several days up to months in case of lifespan studies. Therefore, it is necessary to keep the animals either physically separated, or to track the position of each specimen optically via position tracking software.

Also, for many types of dynamic studies, the environmental conditions have to remain steady over time. This includes control of the amount of nutrients delivered and the control of temperature. Temperature control is particularly critical for lifespan studies; *C. elegans* lifespan varies drastically even at temperatures within its physiological range. Variations of as little as 2 °C can alter mean animals lifespan by several days.

The development of tools and technologies needed to address these requirements has largely been lagging behind the development of tools for biological manipulation. Because of this bottleneck, researchers have to rely on inadequate standard methods or are completely prohibited from certain types of dynamic studies.

#### **1.4 Standard Methods of *C. elegans* Imaging and Handling**

Typically, *C. elegans* are grown and cultured on nematode growth media (NGM) plates. [63] These plates provide a crawling substrate and a balanced pH environment. Nutrients are provided in the form of a lawn of OP50, a non-pathogenic strain of *E. coli* bacteria. Cholesterol is also included in the NGM plate preparation since it is a nutrient required for the animals' ability to molt between larval stages. Though adequate for culturing, these plates do not lend themselves well for experimentation. First, control of environmental conditions is difficult. Controlling the exact amount of bacteria on plates requires precise concentration control prior to seeding and use of antibiotics to curb the bacterial growth. Even then, the lawn thickness can be uneven and the local amount of bacteria different. Animals can thus be exposed to a broad range of nutrients amount, or even crawl off the lawn to an area with no bacteria. Temperature control requires the use of incubators, which for large-scale experiments can be very difficult to manage logistically. Additionally, different temperatures lead to different rates of drying of the agar. This changes the physical crawling conditions and may also alter the rate at which the gel absorbs chemicals such as attractive or repellent stimulants. This can significantly affect the gradients and concentrations of chemicals the animals perceive. Lastly,



manipulation of animals can be very demanding. Studies of individual animals require one plate per each animal. Animals have to be physically moved by picking if stringent dietary control or tracking of animals through egg-laying is necessary. The latter is commonly the case for developmental and lifespan studies. Also, animals can be lost by crawling from the agar to the plastic edge of the plate where they dry out.

Liquid culture protocols mitigate some of these problems but may introduce additional problems. Although maintaining constant concentration of nutrients is more easily achieved and animal loss is more easily preventable, because liquid culture is usually performed in well plates, constant shaking is required for even oxygenation of the solution. Performing a developmental or lifespan study for example therefore remains a difficult endeavor. First, each animal would require its own plate. If the developmental process in question is temperature dependent, plates will require incubator storage. If for example an odorant response change throughout development and lifespan is being evaluated, animals will have to be picked onto new plates after each exposure. Animals will definitely have to be picked regularly onto new plates for lifespan experiments with precise dietary control. Picking increases the risk of physical damage and death of animals. Most importantly, every time animals need to be imaged, they will have to be removed from the plate.

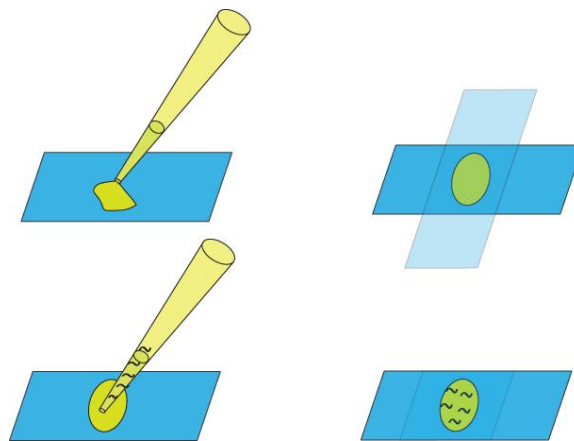


**Figure 1.5** Standard method of agarose pad preparation and *C. elegans* imaging.

The standard imaging technique itself is not adequate for some live imaging and the majority of developmental studies. The technique depends on immobilizing *C. elegans* on agarose pad between a glass slide and cover slip. The two methods of immobilization used are to either glue the animal or to use anesthetics to prevent all movement. Both approaches significantly affect physiology and development. Additionally, animals cannot be fed while immobilized. Also, in the case of glue and some strong anesthetics, the immobilization is irreversible. Because of this, standard methods are no suitable for live imaging for longer periods than several seconds. For example, trafficking of synaptic vesicles can be sufficiently observed over ~30 seconds (as shown in Figure 1.4a), after which the animals are simply discarded. However, formation of growth cones, changes in structures of lipid droplets, changes in gene expression, or tracking of germ cells all require live observation for several minutes up to few hours and would be impossible to perform. The standard approach is also not ideal for developmental studies. Since each animal can only be imaged once, it's impossible to track development on a per animal basis. To get around this problem, it is possible to image animals at different stages of development. This provides a population-base picture (as shown in Figure 1.4b). Though sufficient for gross evaluation, minute details and differences between individuals, which could be used to screen mutants for example, are lost. It is clear therefore that standard techniques are inadequate for live imaging, developmental, and lifespan studies.

### **1.5 The Field of Microfluidics and Its Application in *C. elegans* Studies**

The field of microfluidics is a relatively recent yet rapidly spreading development. The key principle of the field is manipulation of fluids at length scales at which fluid flow becomes extremely predictable and thus controllable, i.e. laminar. This type of flow arises at Reynolds numbers lower than 2300. Because of the length scales and geometries commonly used in microfluidics, the Reynolds number is much lower than

2300. The dimensionless Reynolds number is calculated by the relationship  $Re = \frac{\rho VL}{\mu}$ . At

low values of the Reynolds number, inertial forces (represented by the numerator) become irrelevant and viscous forces (represented by the denominator) dominate, resulting in highly predictable and mostly laminar flow patterns. Since the fluids used are the same as with macro-scale systems, and velocities generally remain within a  $10^1$  m/s maximum, the determining variable is the length scale. The length scales common to microfluidic designs are in the range of nano to millimeters and lead to low  $Re$  numbers. Despite these small lengths scales, most microfluidic systems give rise to a large Peclet number,  $Pe = VL/D$ , where  $V$  is velocity,  $L$  is the length scale, and  $D$  is the diffusion coefficient. This dimensionless number describes the ratio between convective and diffusive mass transfer in a system. Despite the small length scales, in combination with velocities common in microfluidic devices, the numerator term representing convective mass transfer tends to dominate over the denominator, representing diffusive mass transfer. Therefore, two laminar streams co-flowing in the same direction will remain largely unmixed over a long distance, because mixing is dependent on the slow diffusive process. This can be beneficial in delivering well defined pulses of chemical stimuli for example, but it can be detrimental when rapid mixing is required. In case needing rapid mixing, various microfluidic mixers based on folding of the lamina to decrease the diffusion length may be used.

Because of the small length scales, mass and energy transfer achieve equilibrium much faster than at the macroscale. [64, 65] This leads to lower consumption of potentially costly reagents with greater precision and control. Additionally, these length-scales are similar to those of many biological systems, such as cells or small model organisms like *C. elegans*. Because of this similarity and the predictability of flow, microfluidic systems can be designed to physically position, direct the motion of and otherwise physically manipulate these subjects in a minimally damaging and high-throughput fashion.

### **1.5.1 General Microfluidic System Features and Principles**

Original microfluidic devices were fabricated using conventional microfabrication and MEMS principles. This fabrication approach was relatively costly and lengthy. The development of soft lithography as a microfluidics fabrication technique spurred rapid prototyping, cheap fabrication, and provided the ground work for faster adoption and development of microfluidic systems. This molding approach was pioneered and developed primarily by Whitesides and Quake. [66-69] Soft lithography is based on fabricating microfluidic systems in PDMS, or poly(dimethylsiloxane). Devices are molded by pouring the uncured elastomer on top of a master mold and curing it. Though this master is still fabricated using standard lithography techniques, the process is simplified. Here, instead of using photoresist as a mask for subsequently etching the silicon or performing lift-off, 3D features are created directly by photopatterning the resist itself. Thus the master fabrication process is much cheaper and less time consuming. After the elastomer has cured, it can be peeled off and sectioned into individual devices, leaving the master to be re-used. The individual devices can then be bound to a layer of PDMS or glass to seal them via heat or plasma bonding. Another critical step in increasing the utility of microfluidic systems was the development of on-chip fluidic valves. [68] These work on the principle of deflecting a membrane into the area of a channel. This membrane then closes the channel and prevents liquid flow. The deflection is achieved by pressurizing the backside of the membrane. Once the pressure is relaxed, the elastomeric membrane retracts and flow through the channel is re-established.

This pioneering work led to the development of a wide range of microfluidic systems with a plethora of applications. These include but are not limited to cell and particle sorters, DNA capture systems, point-of-care diagnostic systems, droplet generators, micro-reactors, microfluidic mixers, enzyme based capture and analysis systems, and segmented flow particle generators. Microfluidic systems have also found their way into

*C. elegans* research with the goal of improving animal handling and providing more efficient, reliable and high-throughput alternatives for standard methods.

### **1.5.2 Microfluidic Systems for Improved Handling of *C. elegans***

The broad range of research directions with *C. elegans* makes it difficult to design a system capable of addressing every single scenario. Instead, systems were and continue to be developed with specific types of applications in mind. Although not all encompassing, they can be divided into i) immobilization systems, ii) behavior analysis systems, iii) long-term and on-chip developmental studies systems, and iv) lifespan analysis systems.

#### **1.5.2.1 Immobilization Systems**

The focus of immobilization systems is to facilitate rapid immobilization and imaging of a large number of animals. This is highly desirable for forward genetic screens, where animals are mutagenized and then screened for phenotypical mutants. This process is very labor intensive and very low throughput (~5 animals per hour). Microfluidic systems can increase the throughput by 1-2 orders of magnitude. One of the earliest systems was developed by Hulme *et al.* in 2007. [70] This design is a large array of parallel channels with a tapering geometry. Animals are forced into these channels via pressurized flow and compressed by the geometry until immobilized for imaging. A similar system was developed Allen *et al.* for ablation of single synapses. [71] Around the same time, Rohde *et al.* and Zeng *et al.* presented systems based on membrane compression. [72, 73] These systems use suction channels to properly position and grossly immobilize *C. elegans*. A membrane is then used to compress the animals' bodies for complete immobilization. The goal of these systems was ablation of features and sorting of mutant animals from wild type. Kwanghun Chung and Matt Crane from the Lu lab developed an imaging and immobilization system based on cooling of animals in 2008. [74] In this system animals were also properly positioned via suction channels, but they were rapidly immobilized by

cooling to 4 °C. This was the first system to demonstrate automated sorting of animals after imaging. One additional method developed by Chokshi in 2009 used a combination of membrane compression and CO<sub>2</sub> microenvironment. [75] Several additional system and design optimizations, improvements and applications have been presented based on these original designs. [76-78] These immobilization techniques have been shown to work excellently at rapidly immobilizing a large number of animals for high throughput imaging and screening [74, 76-78] and for immobilizing animals for laser surgery and imaging [48, 70, 71, 73, 75].

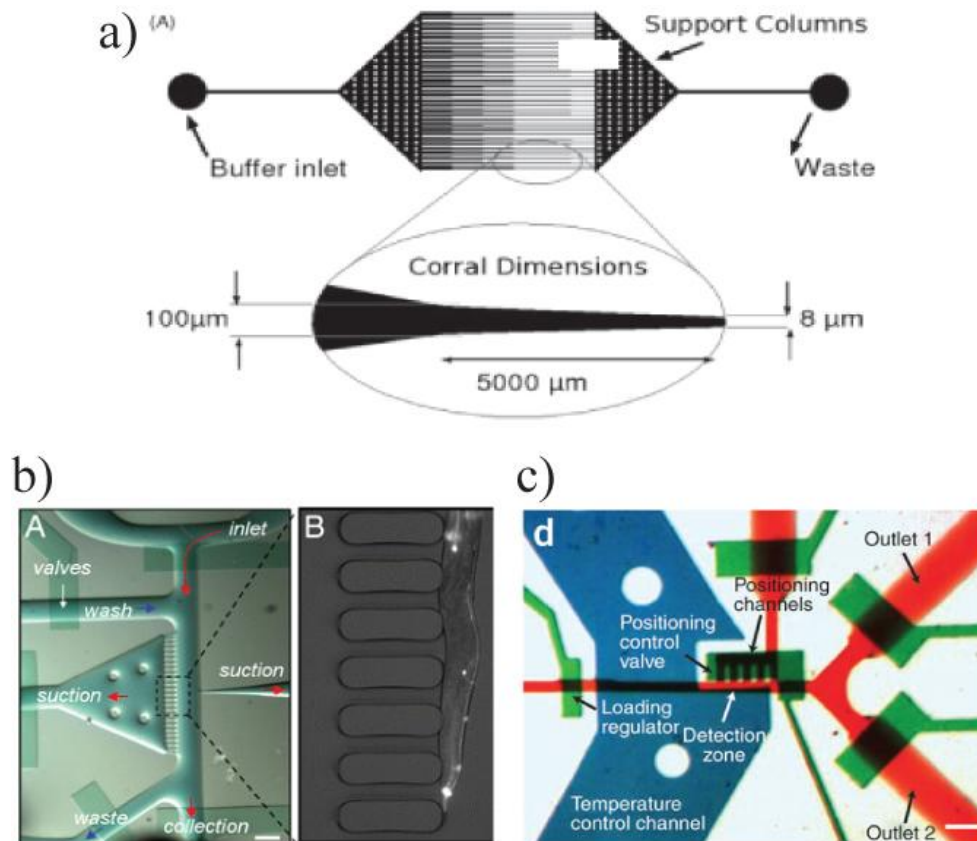


**Figure 1.6** Examples of microfluidic immobilization systems. a) Array of tapering channels for physical compression. (image: Allen *et al.*, Journal of Neuroscience, 2008 [71] Reuse license number: 2158251120582) b) System using suction channels for position and membrane compression for immobilization. (image: Rohde *et al.*, PNAS, 2007 [72] Reuse license number: Permission with proper citation granted). c) Cooling based immobilization system for imaging and automated sorting. (image: Chung *et al.*, Nature Methods, 2008 [74] Reuse license number: 3161480925107).

However, the utility of these systems for live imaging or dynamic long-term studies is limited. In all of these systems, animals are completely immobilized throughout the experiment. As such, animals cannot feed. Moreover, the systems are not set up to deliver nutrients to animals. Therefore, live imaging is possible only for a very short period of time before the animals' physiology is affected. Additionally, the cooling approach and the use of CO<sub>2</sub> directly affect physiology, which makes them unsuitable for live imaging as at all. Furthermore, since the goal of immobilization systems is high throughput imaging, they are not designed or intended to repeatedly image and keep track of individual animals as these animals are developing. Because of this they are not suitable for long-term studies either.

#### 1.5.2.2 Behavior Analysis Systems

Behavior analysis systems have been developed to increase the throughput compared to standard experimental techniques (section 1.3.1), to improve environmental control, and to increase the depth of behavioral response data from each experiment (section 1.3.2). These systems are capable of establishing chemical and thermal gradients or of creating highly spatially confined areas containing odors. One of the earliest assays was presented by Gray *et al.* as a molecular oxygen sensing array, in which a stable oxygen gradient was created across the device by using nitrogen gas as a sink for oxygen at one end of the device. [51] Zhang *et al.* combined chemical signal gradients from pathogenic bacteria with geometric restriction in the shape of a central worm chamber connected to bacteria chambers via channels to analyze olfactory learning in *C. elegans*. [79]. These two systems were not liquid based, yet take advantage of certain microfluidic principles in manipulating gas flows.

A system designed to analyze the activity increase in olfactory neurons via optical detection of fluorescent intensity of the calcium indicator GCaMP was presented by Chronis *et al.* in 2007. [80] In this system, the tips of animals' head can be selectively

exposed to a laminar stream containing olfactory cues. The response in neuron activity can be recorded after shifting the laminar stream to touch the tip and after the stream is moved away from the tip.

In 2008, Lockery *et al.* presented a system designed to mimic a typical crawling environment, while taking advantage of the properties of microfluidic devices for olfactory assays. [81] The design consisted of a large chamber filled with pillars at specific center-to-center distances and pitch. These pillars served as crawl support for *C. elegans*, which would otherwise be swimming in an empty chamber. By taking advantage of laminar flow, sharply defined streams of liquids with differing concentration of stimuli can be established across such a device to study olfactory behavioral response. In 2011, Albrecht *et al.* used a device based on the same principle for high content behavioral analysis. [59] The analysis employed tracking software capable of tracking individual animals over time. The software continuously images the device, uses detection algorithms to identify animals, and tracks their positions and body shape over time. Albrecht was able to extract a large number of features of *C. elegans* olfactory responses to chemical gradients and sharply defined odorant concentration steps. This software is based on the principle of multi-worm tracking software presented by Baek *et al.* in 2002 [82]; since then, several additional individual and multiple worm tracking software packages have become available with the goal of improving behavior analysis throughout and data gathering. [36, 83, 84].

In the Lu laboratory, Kwanghun Chung and Mei Zhan developed a novel approach to behavioral studies. [85] In their system, *C. elegans* are individually loaded into chambers in a large array. Chemical stimuli can then be delivered to the array with precise temporal control. The behavioral response is recorded and then analyzed via custom MATLAB code.



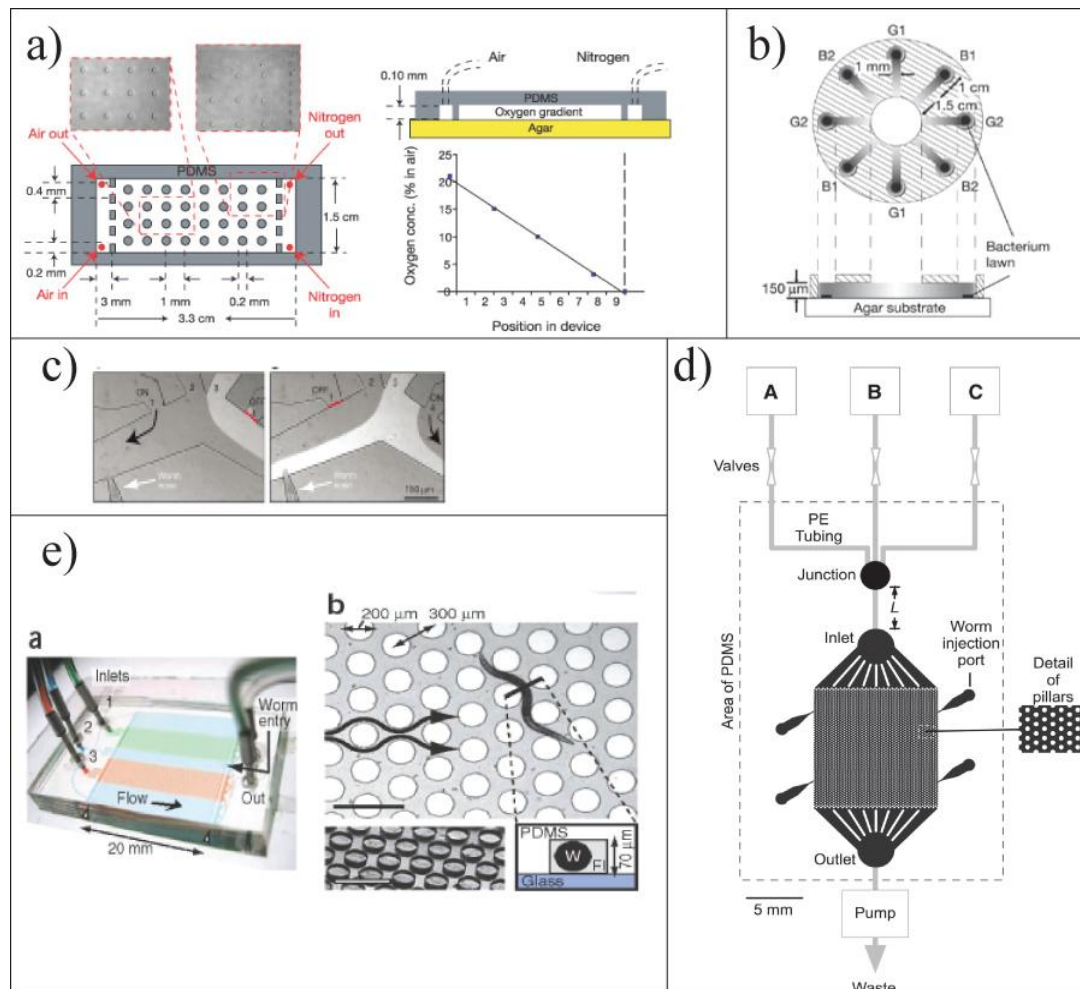


**Figure 1.7** Examples of behavior analysis systems. a) Oxygen gradient generating device designed for studying oxygen sensing in *C. elegans*. (image: Gray *et al.*, Nature, 2004 [51] Reuse license number: 3161480925107). b) Odorant gradient device with geometric restriction to direct movement. (image: Zhang *et al.*, Nature, 2005 [79] Reuse license number: 3161481271215). NOTE: Systems a) and b) utilize microfluidic principles for manipulating gas flows. c) Device for selectively exposing animals to olfactory cues via laminar flow switching. (image: Chronis *et al.*, Nature Methods, 2007, [80] Reuse license number: 3161481433129) d) “Artificial dirt” device; chamber filled with pillar structures designed to mimic crawl like environment, while generating bands of chemical stimuli. (image: Lockery *et al.*, Journal of Neurophysiology, 2008 [81] Reuse license number: Permission not required). e) Pillar array chamber device for generating chemical gradients and sharp transitions between odorants. (image: Albrecht *et al.*, Nature Methods, 2011 [59] Reuse license number: 3161490491141)

These systems have significantly propelled precision and controllability of behavior analysis of *C. elegans*. In addition, worm-tracking systems have allowed for large numbers of animals to be studied simultaneously with individual animal resolution. In

combination, these platforms provide a great conceptual basis for long-term dynamic studies despite lacking certain required features. For example, the principle of individual software tracking or physical isolation is highly applicable to developmental and lifespan studies. Additionally, providing features for crawl support in microfluidic systems more closely mimics the *C. elegans* natural environment. However, a downside of software based tracking is the loss of worm identity in certain occasions, such as two worms moving into close contact. Also, tracking of individual identities requires constant optical tracking. Lastly, these systems are not designed for high-magnification imaging because they lack the ability to immobilize animals. It has to be noted that real-time optical tracking systems do provide high-magnification imaging capabilities. However, such real-time tracking systems can generally only be used to study one animal at a time, which would lead to very low throughput dynamic long-term studies.

#### 1.5.2.3 Long-Term Developmental Studies Systems

In 2011, Rohde *et al.* presented a system with the potential for performing dynamic developmental studies of *C. elegans*. Although not based on microfluidics, the system is capable of repeatedly immobilizing animals, which are being grown in liquid culture in a standard multi-well plate. The immobilization is based in cooling; each well has its own individually actuated peltier-based cooler. Rohde has demonstrated the utility of the system by performing time-lapse analysis of neurite regrowth after laser microsurgery in grown animals. The observed axonal rate of regrowth was significantly greater than predicted by ensemble averaging of many animals, which is a technique used for developmental studies when standard methods of immobilization are used (section 1.4). This supports the argument that population averaging leads to significant loss of detail in describing developmental processes.

However, the application of this system is questionable for developmental studies spanning the earliest developmental larval stages. The difficulty lies in the choice of

immobilization method for imaging. Cooling the animals to 4 °C significantly affects physiological processes. This is not a problem for automated screening systems, because the animal is only imaged once to determine its phenotype. However, such frequent interruption into normal physiological function of developing animals may have significant effects on the development itself.

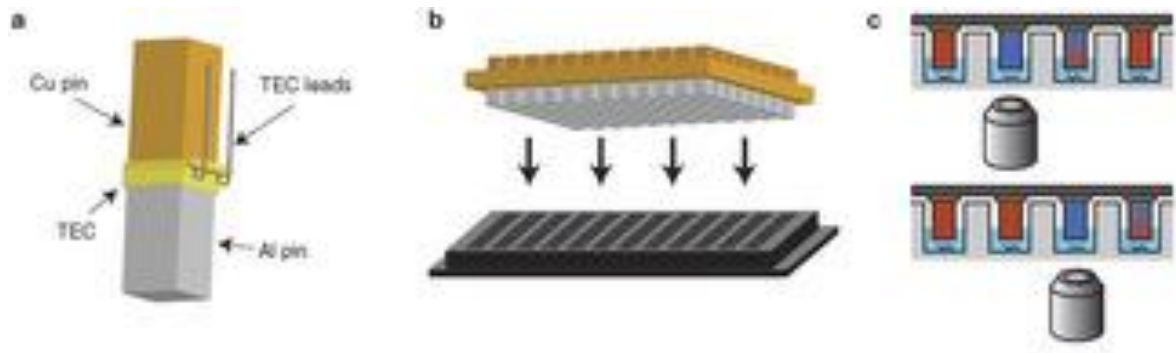


**Figure 1.8** Time-lapse imaging system with peltier cooler based immobilization for imaging. (image: Rohde *et al.*, Nature Communications, 2011 [86] Reuse license number: 3161491152952).

#### 1.5.2.4 Lifespan Systems

Two systems with the goal to perform precisely controlled lifespan on-chip studies have been presented. The first was developed by E. Hulme in 2010. [87] The system is based on an array of chambers, each of which is connected to channel with tapering geometry. Each chamber houses one animal throughout the experiment. These can be moved in and out of the tapering channels for immobilization and imaging. Nutrients in the form of bacteria suspended in liquid solution are continuously delivered to the culture chambers via the tapering channel as well. Progeny are removed from the culture chamber as well. This is important so that the mother is not confused with its progeny during the experiment and so that non-sterile strains may be used. This system allows tracking the lifespan on an individual animal basis and was used to perform a full duration experiment. However, certain shortcomings in the design and methodology led to low acceptance of the work in the life-span community. First, temperature control is critical for lifespan analysis. For example, the generation time of *C. elegans* at 15 °C is 6 days,

while it is only 2 days at 25 °C. Since the system has no temperature control mechanism built in, the use of an incubator is required. Second, since no crawl support is included in the chamber design, animals are forced to constantly swim against a current.

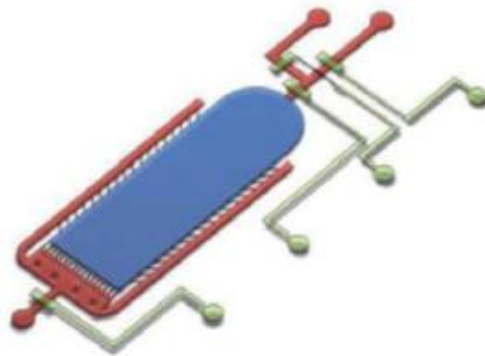
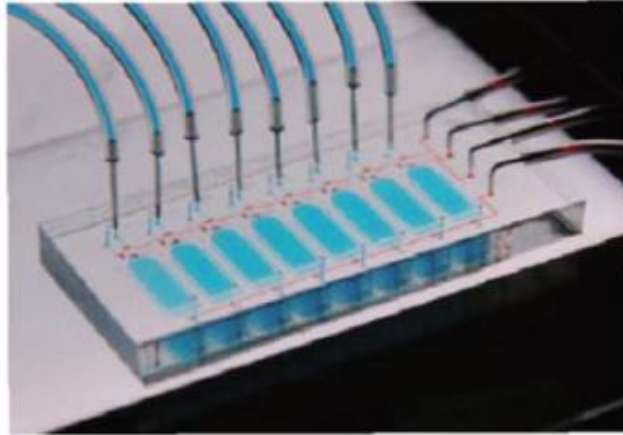


**Figure 1.9** WormFarm device. An array of large chambers designed to perform lifespan experiments on groups of animals. (image: Xian *et al.*, Aging Cell, 2013 [88] Reuse license number: 3161500139097)

The energy requirements of constant swimming may affect lifespan results as well. Third, the nature of the gravity driven flow used in the design requires the system to be open to air, which may lead to contamination. Presence of potentially pathogenic bacteria can drastically alter lifespan of *C. elegans*. Last, the design of the array precludes the option of imaging the array as a whole simultaneously. This prevents certain studies to be performed in parallel, such as analysis in change of behavioral response with ageing.

The second system has been developed by Xian *et al.* and presented recently in 2013. [88]. In this design, an array of large chambers can each be loaded with 30-50 animals. In these chambers, nutrients can be delivered at precise concentrations. Progeny are removed through outlet channels large enough for early larvae, but too small for adult animals. Xian has demonstrated i) the ability of the system to perform several lifespan experiments in parallel, ii) while using a range of nutrient concentrations and additives, and iii) with automated counting of live/dead animals via computer software. The system is also fully closed, thereby minimizing the risk of contamination with pathogenic bacteria.

In comparison with the Hulme device, the throughput of Xian's system is much higher; eight different conditions can be tested on 30-50 animals simultaneously. The trade-off is the loss of individual animal tracking and the inability for observing behavioral response. Similar to the Hulme device, there are no pillars included in the chamber design. Because of this, animals need to swim against a current, and from the collected data it is apparent that over time they are pushed towards the outlet where they accumulate. Whether this affects lifespan is not clear. Also similar device presented by Hulme *et al.*, there is no temperature control built into the system. While these systems perform adequately, they fail to provide the full set of features required for a dynamic lifespan experiment.

## 1.6 Thesis Objectives

This thesis makes contributions to the study of neurobiology, ageing, and development through the development of a toolkit for live and long-term dynamic studies of *C. elegans*. The major contributions are:

- 1) The design of a system capable of robust culturing of developing *C. elegans* and of repeated high-resolution imaging at physiologically benign conditions. This is the first system capable of growing animals from the early L1 larval stage, while

repeatedly and reversibly immobilizing animals for imaging. This immobilization happens at physiological conditions without any damage to the animals.

- 2) The development of a system for studying development of *C. elegans* starting at the embryonic stage all the way through adulthood with the added ability for highly localized temperature control. The temperature control may be used for immobilization of animals for imaging or for studying the effect of temperature on animal development and behavior. This is the first microfluidic system capable of culturing and imaging all developmental stages in a single platform and is designed for easy dissemination to other laboratories.
- 3) The development of a device capable of selectively immobilizing *C. elegans* for continuous live imaging at physiological conditions. This is the first system capable of immobilizing the animal body at physiological conditions while allowing the animals to feed throughout the experiment to maintain normal physiological function.
- 4) The design of a single-package system for lifespan studies with individual animal resolution, integrated nutrient delivery, temperature control, and image acquisition. Compared to other available life-span on chip designs, this is the first system capable of temperature control without the use of incubators and thus can be used as a bench-top system. Additionally, it is designed for control of dietary conditions, temporal control of stimuli for studying effects of aging on behavior, and for use with non-sterile strains without the need to sterilize animals with drugs.

## **CHAPTER 2      MICROFLUIDIC SYSTEM FOR LONG TERM CULTURE OF *C. ELEGANS* WITH HIGH-RESOLUTION IMAGING FOR DEVELOPMENTAL STUDIES**

This chapter describes work on a system for studying the development of *C. elegans*. Developmental studies using multicellular model organisms such as *C. elegans* at the cell or subcellular level rely significantly on the ability to image animals at high-resolution. Standard imaging modalities, such as the use of anesthetics for immobilization, however, do not allow animals to be imaged repeatedly. This leads to the inability to follow the specific development of each individual animal and observe dynamic processes. The ability to image a single animal at high-resolution over a period of time, with no physiological side-effects is therefore critical to thoroughly understand long-term developmental effects. To overcome these difficulties, I developed a microfluidic system, which allows for long-term culture of *C. elegans*, and repeated high-resolution imaging at physiological temperatures without using anesthetics. Animals are cultured in individual chambers in media containing nutrients required for development and immobilized only during an imaging cycle. The immobilization is made possible via a reversible thermo-sensitive sol-gel transition of the solution of a commercially available biocompatible polymer, Pluronic F127. Thus, this method facilitates time-lapse studies of single animals at high-resolution and lends itself to shedding new light on many developmental processes and events. This chapter has been adapted from reference [89], “Long-term high-resolution imaging and culture of *C. elegans* in chip-gel hybrid microfluidic device for developmental studies.”

### **2.1      Overview of the System**

The basic operating principle of this system is depicted in Figure 2.1a. The system operates in three stages. The first stage is initial loading; a suspension of *C. elegans* in

nematode buffer is loaded into the device for trapping individual L1 stage larvae in culture chambers. The second stage is the culture stage; OP50 *E. coli* suspended in nematode buffer are delivered to the device and flow through the culture chambers containing *C. elegans*. This allows animals to feed and develop normally. The third stage is imaging; nematode buffer is temporarily replaced with Pluronic F127 solutions, which is heated to immobilize animals for high-magnification imaging. After the solution cools, it is again replaced with nematode buffer. After completion of the first stage, stage two is maintained for the majority for the experiment. Stage three is engaged whenever animals have to be imaged, after which the system is returned to back to stage two.

The whole system consists of the microfluidic chip and the off-chips components (Figure 2.1b). These include i) a pressure-driven liquid delivery system, a liquid heating element, ii) macrovalves for controlling fluid flow on and off chip, and iii) a compound microscope with a CCD camera and x-y-z stage.

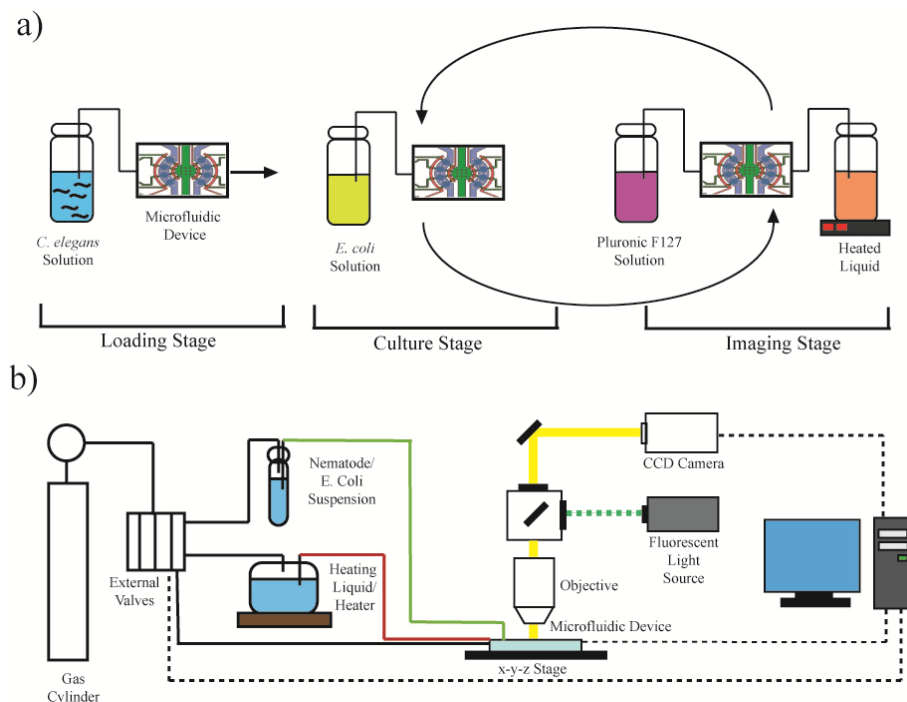


**Figure 2.1** System overview. a) Animals are injected into the device, where they are provided with nutrients to grow and occasionally immobilized for imaging. b) Block diagram of the off chip system components.



## **2.2 System Design Process**

As stated previously, the requirements for dynamic developmental studies include i) the ability to track the development of individual animals, ii) facilitation of normal development, iii) immobilization for periodic imaging without affecting physiology and development and iv) reversibility of the immobilization process.

### **2.2.1 Exploration of Animal Tracking and Immobilization Methods**

Tracking of animals can be facilitated via software as was explored in Section 1.5.2.2 or via physically separating each specimen. Software tracking would require constant observation under a microscope with uninterrupted image processing. This would not only be logistically difficult but computationally intensive. Additionally, worm trackers often receive errors in tracking, such as when two animals touch, and lose record of the animals' identity. For this reason, physical separation of animals was chosen as the preferred alternative. The first design (Figure 2.2a) was based on delivering animals to individual culture chambers with pillar structures included as crawl support. Nutrients were to be delivered to these chambers in liquid form. For imaging, animals would be moved from the chambers to an imaging area via an animal delivery channel. Selection of chambers for imaging and control of flows would occur via pneumatic valves (as described in Section 1.5.1.).

This design was changed into an array to increase scalability and decrease the number of required inputs. Additionally, each chamber was designed with its own imaging area, instead of transporting animals from all chambers to a single area for imaging. The immobilization would occur by pulling animals into a channel with tapering geometry. This was an adaptation of the principles from [70, 71]. In addition to tapering geometry, cooling to 15 °C would be used to decrease activity, yet remain within the physiological range. (Figure 2.2b) After testing, several issues became obvious. First, unlike the previously published designs, this system is intended to study development and has to

accommodate the youngest, early L1 larval stage, and smallest animals. These have a diameter of  $\sim 6 \mu\text{m}$ ; the previous design was intended for animals with diameter  $\sim 40 \mu\text{m}$ . Not only is the fabrication of such small features more difficult, but the pressure drop across a tapering channel of such dimensions is significantly larger and so is the resistance to flow. This makes it difficult to establish sufficient flow to drag animals into the channels. Additionally, since animals reside in large circular chambers where the cross sectional area is several orders of magnitude larger, the flow here is expanded and flow velocity further decreases. Experimentally it became obvious, that any immobilization method would have to be executable on animals inside their culture chambers.

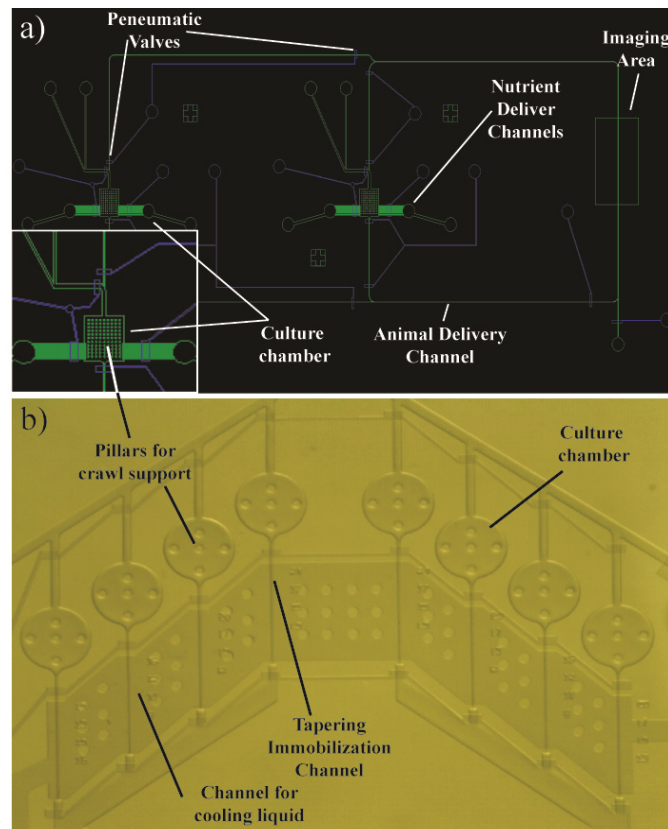


**Figure 2.2** Early design concepts. a) Concept of device with individual culture chambers and a single imaging area. Animals would be moved to and from the imaging area back to the culture chambers via the animal delivery channel. The flow would be controlled via pneumatic valves. b) Array re-design, with an imaging area for each culture chamber. Animals would be immobilized by tapering channel geometry and mild cooling to  $15^\circ\text{C}$ .

The only established methods for immobilization usable on animals in chambers at the time were cooling and membrane compression. Cooling was deemed unacceptable for its effects on physiology. Membrane compression was deemed risky; repeated compression of young and very fragile animals could cause damage. This lack of available options led to the exploration of immobilization agents. These are liquids, which can be used to immobilize animals on demand. Mixtures from molecular gastronomy and the food industry were investigated, such as sodium alginate, gelatin, xanthan gum, and Pluronic brand polymers. Molecular gastronomy mixtures were chosen for presumed biocompatibility. Also, it was anticipated that animals would remain in this liquid, and thus segregation of animals in liquid droplets instead of chambers was explored in addition. (Figure 2.3). Food would be delivered to animals inside droplets via merging with droplets containing *E. coli*. Hundreds of animals immobilized inside droplets could be stored in microfluidic channels.

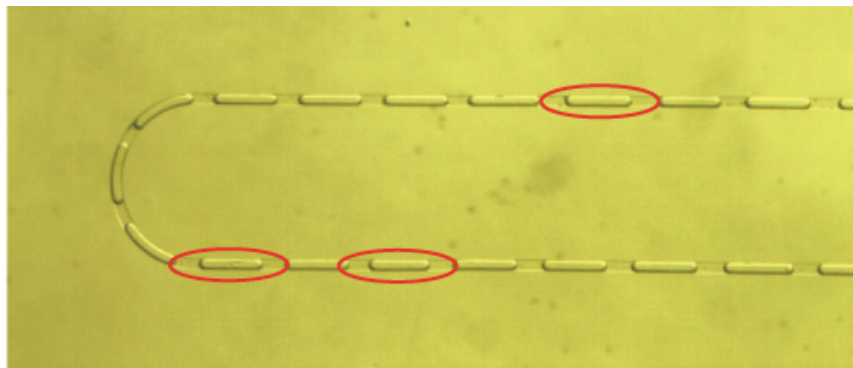


**Figure 2.3** Example of animals trapped in droplets for segregation and long term developmental culture on device.

Droplet implementation proved impractical; growing animals were able to break through the droplet boundary and jump between individual droplets. The only way to prevent this effect was to use surfactants. Although possibly benign, constant exposure to these chemicals could be questioned by the biological community. This would impede the

dissemination of the technology in the community. Even though this idea proved fruitless, the exploration of immobilization agents yielded a promising candidate.

### **2.2.2 Pluronic F127 as an Immobilization Agent**

Pluronic F127 is a tri-block co-polymer from the Pluronic (or Poloxamer) family of products. Pluronic block co-polymers all consist of a block of poly(propylene oxide) with a block of poly(ethylene oxide) at each end of the PPO chain. The different kinds of Pluronic vary in the ratio of the PEO to PPO block sizes and total molecular weight of the block co-polymer. Over the past decades, researchers have investigated the physical properties of these polymers in solution and their possible applications. [90-95] In general, all Pluronic polymers form at least a mixture of free polymer chains and micelles in solution at high enough concentration. The larger the hydrophobic PPO domain is, the lower the critical micellar concentration is and micelles begin to form at lower concentrations and lower temperatures. The larger the hydrophilic PEO domain is, the more difficult it is to form micelles. This effect is however much less pronounced. Additionally, at constant ratio of PEO/PPO, micelles form more readily with higher molecular weights. [90]

Certain polymers from the Pluronic family additionally undergo a thermo-reversible sol-gel transition. During this transition, the solution containing the polymer transitions from liquid state to a gel state. This effect is accompanied by a sharp increase in viscosity which I measured, storage modulus and the yield stress of the solution, as shown in Figure 2.4. [95] This transition occurs very fast on a molecular level; the rate of heat transfer through the gel is thus paramount in controlling gelation kinetics. Thus, the fast and more uniformly the solution can be heated to the transition temperature, the faster the gelation will occur. There is no delay from the gelation process itself. [94]

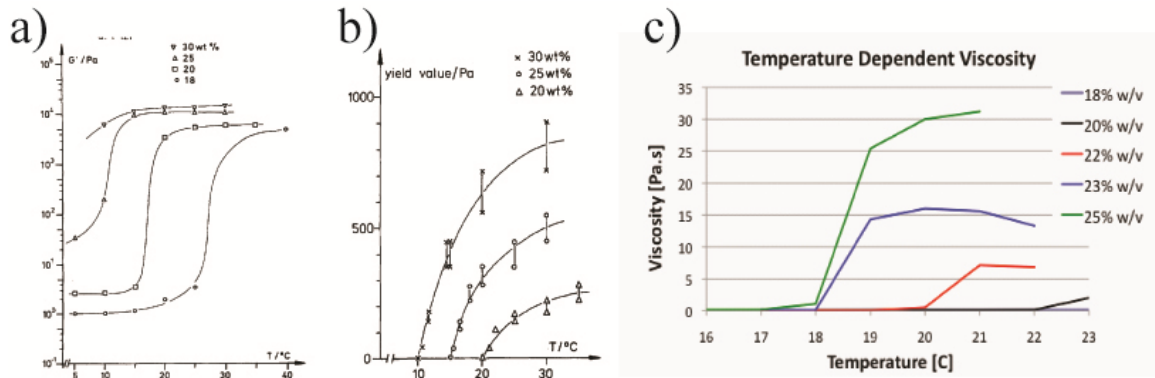


**Figure 2.4** Physical properties of Pluronic F127. a) Storage modulus of PF127 solution with increasing temperature. (image: Wanka *et al.*, Colloid and Polymer Science, 1990 [95] Reuse license number: 3161500986408) b) Yield stress of PF127 solution with increasing temperature. (image: Wanka *et al.*, Colloid and Polymer Science, 1990 [95] Reuse license number: 3161500986408) c) Measurement of viscosity of PF127 solution with increasing temperature.

How the gelation occurs has also been a subject of previous research. Rassing *et al.* proposed a mechanism, in which a structural change in the micellar structure led to the formation of the gel. [96] One such possible proposed mechanism would be the dehydration of the EO blocks in the corona of micelles with a PPO core. This dehydration would lead to the collapse of the corona and formation of a tightly packed structure. Wanka *et al.* confirmed these findings, yet concluded that the gelation effect is triggered by a different process. [95] Wanka confirmed that indeed i) micelles form if the PPO block is large enough and ii) get bigger with increasing temperature. They also become more compact, squeezing out water molecules, until the corona collapses into a dense layer of EO groups. This effect occurs above the critical micelle concentration as confirmed by static light scattering, but prior to the sol-gel transition. The light scattering behavior already corresponded to that and only that of hard sphere particles. Wanka analyzed the small angle neutron scattering patterns and determined that at high concentrations and temperatures the gel appears as an ordered crystalline structure of micelles embedded in an amorphous material. Wang *et al.* subsequently also postulated a 3D structuring.

Most recently, Mortensen *et al.* also used small angle neutron scattering to confirm that i) at low concentrations aggregates are free floating, ii) the PPO block causes the aggregation into micelles with core sizes up to 50 Å, and iii) the gelation process occurs due to an increase in the concentration of micelles with temperature until their volume density is so high, that they lock into a crystalline structure of hard spheres.

Pluronic polymers are approved by the FDA and EPA as direct and indirect food additives, pharmaceutical ingredients, and agricultural products and have very low cytotoxicity. [97-99] Because of this, Pluronic F127 functionality is being investigated in several biotechnology applications, such as an in vitro drug delivery packaging agent [100, 101] or a cell encapsulation agent [99]. Because of its high biocompatibility, and the temperature and concentration controlled and reversible sol-gel transition, Pluronic F127 was our immobilization agent of choice.

### **2.2.3 Compatibility of Pluronic F128 with *C. elegans* Physiology**

Despite being generally accepted as biologically benign for cells and tissues, I have verified this is also the case with *C. elegans*. To evaluate the effect of immobilization with the PF127 gel on animal development, I performed a series of immobilization cycles. The conditions of these cycles corresponded to conditions similar to actual experiments on chip: animals were suspended in PF127 solution, which was heated and cooled to trigger the sol-gel-sol transitions as would happen during an imaging cycle. Besides visually inspecting the gross morphology of the animals, I recorded three indicators of *C. elegans* development, i) time to reach egg-laying, ii) the pharyngeal pumping rate at young adult stage, and iii) the number of progeny in the first 24 hours of egg-laying. As is shown in Figure 2.5, for all three indicators, animals exposed to short (90 seconds) or long (10 minutes) cycles showed no significant difference to the control population (no temperature cycling and no exposure to PF127). Figure 2.5a shows that

time to reach egg-laying varies little between populations. Similarly, the average number of progeny (Figure 2.5b) and the pharyngeal pumping rate (Figure 2.5c) are unaffected,

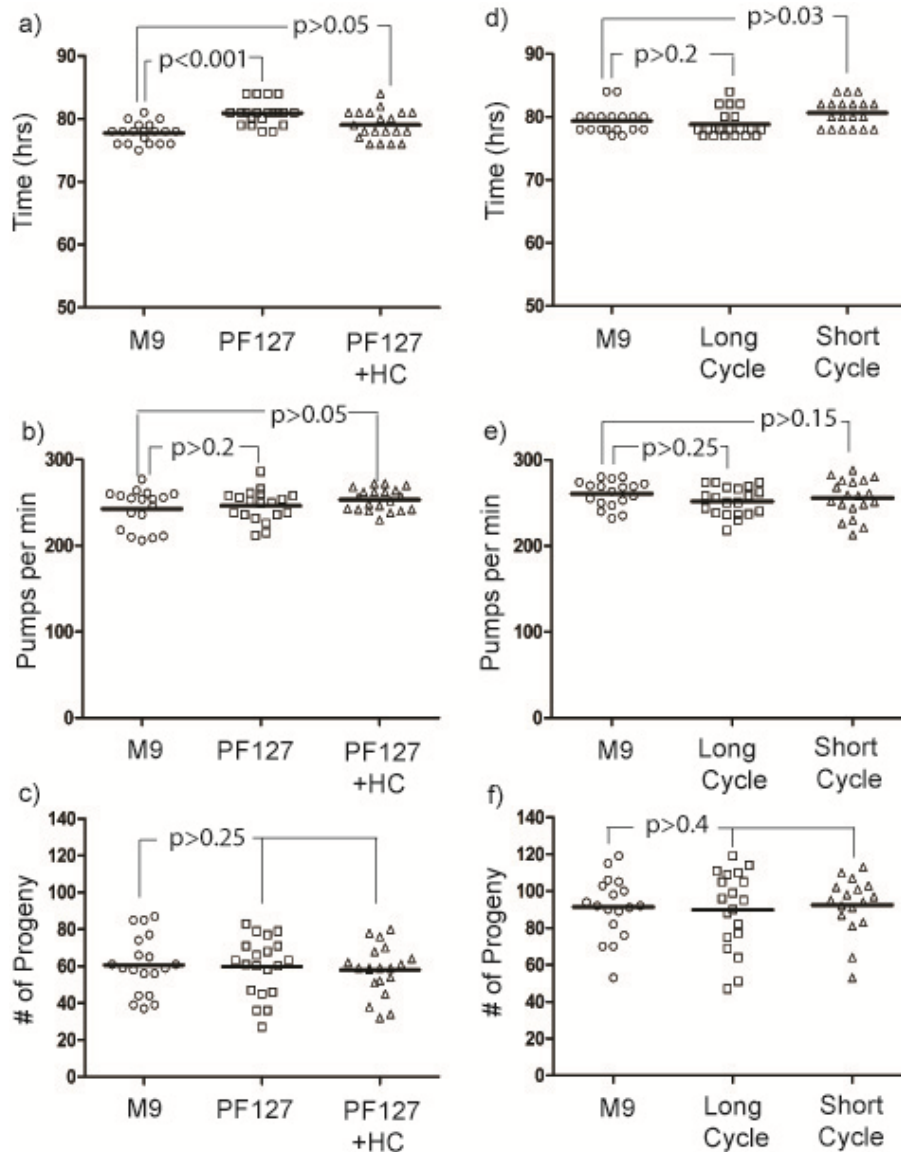


**Figure 2.5** Examination of biocompatibility of Pluronic F127 with *C. elegans* physiology. Analysis of the effect of repeated immobilization cycles (a-c) and exposure during early development (d-f) on animal development. For repeated immobilization, animals were exposed to 50 short cycles (immobilization for 90 seconds) and 5 long cycles (immobilization for 10 minutes). To examine the effects of exposure during early development, animals were exposed to nematode culture medium (M9), PF127 solution (PF127) and PF127 solution containing hydrocortisone (PF127, HC) prior to hatching and during the L1 developmental stages. Afterwards, the following three indicators were observed: (a,d) mean time to reach egg-laying, (b,e) pharyngeal pumping rate at young adult and (c,f) number of progeny in the first 24 hours of egg-laying.  $n \geq 18$ .

suggesting that the nematodes are unharmed by the thermo cycling and the presence of PF127 and proceed with normal development, which is critical for developmental studies. In typical developmental studies, embryos or younger larvae, such as the L1 stage animals, would be used. Since development continues long after hatching, I wanted to ensure that development is not adversely affected by the surfactant-like properties of the PF127 molecules. Therefore I also evaluated the effect of exposure to the PF127 solution during the embryonic and L1 larval stages. In these experiments, I exposed the animals to 25% w/v PF127 solution, which is the highest concentration to be potentially used in experiments, and to PF127 solution containing hydrocortisone, which is a membrane stabilizing agent. I observed the same three indicators as before. Similarly, as can be seen in Figure 2.5d-f, none of these parameters showed statistically significant differences between the PF127 or PF127+HC and the control samples. This suggests that exposure to PF127 solution, even during early developmental stages, has no adverse effects on *C. elegans* development, and the polymer solution can therefore be used for immobilization during live imaging experiments and long term developmental studies.

### **2.3 Final System Design**

Our finalized design is capable of providing both nutrients and proper gas exchange to multiple animals cultured in individual chambers. These chambers are used to keep animals separated at all times, thus guaranteeing that development can be followed on a per-animal basis. Reversible and repeatable immobilization directly inside the culture chambers is facilitated by a solution of Pluronic F127 via the thermo-reversible sol-gel transition. Thus, with efficient temperature control, cycling between a liquid and an immobilizing gel phase is easily achievable. The immobilization occurs anywhere in the chamber without positional requirements, with minimal environmental and physiological disturbances and physical deformation to the animals. This method of immobilization enables observation of physiological processes and events in an unprecedented fashion.



### 2.3.1 Hybrid Platform Design

To successfully culture, immobilize, and image animals, all in a single platform, I designed a hybrid system composed of a microfluidic device and PF127 solution for repeated immobilization. The microfluidic device is a PDMS-based, two-layer device (Figure 2.6). The flow layer contains all flow inlets and outlets and the individual culture chambers. The two inlets are used to load animals into the device and deliver culture medium (loading inlet) and to flow PF127 solution into the device (PF127 inlet). Both inlets join to deliver solution and animals to the loading chamber. From here, animals enter the individual culture chambers, where they are trapped for the duration of the experiment.

There is a total of eight culture chambers per device; four on each side of the loading chamber. These two sets can be operated individually and thus the device can be operated with either four or eight active chambers. Large culture chambers were used for two reasons: i) they allow animals to grow without mechanical constriction and move around freely in an aqueous environment, and ii) the large cross-sectional area leads to the expansion of flow and thus a decrease in linear flow velocity and hence shear. Therefore, unlike in straight channels, sufficient exchange of media and nutrition occurs without animals having to constantly swim against a flow. The slowing of flow also leads to a longer residence time of bacteria in the chambers, which in turn allows animals to feed properly. Partially closed pneumatic valves at the inlet and outlet of the culture chambers function to trap animals for the duration of the experiment. When unpressurized, these valves remain open and permit flow through the corresponding channels. When pressure is applied, the membrane deflects down into the flow layer, increasing the resistance and reducing the flow [68] as shown in Figure 2.6e. Because of the rectangular cross section of the flow channels, these valves do not permit animals to escape while simultaneously allowing flow of liquids through the channels. Excess

animals not loaded into the individual chambers, debris, and wastes are flushed out via the flushing outlet (Figure 2.6).

There is a second layer of the device, which contains valves for flow control and heating conduits for temperature control. The valves are fluid-filled to prevent gas bubble formation in the flow layer. The temperature control channel is used for raising the temperature within the device by a few degrees to trigger gelation of PF127 for immobilization of the animals. Precise temperature control is achieved by controlling the flow rate of the heating fluid and maintaining the heating fluid source temperature.

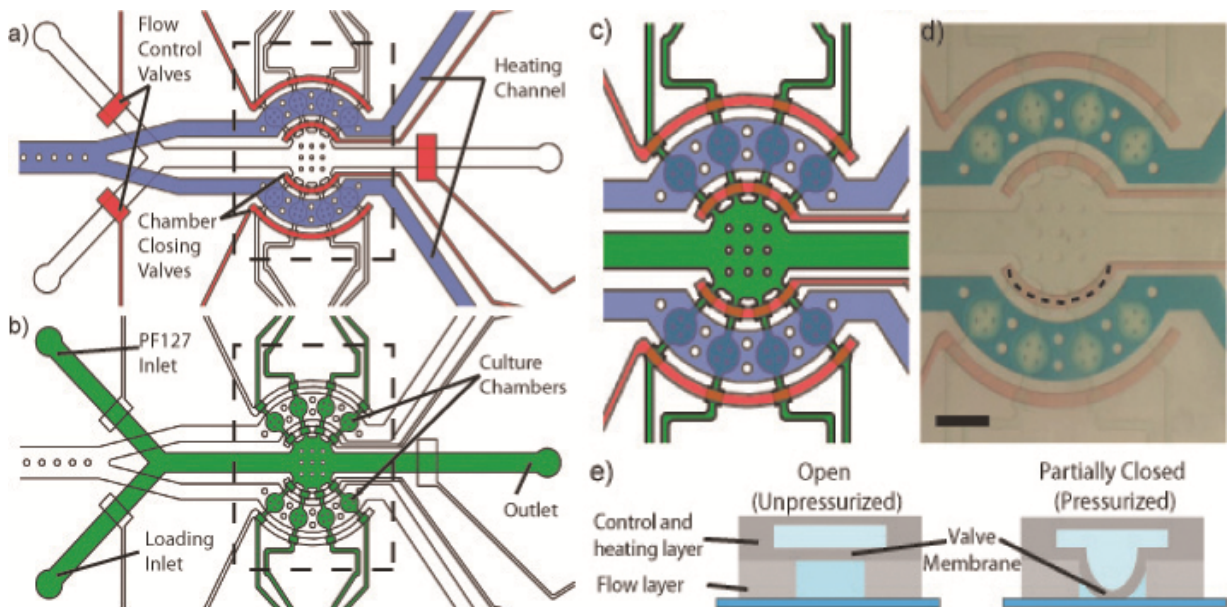


**Figure 2.6** Two-layer microfluidic device used by our hybrid platform. The flow control and heating layer (a) contains pneumatic valves (red) for flow control and trapping of animals inside chambers of the flow layer, as well as the channel used for flowing heating liquid (blue). The flow layer (b) contains the loading inlet (for animals and bacterial solution) and an inlet for the PF127 solution, 8 culturing chambers for individual culture of animals, and a waste outlet. The overall design is depicted in (c); and actual image is shown in (d); both correspond to the areas marked by dashed line rectangles in (a) and (b). The schematic in (e) represents the cross section of a partially closed valve, such as the one marked by a dashed line in (d). While unpressurized, the valve remains open. After pressurization, the valve membrane deflects into the flow layer, partially obstructing the channel. This prevents animals from escaping while allowing flow to continue. Scale bar represents 400  $\mu\text{m}$ .

## 2.4 Materials and Methods

### 2.4.1 Device Fabrication

We fabricated all microfluidic devices in poly(dimethylsiloxane) (Sylgard 184, Dow Corning) using well-established multilayer soft-lithography techniques. [66-68] Briefly, as show in Figure 2.7, each of the two layers of the device was designed in Autocad 2008 (Autodesk); masks were printed by CAD Services (California). The masters were fabricated on a silicon wafer using SU8-2025 (MicroChem) using the manufacturer prescribed procedure, and treated with Tridecafluoro-(1,1,2,2-Tetrahydrooctyl)-1-Trichlorosilane silane (UCT Specialties, LLC). Each of the two layers was then molded into PDMS with the ratio of base polymer to cross-linker to toluene of 20:1:5 (flow layer) and 10:1:0 (flow and temperature control layer).

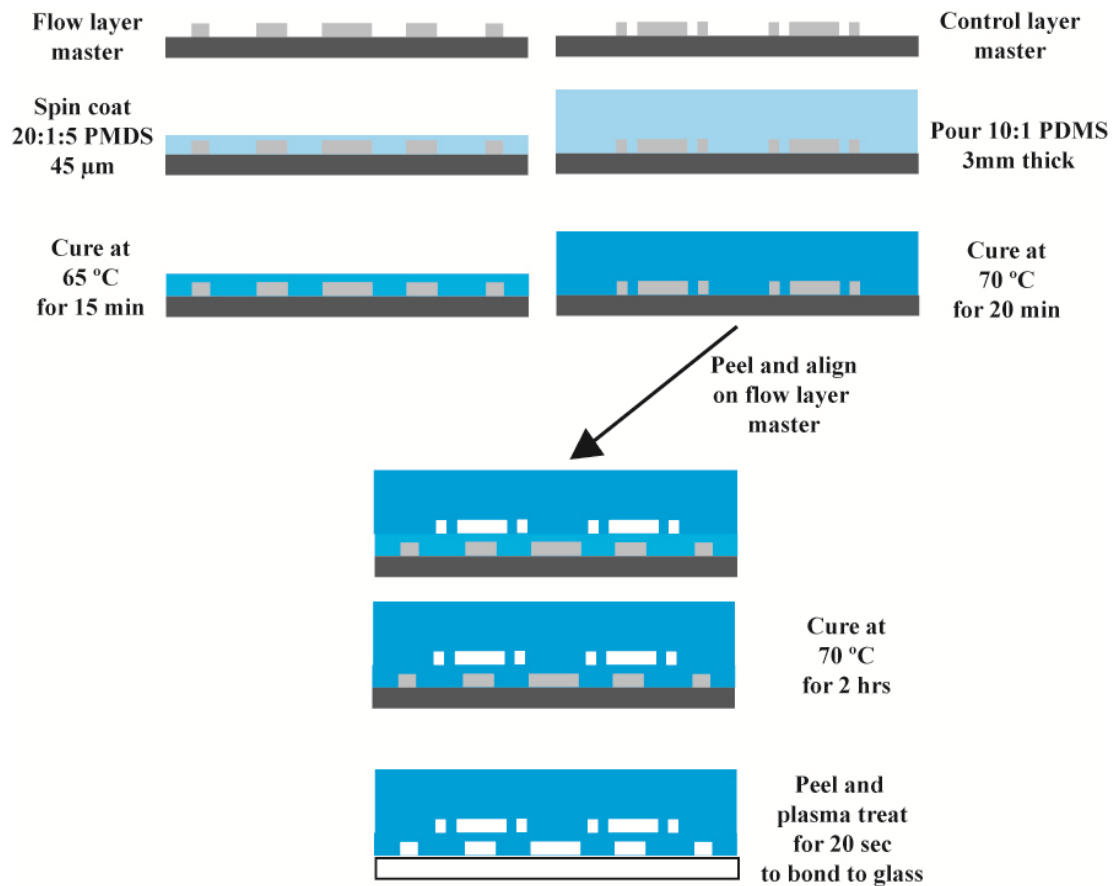


**Figure 2.7** Device fabrication method.

The 50- $\mu\text{m}$  thick flow and temperature control layer was partially cured at 70 °C for 20 minutes at a PDMS thickness of 3 mm. Next, the flow-layer master was spin-coated to a thickness of 45  $\mu\text{m}$  and partially cured on a hot-plate at 65 °C for 15 minutes, providing for a 30  $\mu\text{m}$  membrane between the 15  $\mu\text{m}$  thick flow channels and culture chambers and the top layer.

The two layers were aligned and thermally bonded at 70 °C for 2 hours and irreversibly bonded to a glass substrate via oxygen plasma treatment for 20 seconds (PDC-32G plasma cleaner).

#### **2.4.2 Solutions and Materials**

Fluids, such as culture medium and Pluronic F127 solution, were delivered to the device via plastic PE-60 tubing (Micro Medical Tubing, Scientific Commodities, Inc.) and metal pins, which were inserted into the PDMS device, by a pressure based delivery system. [74] The heating liquid was delivered from a hot bath, which was maintained at a constant temperature of 85 °C. For the heating liquid, the applied pressure not only determines the flow rate, but indirectly affects the temperature of the liquid reaching the device, the residence time inside the device, and the temperature of the culturing channels. I have verified our ability to control the temperature inside these channels via thermocouple measurement at the inlet to the device, as shown in Figure 2.8.

Solutions of Pluronic F127 (Sigma Aldrich) in water were prepared at concentrations of 23%, and 25% w/v. The suspension was agitated for 4 days at 4 °C until the polymer pellets were completely dissolved. Solutions of Pluronic F127 at 25% w/v with hydrocortisone were prepared by suspending 10  $\mu\text{L}$  of hydrocortisone solution (6.06  $\mu\text{M}$  in ethanol) (Sigma Aldrich) in 10 mL of the pre-mixed PF127 solution. Standard nematode buffer [1] solution containing OP50 bacteria was prepared by centrifuging OP50 bacteria suspended in LB medium, removing the supernatant and re-

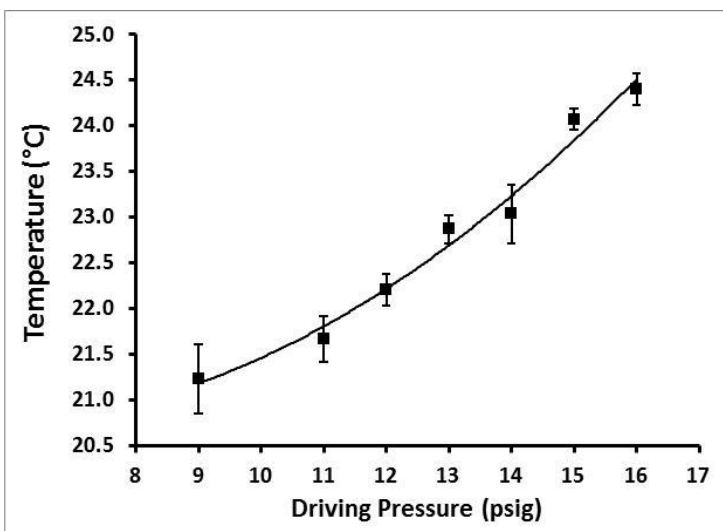


**Figure 2.8** Temperature measurement of heating liquid at inlet of microfluidic device.

suspending bacteria in M9 buffer at OD600  $\approx$ 0.9. The solution was filtered through a 5  $\mu$ m filter to remove clumps and debris.

### 2.4.3 Animal culture, assay and microscopy

*C. elegans* were cultured at 20 °C on standard agarose plates with OP50 bacterial lawns, and were suspended in standard nematode buffer for experiments. I used the N2 strain for all experiments where fluorescence was not required. The CZ456 (a strain that carries *juIs1=Punc-25::gfp*) [58] was used for all fluorescence studies.

Repeated immobilization experiments to assess animal viability were performed in Eppendorf tubes. Animals were age-synchronized by allowing them to hatch in M9 solution for a period of 24 hours after embryo isolation. After 24 hours, L1 animals were extracted from M9 and suspended in 25% w/v solution of Pluronic F127. Two different immobilization periods were tested; short cycles consisted of sixty seconds at 15 °C to trigger gel-to-liquid transition and ninety seconds at 21 °C for complete gelation, and long cycles consisted of five minutes at 15 °C and 10 min at 21 °C. Age-synchronized animals were divided into two groups, one exposed to a total of fifty short cycles and the other to five long cycles.

After the temperature cycling, animals were extracted into M9 solution, washed to remove the residual PF127, and placed on standard agar culture plates seeded with OP50 bacterial lawns. The control sample consisted of the same batch of animals, which were kept in M9 solution for the duration of the experiment and were placed on agar plates at the same time, and not exposed to the temperature cycling. After being placed on culture plates, animals were allowed to grow at 21 °C, and the time to reach egg-laying, pharyngeal pumping rate at young adult stage, and the number of progeny in the first 24 hours of egg-laying was compared for all three samples.

To determine the effects on early development, unhatched embryos were suspended in 25% w/v solution of PF127, and PF127 with 60 nM hydrocortisone. Embryos were allowed to hatch, and were maintained in the solution for a period of 24 hours. After 24 hours, animals were processed in the same manner as during repeated immobilization experiments.

Fluorescent images were acquired using a Leica DM4500B microscope with a Hamamatsu C9100-13 EM CCD camera at 5x magnification to monitor the device operation and at 100x magnification for subcellular imaging. Images were acquired using Image-Pro (MediaCybernetics) and processed and pseudo-colored with ImageJ (NIH).

## **2.5 Results**

### **2.5.1 Immobilization Cycle for Imaging**

To demonstrate how our system can be used to track live events in a physiologically active animal, I used our chip-gel hybrid platform to perform repeated imaging cycles. For this purpose, animals were loaded into the individual culture chambers suspended in buffer with food through the loading inlet; the buffer was continuously perfused through the device while animals were not being imaged (Figure 2.9a). During an imaging cycle, flow of the buffer was stopped and was replaced by PF127 solution (Figure 2.9b). Once the solutions were completely exchanged, flow of a warm fluid through the heating

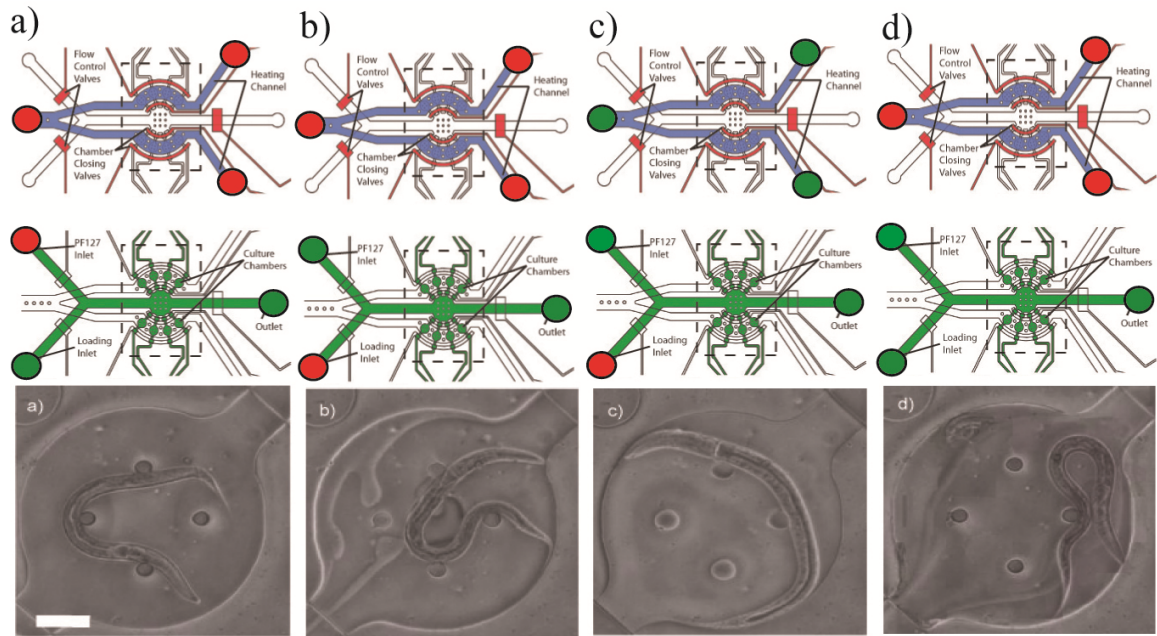


**Figure 2.9** Immobilization cycle. While being cultured on device, animals are suspended in a solution of M9 containing OP50 bacteria (a). During an imaging cycle, the M9 buffer is first replaced with PF127 solution (b). The device is then heated to trigger the sol-gel transition and thus immobilize the worm (c). After the cycle is complete, the device is allowed to cool off and the PF127 solution is flushed out (d). Scale bar represents 60  $\mu\text{m}$ .

channel above the imaging chamber was turned on. This leads to a temperature increase of  $\sim 2^\circ\text{C}$  in the culture chambers and the subsequent gelation of the solution immobilization of animals inside the chamber (Figure 2.9c). The time required for onset of gelation using this method is  $\sim 45\text{-}60$  seconds after initialization of the heating cycle by visual inspection. After the imaging sequence is complete, flow of heating fluid was turned off and the device cooled off to ambient temperature; the cool-off time plus the phase transition of the gel is approximately 30 seconds. Once the temperature of the Pluronic F127 solution is decreased below its gelation temperature, it becomes a liquid and can be easily flushed out of the device and exchanged for buffer solution until the next cycle (Figure 2.9b). The liquid driving pressure in the temperature control chamber is always set equal to the driving pressure in the flow layer to prevent deflection of the culturing chamber membrane and thus flattening of animals. Using this method, I can repeatedly image individual animals without direct manipulation by simply exchanging

the suspension liquid inside the device and raising the temperature within the device by 2 °C. The method is also age independent and doesn't have positional requirements. Unlike tapered-channel geometry for example, which would require animals to enter a channel narrowing from ~50 μm to ~5 μm to sufficiently immobilize animals throughout all developmental stages, animals of all ages can be immobilized anywhere in the chamber at any time using our technique.

### **2.5.2 Image Quality with Pluronic F127 as Immobilization Agent**

Low scattering and low autofluorescence are critical for imaging extremely small features, such as subcellular or synaptic expression patterns. For this purpose, I compared the ability to observe the expression of the green fluorescence protein near the synapses (Figure 2.10). To show that image quality does not degenerate by the presence of Pluronic solution, I imaged animals containing *juIs1*, the integrated *Punc-25::Snb-1:GFP* marker. The *unc-25* promoter is expressed in 26 GABAergic neurons immediately after their generation and is localized in cell bodies, axonal branches, and synaptic regions<sup>31</sup>. The expression from this transgene is dim and photobleaches rapidly, and is thus difficult to observe even using standard methods.

We thus compared quality of images obtained using a standard agar pad and sodium azide as the immobilizing agent with that of images obtained using 25% w/v PF127 gel inside our microfluidic device. As can be seen in Figure 2.10a-d, both methods yielded similar high quality images. It was possible to identify neuronal cell bodies and synapses (some ~1 μm) along the ventral and dorsal nerve cords, even in the presence of autofluorescence from the animal intestine. The PF127 gel itself did not exhibit any noticeable autofluorescence, and I did not observe more scattering from the polymer. Photobleaching was comparable to that of the standard method.



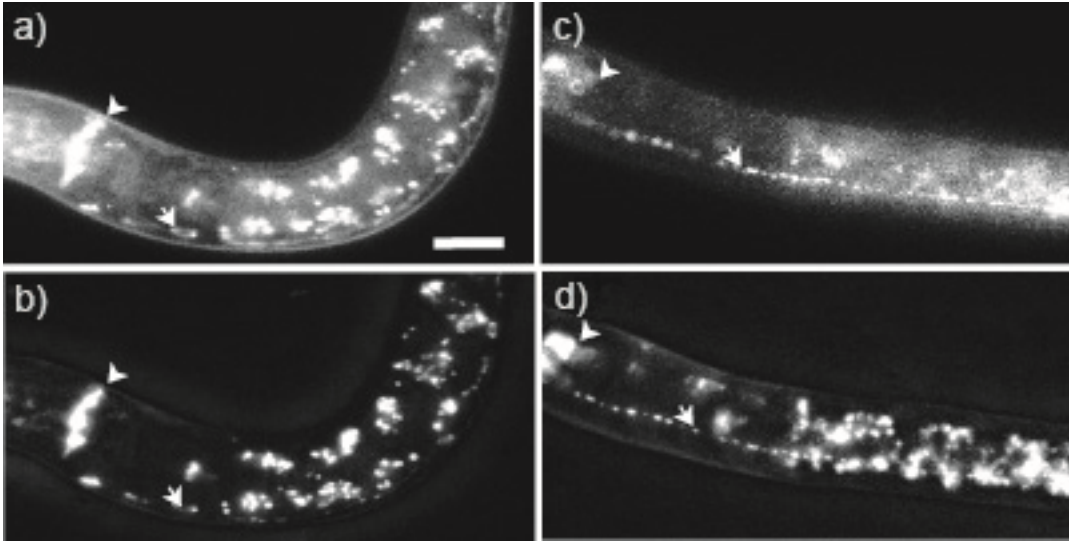


**Figure 2.10** Comparison of image quality between standard procedures (on agarose pads with anaesthetics) (a,b) and using PF127 gel in microfluidic devices (c,d). Imaged animals contain *juIs1*, a very faint and easily photo-bleachable synaptic GFP marker. (a,c) Single image at a focal plane, (b,d) flattened z-stack (40 images, step size 0.5  $\mu\text{m}$ ). Scale bar represents 5  $\mu\text{m}$ . Arrows point to GFP expression localized to synapses, arrowheads point to neuronal expression.

### 2.5.3 Extent of Immobilization with Pluronic F127 Solution

To assess the efficacy of PF127 in immobilizing animals for imaging, I characterized the extent of immobilization after a sol-gel transition has occurred (Figure 2.11). I tested animals in 23% w/v Pluronic F127 solution. Animals were loaded into the device at a temperature below the critical gelation temperature and trapped in individual chambers while suspended in the PF127 solution. After temperature in the device equilibrated to 22  $^{\circ}\text{C}$ , which is above the sol-gel transition temperature of the polymer at this concentration, a sequence of images (100x magnification, 2 seconds apart) was taken. The sequence was then analyzed to determine whether individual synapses shifted during the imaging. False-coloring the images from different time points with different colors and overlaying images (Figure 2.11a-d) illustrates the movement and I can also quantify positions of objects (e.g. synapses) of interest over time. Animals remained immobilized for a period of at least 10 seconds or more; within this time period the shift in position was less than

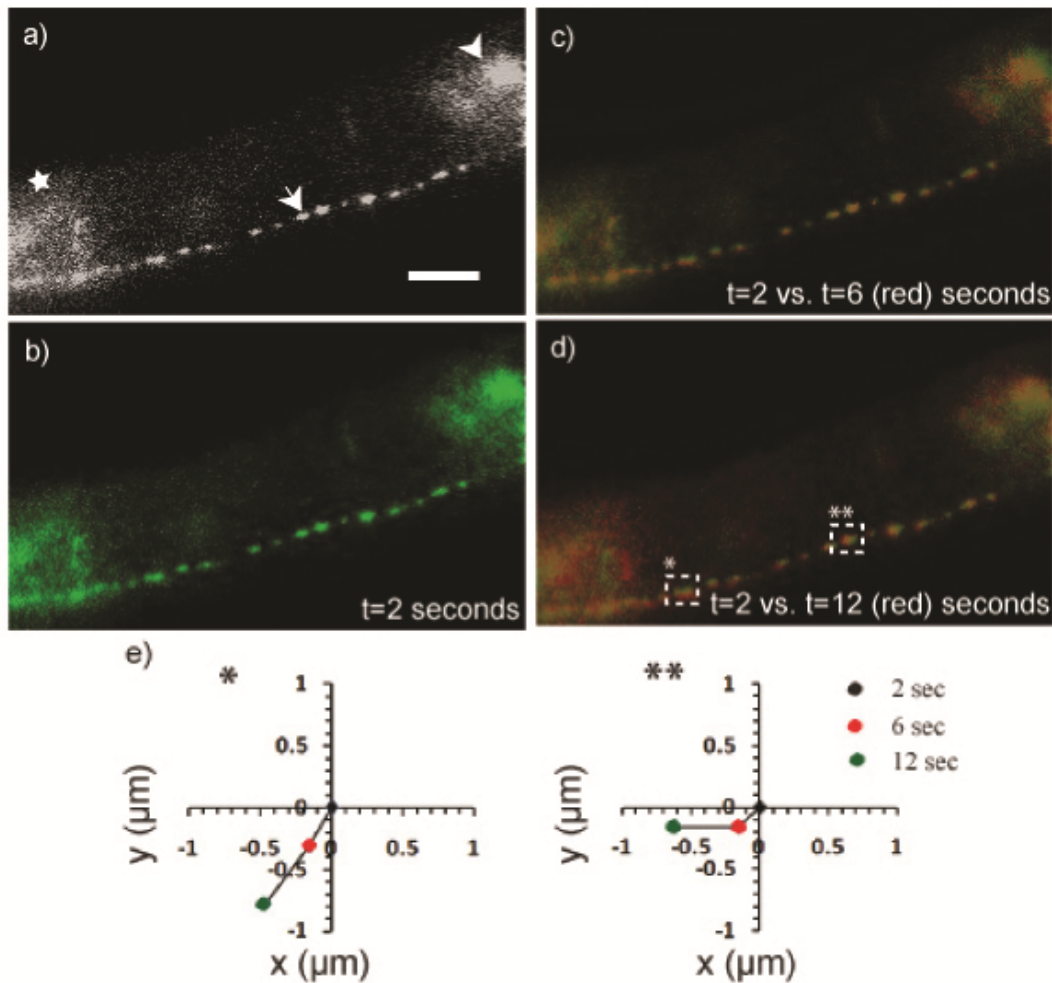


**Figure 2.11** Verifications of the extent of immobilization by the PF127 gel inside the microfluidic device by imaging animals. The single z-plane greyscale images (a) were processed and false-colored green (b). Images at later times from the same z-plane were false colored red. The green colored image was then merged with the red colored images taken at 6 seconds (c) and 12 seconds (d), showing completely overlap and hence proving no movement of the sample. Dashed-line squares in d) show the synapses selected for positional tracking in (e). The x,y position of these synapses was tracked and graphed over time (2, 6, and 12 seconds) to show the extent of movement. Scale bar represents 5  $\mu\text{m}$ . Arrows point to synapses labeled by the presence of *unc-25::GFP*, arrowhead points to neuronal localization, and star denotes intestinal fluorescence

0.5  $\mu\text{m}$ . This is sufficient for obtaining at least two stacks of 40 images with planes in the z-direction separated 0.5-2  $\mu\text{m}$  without any x,y movement. Longer than 10 seconds, some animals struggle against the constraint of the gel, which may lead to a shift in position or rotation of the animal body?

It is critical to point out, that even though the immobilization is ultimately mechanical, no deformation of the animal body occurs. This is because the formation of the gel from the liquid solution is relatively uniform around the animal body. Since the formation of the stiff gel is uniform, there is no directional imbalance in the compressive force, which would lead to deformation of body shape, such as flattening. Thus, animals retain their body shape, and no distortion of features occurs.

#### **2.5.4 Long-Term Culture Inside Microfluidic Device for Early Stages of Development**

The features of our method make it very useful for longitudinally live-imaging animals throughout their developmental stages in combination with long term culture directly on the microfluidic device. I therefore tested the ability of our microfluidic system to maintain culture conditions optimal for normal development of *C. elegans* by culturing animals on the device long term.

We loaded animals into the device and trapped individual worms in the culturing and imaging chambers (Figure 2.12a). Animals are loaded through the loading channel and the loading chamber into the culture/imaging chambers while suspended in buffer with food and supplemental cholesterol at a concentration of 0.1 °g/mL, which is required for the animals to molt. [1] Upon loading and trapping inside the channels, flow was continued to provide a steady supply of nutrients and fresh medium. The flow rate through the device was maintained at 0.02 mL per hour to sustain growth. Animals were maintained in this state for a minimum of 12 hours (Figure 2.12c) during which time they maintained normal locomotory behaviors and a pharyngeal pumping rate similar to that of animals on standard agar culturing plates (data not shown).

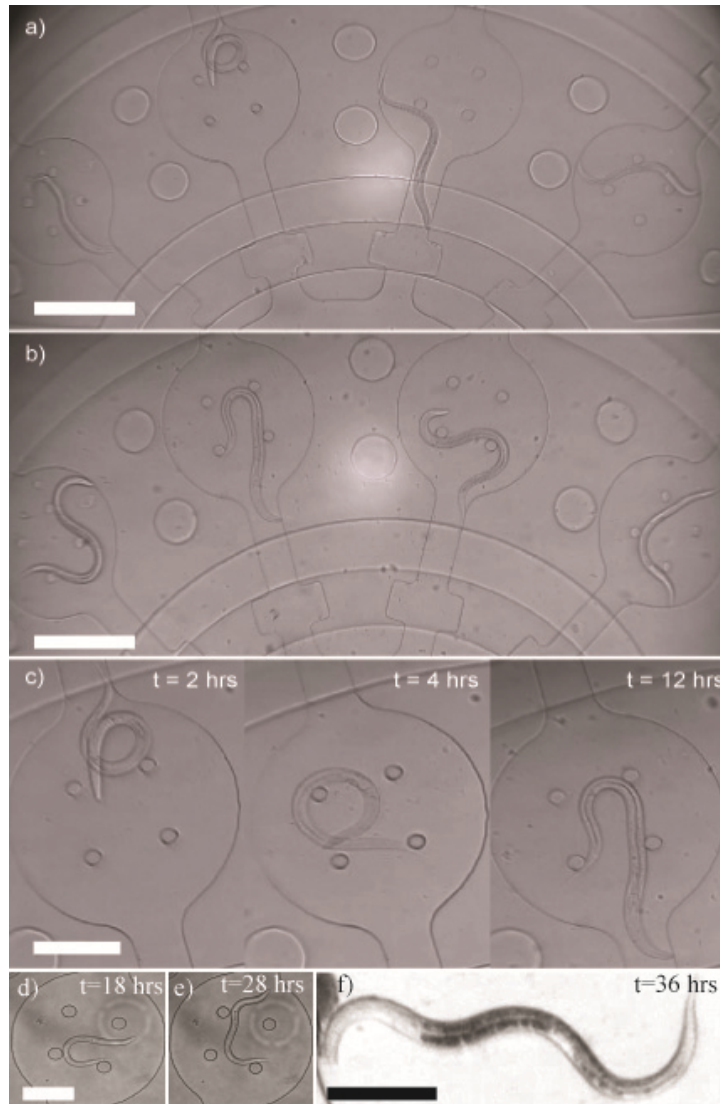


**Figure 2.12** Long-term culture on chip. To culture animals long-term, they were loaded into the device and trapped individually inside culture chambers (a), where they can remain for 12 hours (b) or longer. Animals are provided with bacterial food, allowing them to grow and develop normally (c). Scale bars represent 200  $\mu\text{m}$  in (a) and (b), and 100  $\mu\text{m}$  in (c).

## 2.6 Conclusions

In this chapter, I have demonstrated the ability of our hybrid chip-gel platform to perform long-term culture with individually trackable animals (from L1 and on), and repeated live imaging at high resolution at physiological conditions. I verified that repeated immobilization for various durations and exposure to the immobilizing agent - Pluonic F127 - during early larval stages has no discernable effect on animal development. Our

platform can be easily expanded into larger arrays to facilitate more rapid acquisition of data; more importantly, in contrast to currently available methods, this technology is advantageous in gaining new insights on developmental and dynamic processes such as vesicle transport, synaptic re-arrangement, and growth cone development.

## CHAPTER 3      MICROFLUIDIC TRAP ARRAY FOR CHEMICAL AND THERMAL MANIPULATION OF *C. ELEGANS* EMBRYOS

### 3.1      Introduction

This chapter discusses the work on a system for chemically and thermally manipulating *C. elegans* embryos in a simple but highly controlled manner. The embryo stage and the various developmental processes occurring during this time have significant effects on the survivability, development, and functionality of the animals during the following larval and adult stages. Various studies of the embryonic developmental stage have identified the major genetic players of this process. [102-111]. How the process itself can be altered by exposure to alcohol or drug agents such as cancer treatment drugs has also been a point of interest. [112-115] Understanding normal development and perturbations to this process from external factors such drugs and various types of stress is highly beneficial to understanding similar processes in humans. This is largely possible due to the significant percentage of homologous genes and conserved biological pathways been *C. elegans* and humans.

Such studies require i) physically handling large numbers of embryos in a uniform way without physically or otherwise damaging them in the process, ii) precise temporal and chemical stimulus control for purposes of accurate timing relative to developmental events and frequency control, and iii) frequently the ability to track animals after hatching for observing their development and functionality. This combination of requirements can be difficult to implement practically and in a high throughput fashion. Several microfluidic designs have been successful at efficient manipulation and studying of embryos in the zebra fish and *Drosophila melanogaster* model organisms. [116-122] No such system however exists for working with *C. elegans* embryos.

Here I present a system designed to efficiently trap individual embryos, to thermally or chemically stimulate them with temporal control, and to study the effect of the stimulation on the animals after hatching. It is based on a large and easily scalable array of embryo traps designed to each trap one embryo. Each trap is connected to an individual culture chamber in which these embryos can hatch and develop. Rapid fluid exchange across the array allows for precise timing for chemical exposure. Additionally, integrated electrodes used for resistive heating serve to control the temperature for embryo stimulation and a broad range of additional applications, such as heat shock and immobilization with Pluronic F127 for imaging. As such, the device may be used not only to study embryonic development, but any developmental process of interest and the effects of external stimuli on these processes. This work was completed in collaboration with two undergraduate students, Iva Franjkic and Michael Ryan Warner.

### **3.2 General System Overview**

The basic operating principle of this system is depicted in Figure 3.1a. The system operates in three stages. The first stage is initial loading; a suspension of *C. elegans* embryos in nematode buffer is loaded into the device for trapping. Trapping occurs passively without any direct researcher involvement via flow dynamics and feature design. From the traps, embryos are moved to culture chambers by pressurizing the device and opening a path between the trap and its corresponding chamber. The second stage is the exposure stage; the embryos are exposed to chemical or thermal stimuli. Temperature on device is increased by using individually addressable electrodes as resistive heaters. The third stage is the culture stage; OP50 *E. coli* suspended in nematode buffer are delivered to the device and flow through the culture chambers containing embryos and hatched *C. elegans*. Animals can be exposed to external stimuli during this stage as well. Additionally, the buffer can be temporarily replaced with Pluronic F127 solution, which can be heated to immobilize animals for imaging.

The whole system consists of the microfluidic chip aligned on a slide with patterned electrodes and the off-chips components (Figure 3.1b). These include i) syringe pump driven liquid delivery system ii) external valves used for selecting the solution to be delivered to the device, iii) a compound microscope with a CCD camera and x-y-z stage, and a iv) digital input output controller to actuate individual electrodes.

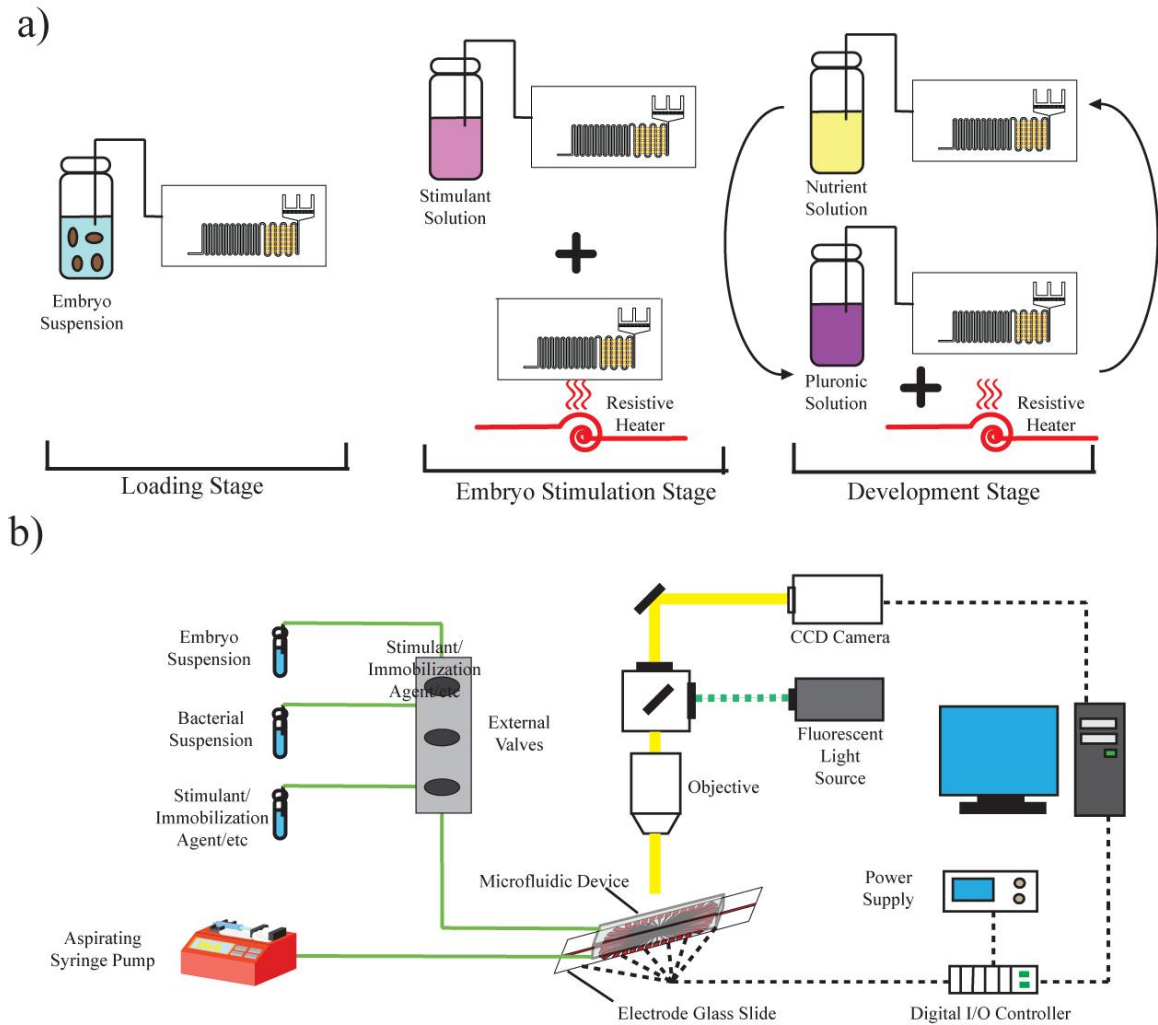


**Figure 3.1** Schematic of the system operation and components. a) Three modes of operation of the device are loading, embryo stimulation, and the development/culture stage. b) Comprehensive system schematic.



### 3.3 System Design

#### 3.3.1 Microfluidic Component

The roles of the microfluidic device is to efficiently handle trapping of embryos, facilitate highly temporally controlled chemical stimulation, and if necessary provide the environment needed for proper *C. elegans* development in a high-throughput manner. Typically, high throughput in microfluidics for *C. elegans* applications has been achieved by processing large numbers of animals serially and rapidly. [70-72, 74-78] Most commonly this was done for automated sorting or microsurgery. [72, 74, 76-78] This approach however is not suitable for embryo handling and possible stimulation, such as exposure to chemicals or thermal stress. Serial processing of embryos would introduce significant differences between the ages of embryos at the time of stimulation, especially in case where stimulation lasts for several minutes or hours. Moreover, observing the subsequent embryonic and larval development on an individual animal basis would be impossible. This for example is highly desirable for studying distribution of P granules after hatching [123-126], for studying distribution of heat shock proteins in adulthood after embryonic stimulation [127-129] or for studying developmental effects after drug treatment in the embryonic stage [112, 130, 131]. A more suitable approach therefore is parallel simultaneous processing of a large number of embryos. This places the additional requirement of easy scalability on the system to be used.

In Chapter 2, I have introduced a system for isolating individual L1 larvae to observe their development with repeated high-magnification imaging. Although the chamber isolation principle from that system remains applicable, scalability is an issue due to the active control of animal trapping. In fact, scalability is problematic in most actively controlled microfluidic systems. In the case of the system from Chapter 2, four chambers are controlled by a joint inlet and outlet valve. Achieving loading of one animal per chamber requires monitoring from the researcher and actuation of the inlet and outlet

valves. Since the loading process is random, this can take several minutes. With an increasing number of chambers controlled by a joint inlet and outlet valve, the probability of single loading across all chambers decreases drastically since probabilities are multiplied as  $P_{Overall}=P_1 \times P_2 \times P_3 \times \dots \times P_N$ . Each additional chamber thus decreases the overall probability of single loading for all chambers controlled by a single valve. This in turn leads to an ever increasing loading time as the chamber numbers grow. For this reason, the number of chambers that can be loaded is limited. If we assume that four chambers are per valve are ideal, then the number of valve control connections to the device (inlet and outlet) scales by  $n/2$ , where  $n$  is the number of chambers. For an array of 48 chambers, only the valve connections would total 24. From a practical and design point of view, this is not acceptable.

For this reason, I have decided to pursue a design that is passive in nature without direct user action. In the case of a design for high throughput manipulation of embryos, this means that once embryos are injected into the device they are trapped by the design of the trapping features and the flow pattern on the device. This eliminates the need for valves to control loading, and the only connections to the device necessary become the fluid flow inlets and outlets. Thus, regardless of the size of the trap array, the number of connections remains the same and the only scalability restriction is becomes the footprint of the device.

Figure 3.2a shows one such initial design. Traps in the shape of an oval protrude from a main delivery channel. At the outlet of each trap is a narrow opening, which serves to hold embryos in the trap while permitting flow past it into the connecting channel. After traps are loaded, the device is pressurized to open the restriction and allow embryos to flow down the channel to another restriction at the inlet of a culture chamber. This restriction serves to stop all embryos at the chamber inlet, so that lagging embryos can catch up. By pressuring the device again, embryos can be loaded into culture chambers. The loading efficiency of these traps was ~60% (single embryo per trap). However, over

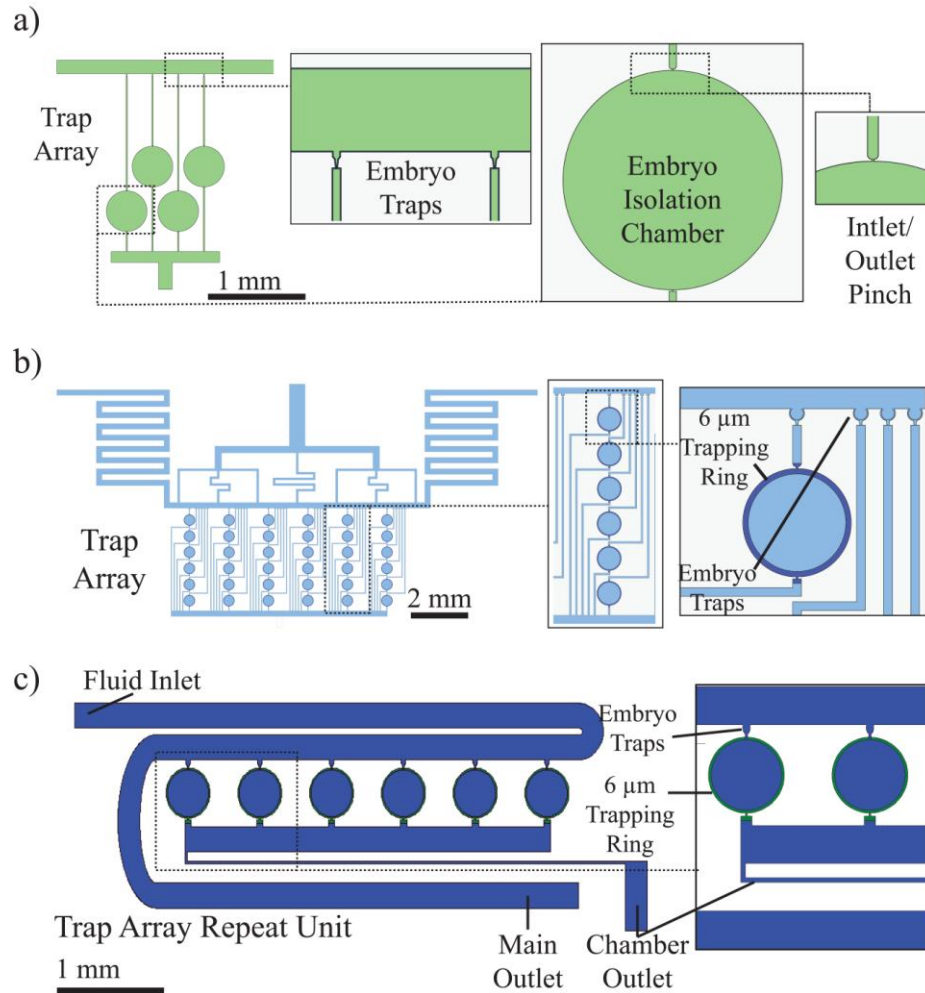


**Figure 3.2** Early microfluidic device designs. a) Embryo traps connected to individual culture chambers requiring embryo transport. b) Embryo traps design to keep embryos until hatching, when animals would be transported to a culture chamber with passive trapping. c) Embryo traps directly connected to culture chambers with passive trapping.

80% of the embryos would remain stuck in the channels connecting the traps to their chambers. I concluded that though trapping can be efficient, further manipulation can be difficult. In the next design (Figure 3.2b), traps were designed to hold embryos immobilized until they hatched. At this point, animals would be flushed through a connecting channel towards a culture chamber as in the previous design. This time, the 65 μm tall chamber was surrounded by a 6-μm ring to stop the animals from escaping the chamber. Once inside the chamber, over 99% of animals remained. However, less than 10% of the embryos loaded actually hatched and had their progeny moved in towards the

chamber. This may have been due to damage to embryos from constant high flow rates, as well as washing of hatched *C. elegans* along the main channel. The next design principle combined the trap design, but each trap was connected directly to a culture chamber with a restriction (Figure 3.2c). This chamber was also surrounded by a low height ring to prevent hatched animals from escaping. This facilitated efficient transport from embryo traps to chambers by simply pressuring the device to open the restriction, while retaining the ability to keep animals trapped passively. This principle was applied for the finalized embryo trap array design.

### **3.3.2 Temperature Control on Device**

The ability to increase temperature on device is critical for a broad range of applications such as inducing heat shock, increasing metabolic rate, or even immobilization for imaging. Robust cooling and heating methods for *C. elegans* microfluidic applications based on delivering hot or cold liquid have been developed in our laboratory. [74, 89] These have been shown to accurately control temperature in a target location such as a trapping channel or an array of culture chambers. The implementation of this technology is however difficult when a large number of specific locations needs to be controlled on an individual basis, such as a very large array of chambers and traps. This would require a complex network of on chip channels and control valves and significantly limit usefulness. An alternative approach for locally increasing temperature is Joule heating. Electrodes integrated into microfluidic devices can be used as highly localized heaters. A multitude of electrode patterning techniques and designs have been used in the field for applications such as dielectrophoretic separation, flow focusing, PCR, and as components of sensors. [132-140]. Traditionally, these electrodes are patterned onto a glass or silicon substrate via a combination of standard metal deposition and etching techniques. However, without the ability to re-use each device multiple times, large scale

experimentation would make device fabrication very resource and time intensive and in some cases require the use of a cleanroom.

Siegel *et al.* used a novel molding method for creating metallic components inside a microfluidic PDMS chip. [141] The components were created by injecting molten solder into channels of a PDMS device heated to 180 °C and then allowing the solder to cool. I have adapted this technology with a more easily implemented fabrication method for fabricating large numbers of devices reliably and cheap.

**Table 3.1** List of available low-melting/fusible alloys available from RotoMetals (rotometals.com)

Type/ Approx Temp in F	Antimony	Bismuth	Cadmium	Lead	Tin	Indium
Roto117F	0%	44.7%	5.3%	22.6%	8.3%	19.1%
Roto136F	0%	49%	0%	18%	12%	21%
Roto140F	0%	47.5%	9.5%	25.4%	12.6%	5%
Roto144F	0%	32.5%	0%	0%	16.5%	51%
Roto147F	0%	48%	9.6%	25.6%	12.8%	4%
Roto158F	0%	50%	10%	26.7%	13.3%	0%
Roto158-190F	0%	42.5%	8.5%	37.7%	11.3%	0%
Roto203F	0%	52.5%	0%	32%	15.5%	0%
Roto212F	0%	39.4%	0%	29.8%	30.8%	0%
Roto217-440F	9%	48%	0%	28.5%	14.5%	0%
Roto255F	0%	55.5%	0%	44.5%	0%	0%
Roto281F	0%	58%	0%	0%	42%	0%
Roto281-338F	0%	40%	0%	0%	60%	0%

Instead of using molten solder, I have selected a low melting point alloy from a range of low-melting/fusible alloys. There are primarily composed from Bismuth, Indium, Tin, and other metals, as shown in Table 3.1. Alloy Roto144F does not contain any Lead and melts at 62 °C, making it an ideal candidate. The melted alloy was simply injected into a microfluidic channel with a design, which would lead to high electrical resistance (Figure 3.3a). The resulting electrodes (Figure 3.3b) could then be connected to an outside current source via metal pins inserted into holes filled with the alloy. To keep all the device, alloy, and injection syringe at 70 °C during the molding, the injection was performed inside a hot bath (Figure 3.3b). The high cohesiveness of liquid metals in an

aqueous solution allowed for formation of continuous alloy wires inside the device. When current was subsequently applied to a sample design, a steady 2 °C temperature change could be achieved, which melted thermochromic crystals in a liquid solution.

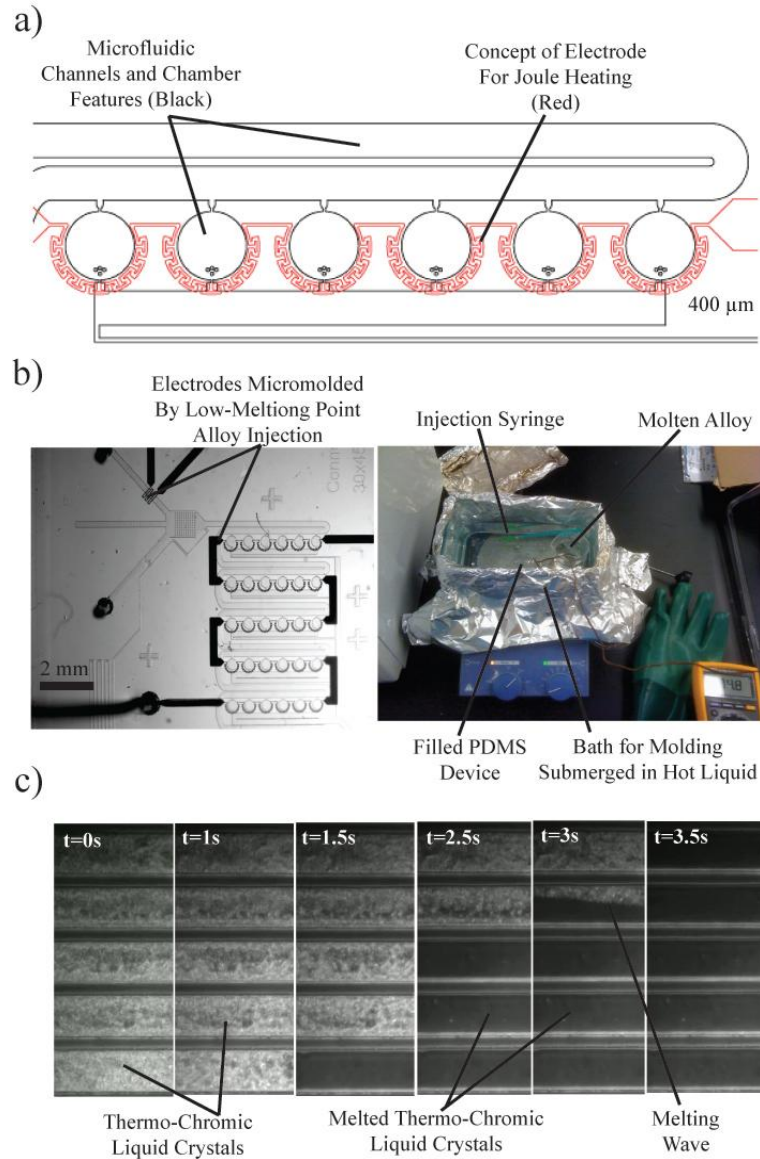


**Figure 3.3** Concept of electrodes molded in PDMS. a) Schematic of channel for making electrodes from molten alloys. b) Alloy injected into microfluidic device inside hot bath formed alloy wires inside the PDMS device. c) Alloy wire was used to rapidly heat a small area filled with thermochromic crystals by 2 °C.

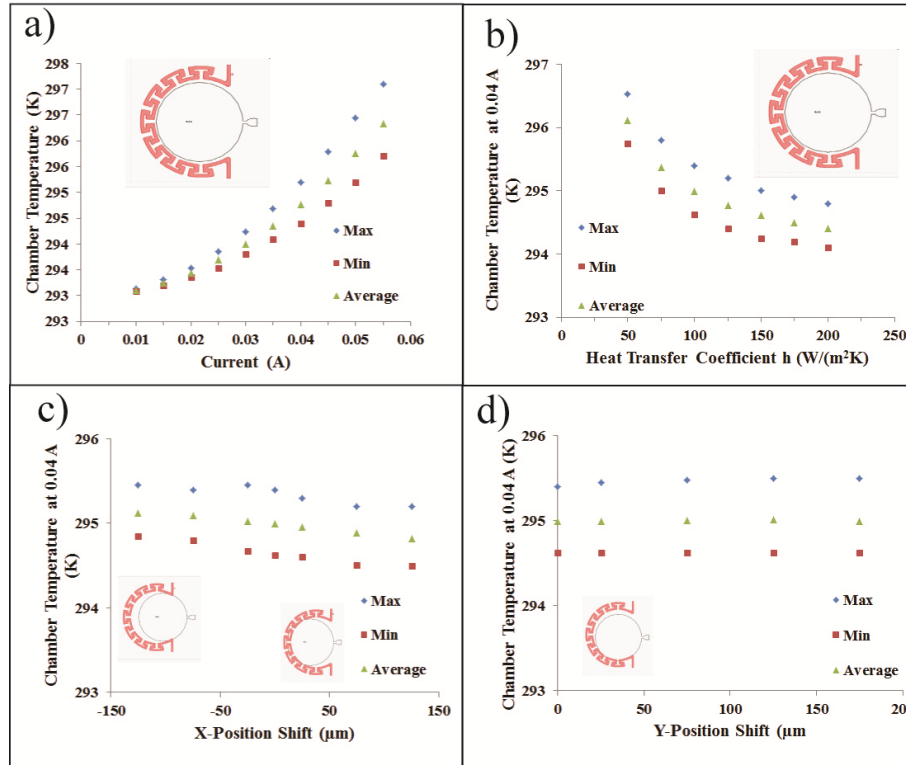


**Figure 3.4** COMSOL Simulation results. a) Current vs. Temperature relationship. b) Effect of changing heat transfer coefficient on chamber temperature. c-d) Effect of x and y positional shift on chamber temperature.

Since the future electrode wires have to cross fluid channels, they have to be on a different PDMS layer, making the design a multi-layer PDMS device, which requires alignment of the various layers. I used a COMSOL simulation to test the robustness of the assembled device to misalignment of the two layers and thus the shift between the position of a culture chamber and the electrode around it and to a change in the heat transfer coefficient of the device. The model consisted of a single quadrant of the microfluidic device with accurate dimensions. The boundary conditions on all external surfaces were set to heat transfer, with the coefficient of heat transfer values corresponding to forced air flow. The quadrant external surfaces corresponding to faces sectioned from PDMS were set at symmetry boundary conditions. The general equation solved was  $\nabla \cdot (\cdot k \nabla T) = Q$ . The heat source for in the domain corresponding to an

electrode was calculated via  $Q=I^2 \cdot R$ . The results of the simulation are shown in Figure 3.4. The figure shows results of temperature vs. current simulation in a perfectly aligned chamber, for various heat transfer coefficients, and for various degrees of misalignment in the x and y directions. As expected, while positional shift is negligible, changes in the heat transfer coefficient can cause significant temperature changes and need to be accounted for in any experiment.

The molten alloy injection approach is very simple and easily implemented. However, one difficulty lies in the designing electrodes for addressing individual chambers. Because these electrodes are formed by microfluidic channels, forming a large array of electrodes requires a large area and an inlet and outlet for each electrode. This requirement can be reduced, but only at the cost of heating multiple chambers at once. Because of this, the technology isn't fully suitable for individual targeting, but for whole device or multi-chamber heating. Therefore, a different electrode fabrication method has been chosen for the final design. Nevertheless, the electrode heater concept is highly applicable to localized heating and is robust enough to function even with fabrication defects.

### **3.4 Final Design**

The final design is a microfluidic array of embryo traps, each of which is connected to a single culture chamber as shown in Figure 3.5b. Fluids are delivered to the array via a serpentine delivery channel. Each embryo trap connects to this channel and serves as a trap for embryos as well as the inlet into each chamber. Trapping is passive; flow through the serpentine channels is partially diverted through the embryo traps and delivers embryos into the proper position. The outlet of each chamber is connected to the serpentine delivery channel as well. This design feature increases right-to-left cross flow and increases the rate of fluid replacement in the array, which is of benefit to temporal control of chemical stimulation.



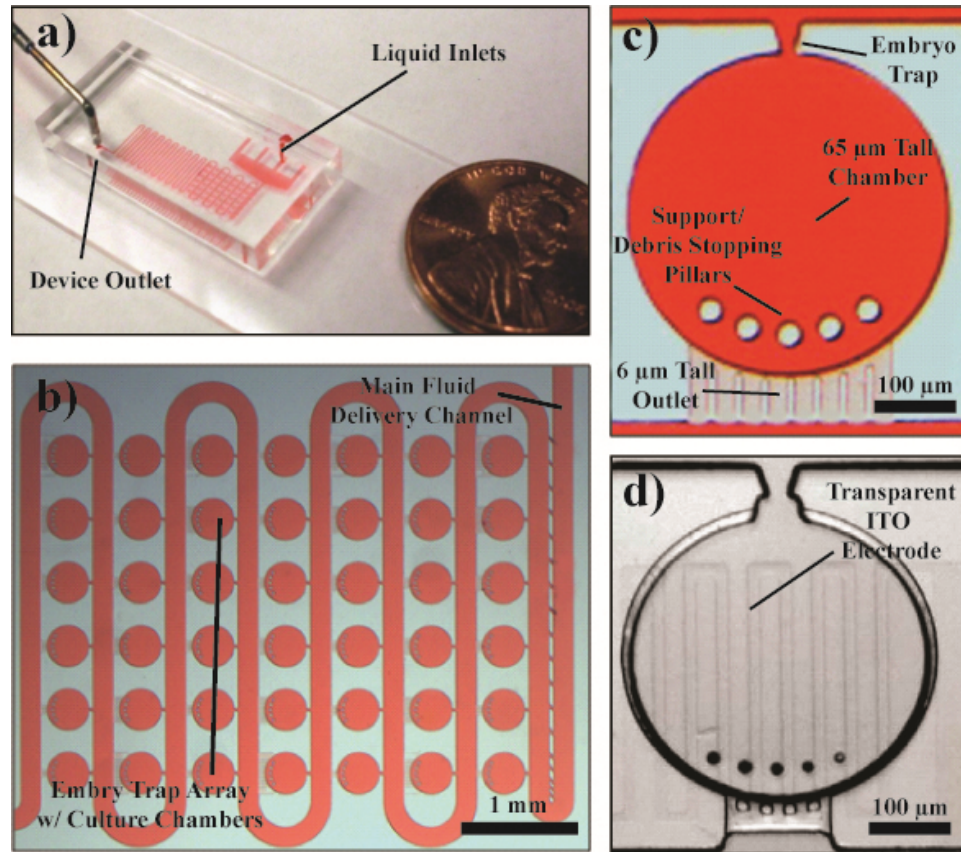


**Figure 3.5** Final design. a) Scale comparison of microfluidic device to a penny. b) Embryo trap and culture chamber array. c) Embryo trap and chamber concept. d) Microfluidic device aligned on top of a transparent microelectrode resistive heater.

Embryo traps are separated from their corresponding chambers by a narrow restriction (Figure 3.5c). This restriction prevents embryos from entering the chambers prematurely and thus prevents double loading. It also helps to prevent hatched animals from escaping through the inlet. The chamber is 65  $\mu\text{m}$  tall to accommodate development through adulthood. Pillars at the outlet of the chamber serve as structural support and a debris filter. The outlet channels are only 6  $\mu\text{m}$  tall and passively prevent animals from escaping.

This microfluidic array is aligned on an array of transparent electrodes as shown in Figure 3.5d. Each electrode is individually connected to a computer controlled digital I/O controller and can be selectively turned on. These electrodes are fabricated from Indium

Tin Oxide (ITO) as serve as individually addressable resistive heaters for a broad range of applications.

### 3.4.1 Passive Trapping Principles

#### 3.4.1.1 Embryo Trap Concept

The embryo trap is an oval shaped protrusion out from the liquid delivery channel with two height layers as shown in Figure 3.6. The dimensions of the oval are specific to the average size of a *C. elegans* embryo. Embryos flowing through the liquid delivery channel are pushed by flow into the trap. Once an embryo trap is filled, flow is re-directed to the remaining traps. This helps to hold the embryo in position while increasing the rate of trapping for the remaining trap positions.

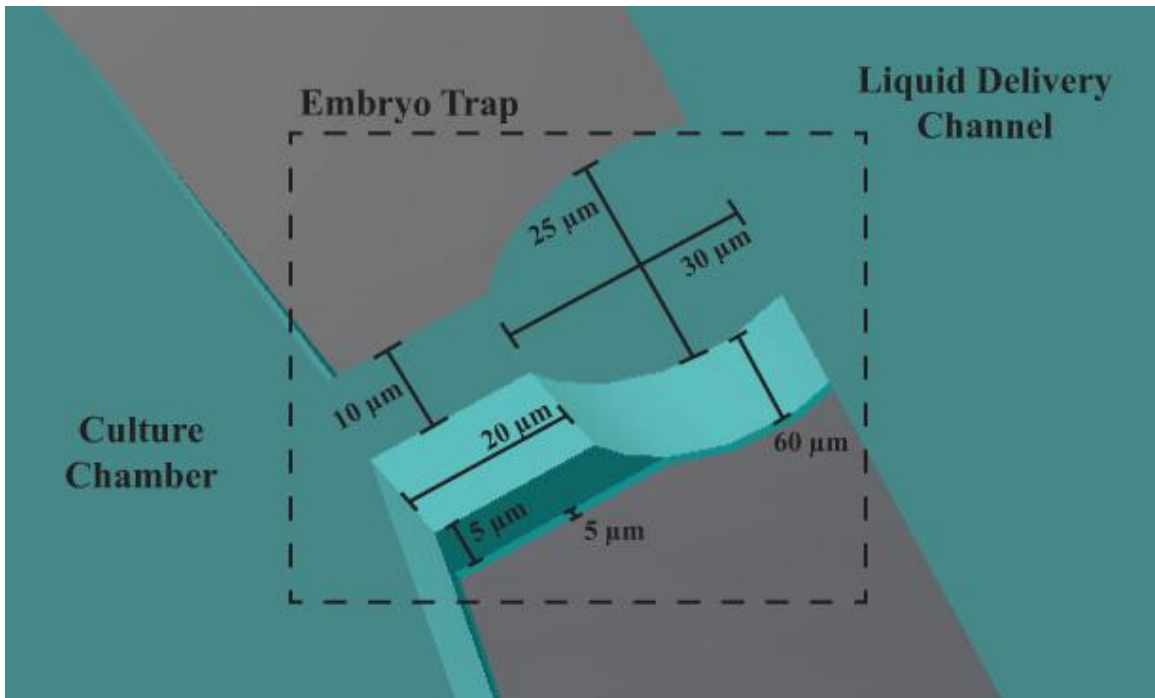


**Figure 3.6** Embryo trap features and dimensions.

At the outlet of each embryo trap is a 10 μm wide and 20 μm long channel connecting the trap to its culture chamber in the top layer. The bottom layer is 5 μm wider on each side, but also only 5 μm tall. The features of the top layer are 60 μm tall. The narrow channel

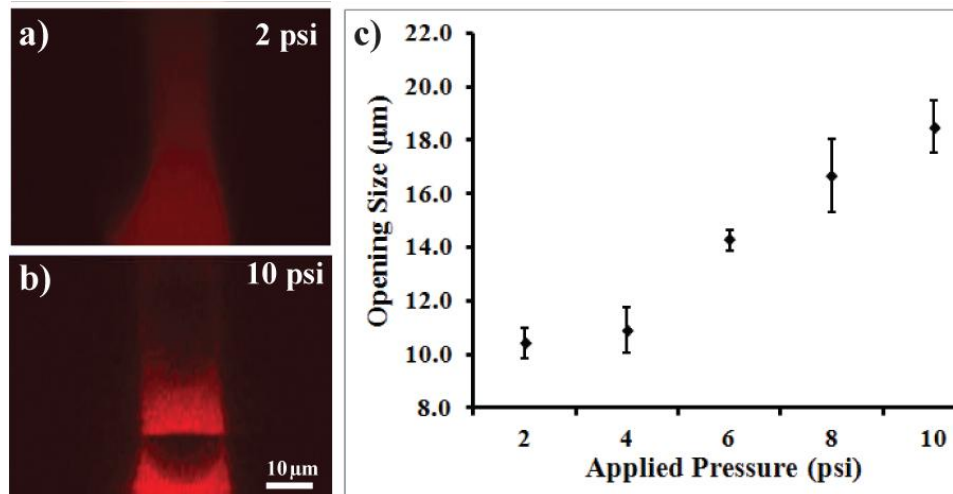


**Figure 3.7** Opening of the narrow channel of the embryo trap. a) Confocal image cross-section in the x-z plane across the narrow channel at 2psi. b) Confocal image cross-section in the x-z plane across the narrow channel at 10psi. c) Narrow channel width dependence on applied pressure.

serves two functions. First, it helps to hold the embryo in its trap until all traps are filled. Once the array is completely loaded, the device is pressurized to widen the restriction, as shown in Figure 3.7. This widening is further facilitated by the increased width of the bottom layer, which allows the restriction to flare outwards upon pressurization. The widening allows the embryo to pass into the culture chamber and remain trapped there until hatching, as shown in Figure 3.8. Once animals hatch, the second function of the narrow channel is to help prevent the animals from escaping through the embryo trap. The narrow channel geometry is difficult for animals to penetrate. It also focuses flow into a smaller cross-sectional area, which drastically increases the velocity of flow.

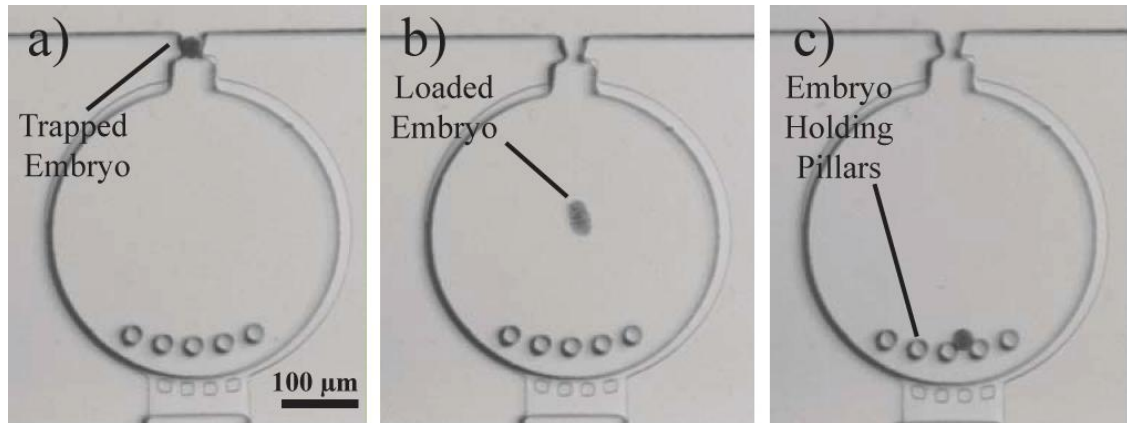


**Figure 3.8** Time lapse of embryo trapping. a) Flow dynamics position and hold embryo in a trap. b) Device pressurization allows the embryo to pass through a widened narrow channel restriction. c) Embryo is positioned inside a culture chamber.

### 3.4.1.2 Passive Holding of Trapped Embryos and Hatched Animals in the Culture Chamber

The principle of passive trapping of hatched animals inside the culture chamber relies solely on geometry and flow. The chamber, just like the trap, has two different height layers (Figure 3.9a). The top layer is 60  $\mu\text{m}$  tall to allow animals to develop up to the adult developmental stage. The diameter of the chamber can be scaled to accommodate any size animal. The two designs I have found most useful are an array with 400  $\mu\text{m}$  diameter for observing the embryo through early L4 larval stages and an array with 1 mm diameter for observing development through adulthood. The trade-off between choosing a different chamber size is the number of animals, which can be observed simultaneously within one field of view at high enough magnification to measure rate of growth. At  $D=400\ \mu\text{m}$ , the number is 36, while at  $D=1\ \text{mm}$  the number is 16 at 2x magnification.

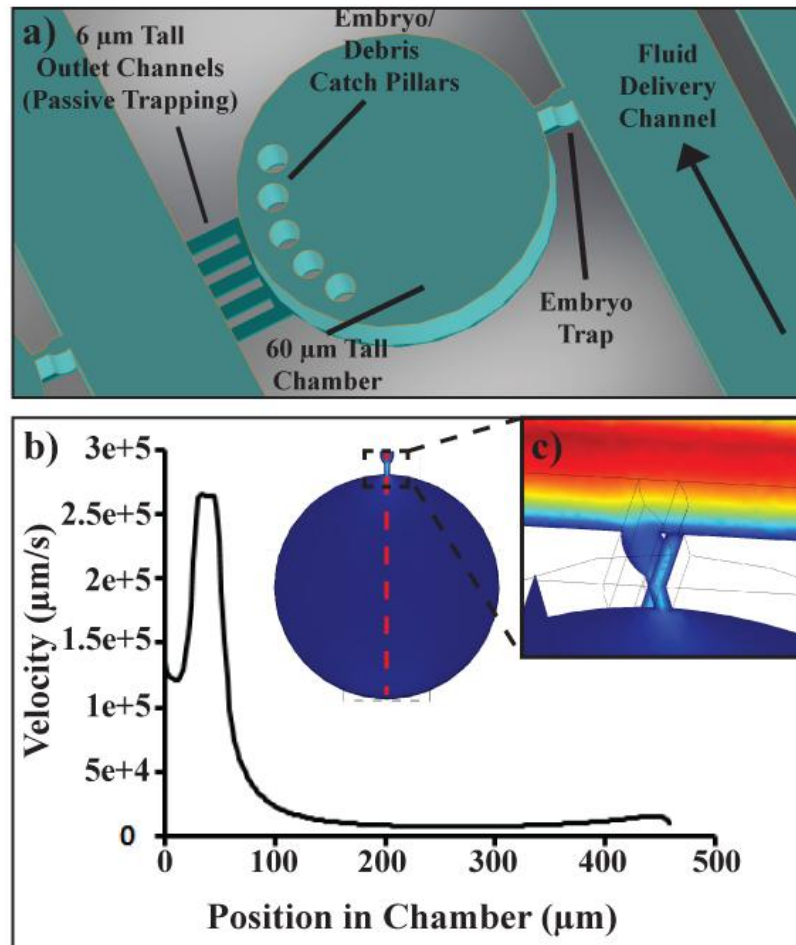


**Figure 3.9** Microfluidic chamber design for passive holding of animals. a) 3D rendering of the chamber features and dimensions. b) Flow velocity across a chamber. The high velocity in the inlet helps prevent animals from escaping. In the bulk of the chamber the flow velocity significantly decreases, leading to lower shear rates and higher bacterial residence time. c) Close-up view of the flow velocity profile through an embryo trap.

The bottom layer of the chamber is also 5 µm tall, as was the case with the trap. The main features of this layer are the outlet channels connecting the chamber to the fluid delivery channel. The low height of the layer makes it very difficult for even freshly hatched larvae to escape, even though their diameter is only ~7 µm. To escape, the animals would have to crawl through the channel with their body compressed. Immediately after hatching, they are not capable of doing this. Additionally, there is very little drag from flow to help them move into the channels. This is because the flow in the chamber is expanded, and so the velocity is much lower as compared to the inlet for example. (Figure 3.9b-c).

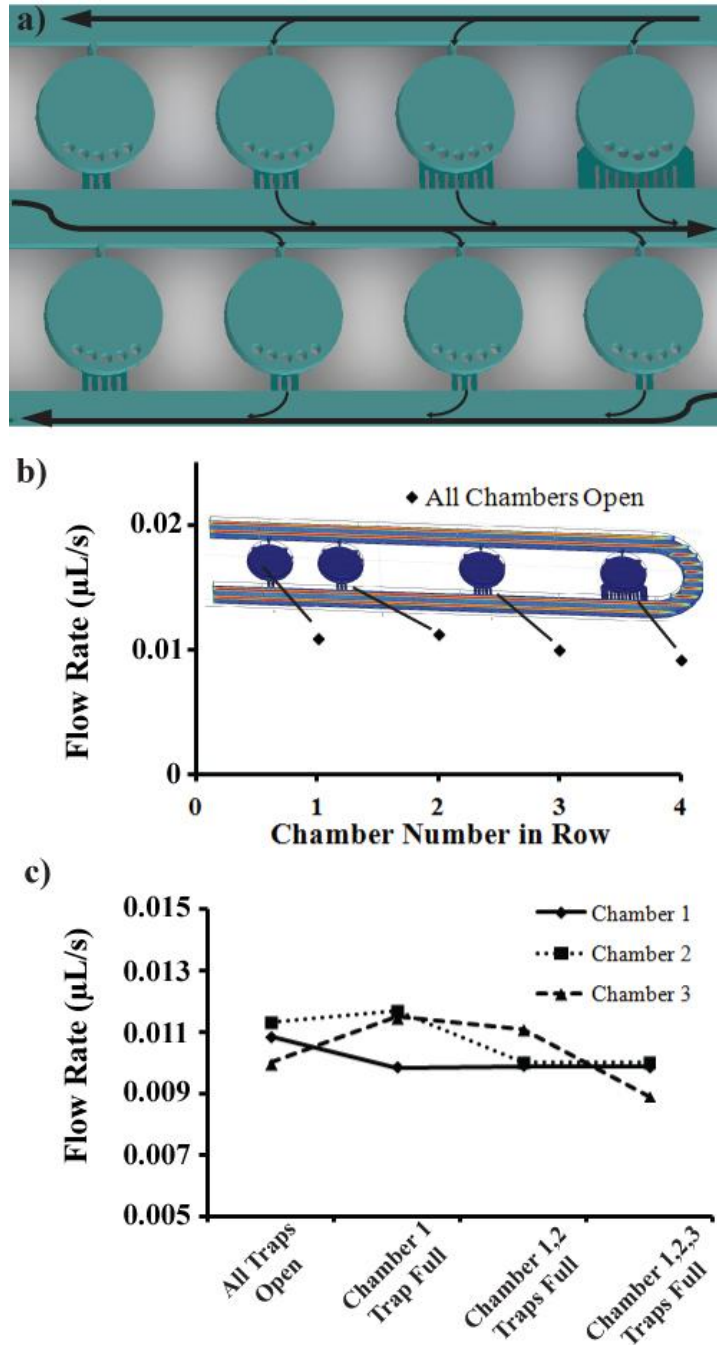


**Figure 3.10** Flow routing principles in trap array. a) Schematic of the direction of flows through the device. Flow across chambers connecting to the serpentine delivery channel leads to cross flow across the device. b) Results of COMSOL simulation of flow rates across chambers with different outlet designs to even out the pressure drop across a row of chambers. The flow rates across all the positions are very even as is desired. c) Effect of an embryo being trapped on flow rate to chambers. Filling the trap of the first chamber decreased flow to the chamber and increased the flow rate of the second and third chambers. This effect is repeated as embryos gradually fill traps.



A COMSOL simulation was performed to characterize the flow velocities across a chamber and across the array (Figure 3.10). The simulation was modeled with a single repeating unit (row) of the array with accurate dimensions as an incompressible Navier-Stokes flow. The general equation solved was  $\rho(v \cdot \nabla)v = \nabla \cdot \{PI + n(\nabla v + (\nabla u)^T)\} + F$ ,  $\nabla \cdot v = 0$ . The inlet and outlet boundary conditions were set as normal flow-rate of 2 mL/hr and the fluid modeled was water at room temperature. The other materials used were PDMS and glass. The mesh was set to extra fine with the maximum element size condition changed to  $2 \cdot 10^{-6}$ ; the total number of elements used in the simulation was  $5.34 \cdot 10^5$ . Values of flow rates and velocities were determined via boundary integration of the velocity field and via cross domain measurement of velocity respectively.

#### 3.4.1.3 Design of Flow Through the Array

The flow across the whole microfluidic array has been designed for rapid fluid exchange across the whole array, for even flow rate to each chamber, and for rapid loading. The rapid exchange across the array is aided by a cross flow, which exists because the outlets from each chamber connect back to the liquid delivery channel. This creates a flow direction which is perpendicular to the serpentine fluid delivery channel and aids in rapid exchange (Figure 3.10a). Even flow rates through each chamber are achieved by pressure balancing flow across each chamber via different outlet geometries, as shown in Figure 3.10b. The results of the COMSOL simulation corresponding to the actual array design show that flow-rates remain within 10% across a repeating unit of the array, as determined by comparing flow-rates at the inlet of each chamber. Rapid loading is achieved via diversion of flow from filled traps to empty traps (Figure 3.10c). Once a trap is filled by an embryo, the flow through this trap is blocked. This increases the flow to the remaining traps, increasing the likelihood of embryo trapping. In the COMSOL simulation, loading of an embryo was simulated by creating elliptical void space in the embryo trap itself.

## 3.4.2 Temperature Control Mechanism

### 3.4.2.1 Temperature Control Via Resistive Heating

An array of transparent ITO electrodes patterned onto a glass slide serves as the temperature control component (Figure 3.11). The array layout can be altered to accommodate different chamber sizes, but the electrode design remains uniform. The fact that ITO is transparent (>85% light is transmitted through a 160 nm ITO layer) enables positioning of electrodes directly under a culture chamber. Each microfluidic culture chamber is thus actuated by a single electrode for highly localized and individual temperature actuation based on the applied current. The microfluidic device has to be aligned and assembled on top of a patterned glass slide or cover slip (Figure 3.11b). However, we have developed an assembly method, which makes the patterned electrodes re-usable.

### 3.4.2.2 Uniformity of Fabricated Electrodes is Critical for Temperature Control

Electrodes were patterned [142-144] on purchased slides with a pre-deposited layer of ITO. These slides come with a pre-specified thickness of 120 – 160 nm, and possible roughness of 20nm per 5mm length peak to peak (per manufacturer specifications). The thickness of the ITO layer has a direct effect on the resistance distribution of the electrode array. This array is designed to provide even resistance across each electrode path for the purpose of simple operation; if the resistance is even, then the same current will yield the same temperature increase over any electrode. If the surface roughness is significant enough, the array will have widely varying resistances. I have encountered this difficulty, as can be seen in Figure 3.12, where the resistance from the left to the right side of the device varies greatly, and thus the current for each electrode would have to be individually calibrated.



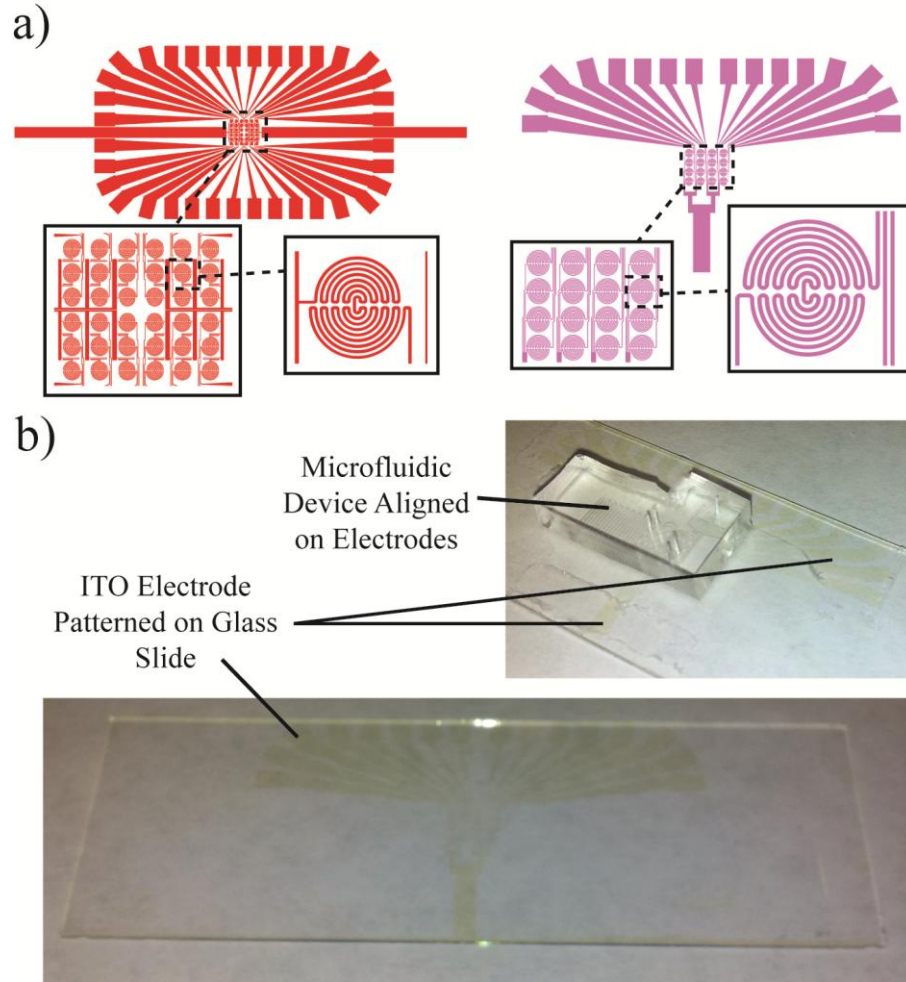
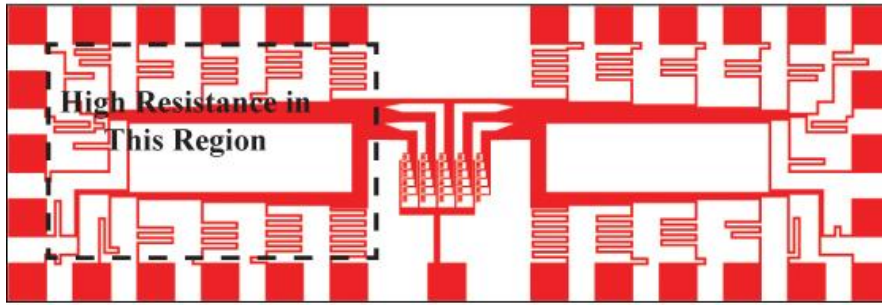


**Figure 3.11** Transparent electrode heaters. a) Different layouts are used to accommodate different chamber sizes, but the electrode itself remains the same. b) Contrast enhanced image of a glass slide patterned with the conductive and transparent ITO, and of a slide with a microfluidic device positioned and aligned on top of it.

To be able to work with purchased slides, a specific electrode array design is required. The majority of the resistance across the complete path of each electrode has to be focused into the electrode itself. I have proposed and tested several designs, where over 97% of the resistance is in the heater electrode itself. This value was calculated during the design process. This allows focusing the resistance into a very small area with presumably smaller variations in layer thickness. Variability is still present, but it becomes negligible for the purposes of heating a microfluidic chip, as shown in Figure 3.13.

a)



b)

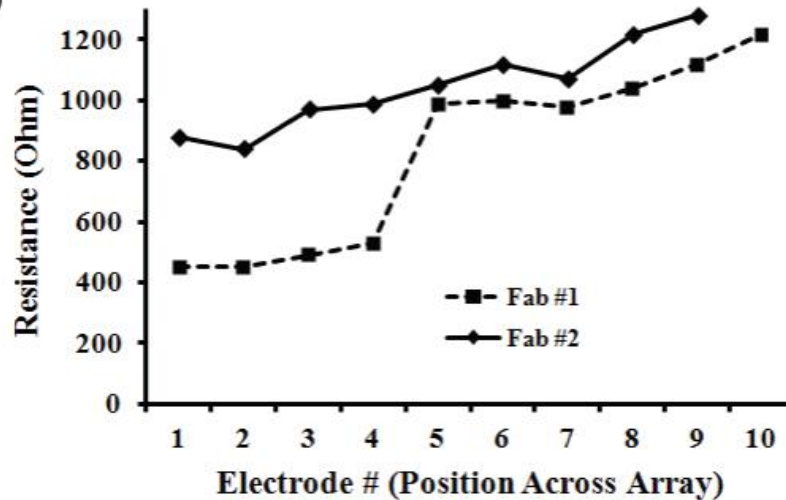


**Figure 3.12** Non-uniform electrode resistance due to substrate un-evenness. a) Sample design, where approximately 50% of the resistance across an electrode path is outside the heater electrode. b) Measurement of resistances from random electrodes from left to right along the array. Electrodes patterned from purchased slides.

Even with an even resistance across electrodes, the absolute values may still differ between fabrication runs. Therefore, individual calibration is needed for each slide. The alternative approach is to deposit ITO onto a glass substrate and ensure uniform thickness. [145-149] This can be done on a glass slide or cover slip. The advantage is that any glass substrate thickness can be chosen, which is critical in cases where high magnification imaging is required and glass thickness has to be minimal. Also, this method precludes the need for a specialized electrode array design.

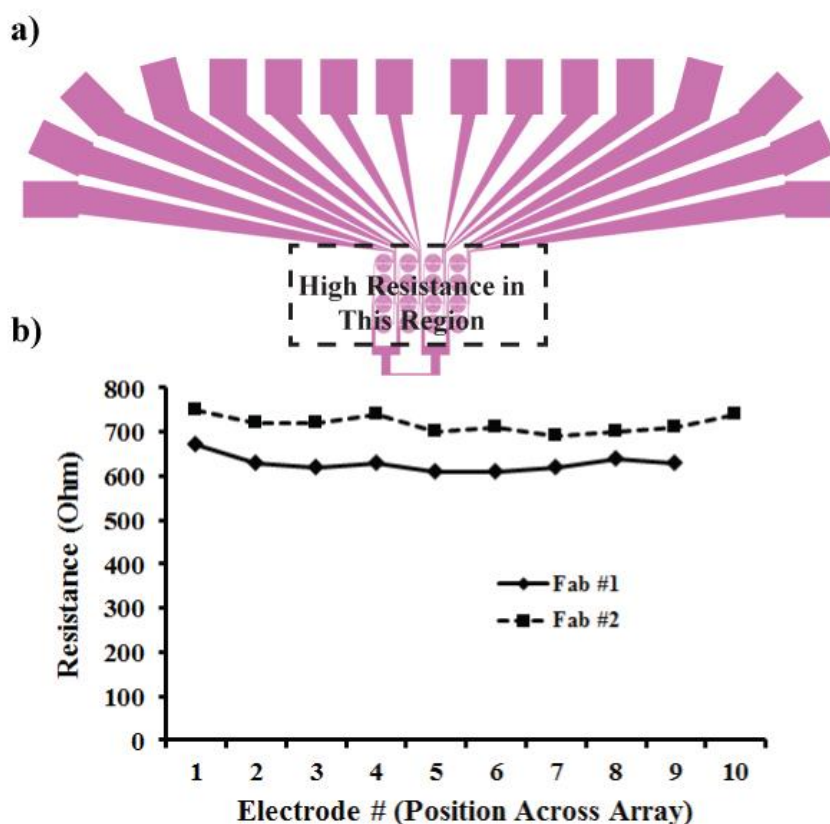


**Figure 3.13** Uniform electrode resistance despite substrate un-evenness. a) Sample design, where approximately 97% of the resistance across an electrode path is centralized the heater electrode. b) Measurement of resistances from random electrodes from left to right along the array. Electrodes patterned from purchased slides.

### 3.5 Methods

#### 3.5.1 Fabrication

We fabricated all microfluidic devices in poly(dimethylsiloxane) (Sylgard 184, Dow Corning) using well-established multilayer soft-lithography techniques. [66-68] Briefly, each of the two layers of the device was designed in Autocad 2012 (Autodesk); masks were printed by CAD Services (California). The master were fabricated on a silicon wafer using SU8-2025 (MicroChem) using the manufacturer prescribed procedure for multi-layer SU-8 processing, and treated with Tridecafluoro-(1,1,2,2-Tetrahydrooctyl)-1-Trichlorosilane silane (UCT Specialties, LLC). The master was then molded into a 4mm thick layer of PDMS and cured at 70 °C for 2 hours.

The electrodes were patterned using standard ITO wet etch technique. [142-144]. In short, the array was designed in Autocad 2012 (Autodesk); masks were printed by CAD Services (California). Slides coated with ITO to a maximum thickness of 160 nm (Delta-Technologies, Inc.) were coated with SPR-1813 (MicroChem) to a thickness of 2  $\mu\text{m}$  and patterned using the manufacturer prescribed procedure. Following patterning, a wet etch of ITO was performed with HCL at a ratio of 37% HCL: DI water of 1:1 for 12 minutes until the resistance between segments where ITO was etched away matched that of a glass slide. This was done to confirm complete removal of ITO. Lastly, the photoresist was removed using acetone to expose the patterned ITO electrodes.

The microfluidic device and the electrode slide were assembled with a method that allows the slide to be re-used multiple times. The method is depicted in Figure 3.14. First, the ITO electrodes were protected with a stripe of clear tape. Next, a 10- $\mu\text{m}$  thick layer of 20:1:5 mixture of PDMS (prepolymer: crosslinker: toluene) was spun-coated onto the slide. Then, the PDMS microfluidic device and membrane coated slide were bonded together via oxygen plasma treatment for 20 seconds (PDC-32G plasma cleaner). This allows the device to fully seal to the glass slide without permanently bonding directly to it. After, the clear tape was peeled away to expose ITO electrodes. Magnetic tape (VWR) was then used to position 24gauge copper wire on the electrode connection pads. Another piece of magnetic tape on the other side of the glass slide was then used to hold the copper wire in proper position. The wire used cannot be solid, but has to be a bundle which can be flattened. At this point the device is ready to be used. Afterwards, the membrane can simply be peeled off the device and any remaining fragments removed after treatment with toluene to swell the PDMS.

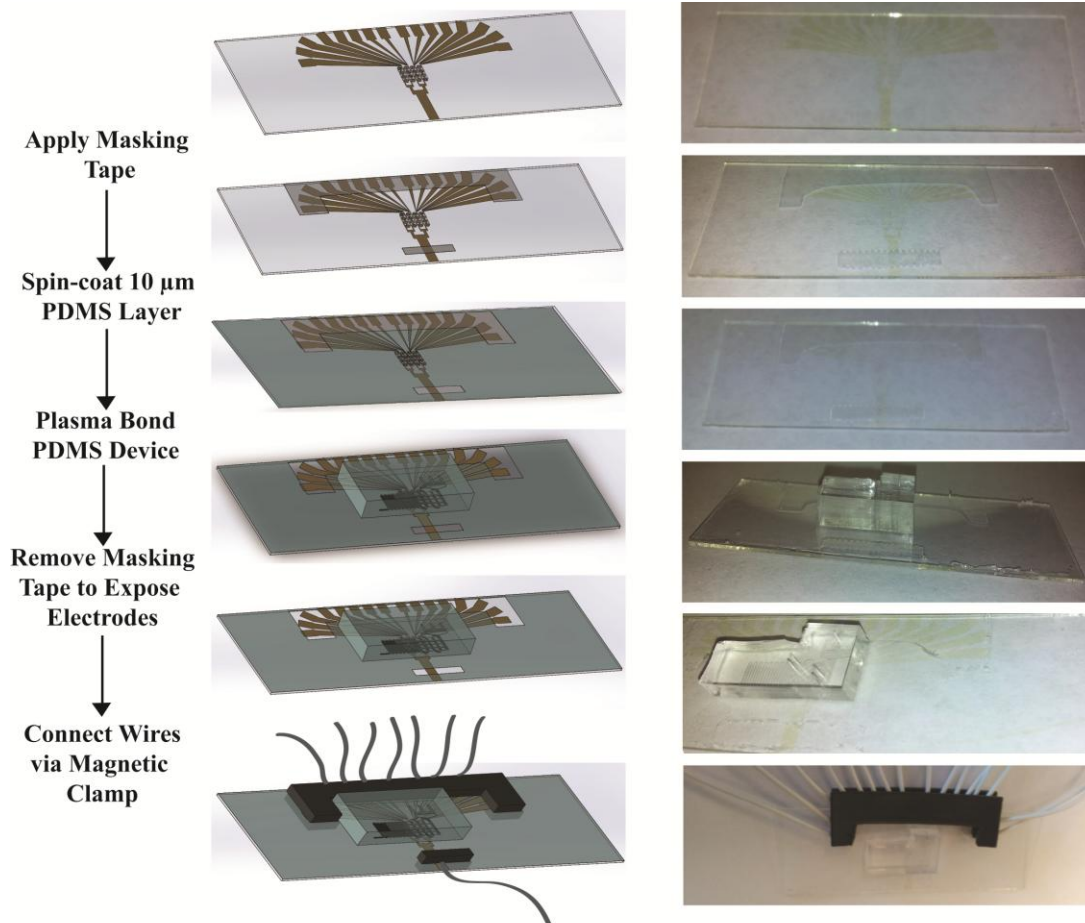


**Figure 3.14** Device and electrode slide alignment procedure.

### 3.5.2 Culture of *C. elegans* and Extraction of Embryos

*C. elegans* were cultured at 20 °C on standard agarose plates with OP50 bacterial lawns, and were suspended in standard nematode buffer for experiments. I used the N2 strain for all experiments where fluorescence was not required. The CZ456 (a strain that carries  $juIs1=Punc-25::gfp$ ) [58] was used for all fluorescence studies. On-chip long culture was performed in a solution of OP50 bacteria suspended in standard nematode buffer (M9) [1] at an  $OD_{600}=1$ . Embryos for experiments were collected by allowing young adult *C. elegans* to lay embryos on agar plate for 4 hours, then removing the animals, followed by washing embryos off the plate.

Fluorescent images were acquired using a Leica DM4500B microscope with a Hamamatsu C9100-13 EM CCD camera at 5x magnification to monitor the device

operation and at 100x magnification for subcellular imaging. Images were acquired using Image-Pro (MediaCybernetics) and processed and pseudo-colored with ImageJ (NIH).

### **3.5.3 Solutions**

All solutions were filtered through a 0.2  $\mu\text{m}$  nylon membrane filter (MF-75, Nalgene) to remove particulates. Solution of Pluronic F127 was prepared at 20% and 1% w/v. Nutrient solution containing OP50 bacteria was prepared by centrifuging OP50 bacteria suspended in LB medium, removing the supernatant, and re-suspending the bacteria in standard nematode buffer at  $\text{OD}_{600}=1.0$ . Nutrient solution was filtered using a 10  $\mu\text{m}$  pore size filter to remove clumps. Solution of Rhodamine 110 Chloride was prepared at 0.01mg/mL in deionized water.

### **3.5.4 Experimental Methods**

#### 3.5.4.1 Resistance Measurement

The resistance across electrodes was measurement with a standard multi-meter (E-SUN ECS820B) for sample electrodes in the array. All electrodes were tested for resistance; the sample electrodes reported in figures were the same for all fabrication runs.

#### 3.5.4.2 Temperature Measurement

Temperature measurement inside the chamber was performed using a micro-thermocouple (Omega). A hole was cut into the PDMS device for each chamber, and the electrode was inserted into the hole. Temperature was measured as current was applied across the electrode, until the temperature in the chamber stabilized. The current source used was a Mastech HY5003 power supply (Mastech).

#### 3.5.4.3 Fluid Exchange Measurement

Measurement of fluid exchange was done with a solution of Rhodamine 110 Chloride fluorescent dye. The dye was used over Rhodamine B because it doesn't absorb as

readily into PDMS, which would skew measurements. Fluorescent intensity was recorded while flow of pure deionized water and solution of Rhodamine 110 Chloride were alternated at specific time intervals. Average chamber intensity was extracted at individual time points from three chambers in the array; first chamber in the first column, middle chamber in the middle column, and last chamber in the last column.

#### 3.5.4.4 On-Chip *C. elegans* Culture

On-chip culture after embryo loading was performed by constantly perfusing nutrient solution with cholesterol through the device. The device was pre-treated with Pluronic F127 solution at 1% to minimize biofilm formation. The PF127 solution was washed out prior to the experiment and only PF127 absorbed to the surface remains. Nutrient solution (OP50 suspended in M9 buffer) was delivered at a flow rate of 2mL/hr.

#### 3.5.4.5 Immobilization of *C. elegans*

Immobilization of animals was performed using solution 20% w/v Pluronic F127 and electrode heaters. Nutrient solution in the device was replaced with PF127 solution prior to immobilization. Then, heat was turned on for 5 seconds to heat the solution and form PF127 gel. Complete transition from the solution to the gel state was set as the point at which animals were no longer moving. Animals were then imaged while the chamber cooled and the gel transitioned back to liquid state.

### **3.5.5 Auxiliary Hardware**

The auxiliary hardware used for the system is syringe pump capable of withdrawing fluids (NewEra Pump Systems, NE-1000) and the components used to control the patterned electrodes. These components consists of a HY-5003 DC power supply (Mastech) and a PacDrive digital I/O controller (Ultimarc) connected to the PC and controlled via a LabVIEW GUI.

## 3.6 Results

### 3.6.1 Embryo Trap Efficiency

The embryo trap loading efficiency is one of the most critical properties of the system, because it correlates directly to throughput and the sample size per experiment. We observed an overall loading efficiency of 65% (Figure 3.15). The ideal loading is not one embryo per trap, but one embryo per culture chamber. Thus, even though the trap itself is designed specifically towards the average size of a *C. elegans* embryo, loading is not perfect. (Figure 3.15). Several factors contribute to the loading efficiency being approximately 65%. First, the collected embryos are of various sizes (observed empirically during experiments). Large embryos fill traps while protruding into the fluid delivery channel. They serve as an obstruction to other flowing embryos and may cause formation of clumps at the trap. Once the device is pressurized, the whole clump can enter the culture chamber and thus multiple embryos are loaded. On the other hand, smaller embryos do not fill the trap completely, allowing other embryos to partially fill the rest of the trap. Again, once pressurized, multiple embryos will be loaded into a chamber. Therefore, it is critical to age synchronize the collected embryos to minimize size variation.

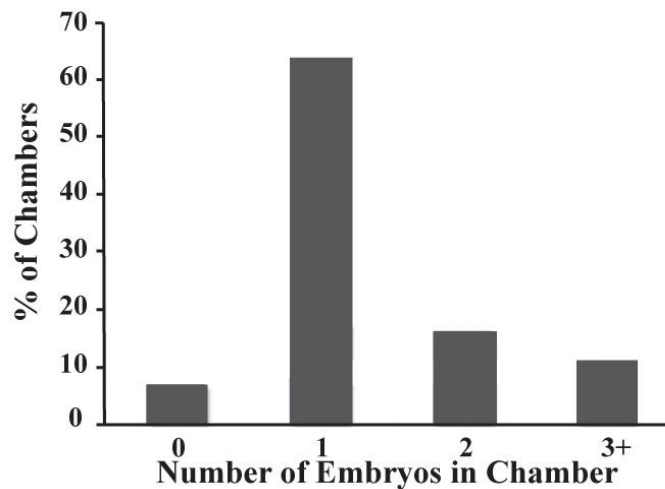


**Figure 3.15** Loading efficiency of embryos into chambers in the microfluidic array.



The second factor is proper transfer of features from the mask to the mold during fabrication. Since the features of the trap are small and strictly geometrically defined, fabrication errors resulting in deviation from the design dimensions decrease the trapping efficiency. For example, un-even exposure of photoresist to the curing UV light can cause certain features to become overexposed and some to become underexposed. Overexposed features result in increased narrow channel dimensions, leading to high probability of embryos passing through to the channel prior to pressurization. This would lead to multiple-loading. Under-exposing the features may make the narrow channel too narrow, thereby limiting flow sufficiently enough to prevent initial trapping of embryos. These issues become particularly difficult if uneven feature size is manifested across a single array. Through several fabrication runs, I have observed up to ~35% feature size change due to over- or underexposure. As an estimate, roughly 20% of traps on a single array would become dysfunctional in such extreme cases. Therefore, extreme care has to be taken during fabrication.

### **3.6.2 Temperature Control on Device**

I measured temperature inside the microfluidic chamber when a solution of 20% w/v Pluronic F127 was flowing through the device at 3mL/hr with 1 mm diameter chambers. The average electrode resistance was 640  $\Omega$  and the ambient room temperature was 18.5 °C. As can be seen from Figure 3.16, a direct correlation between applied current and chamber temperature can be established. This is critical since a direct relationship between current applied to electrodes and the resulting chamber temperature must hold. However, the slope of this relationship may differ for various applications. For example, if solutions with different heat capacities are used, a calibration curve has to be established for each solution. More importantly, the difference between flowing and stationary liquid is very significant due to convective heat transfer. The current

requirement will also depend on the average electrical resistance of the electrode array used. However, for each specific situation, a relationship can be well established.

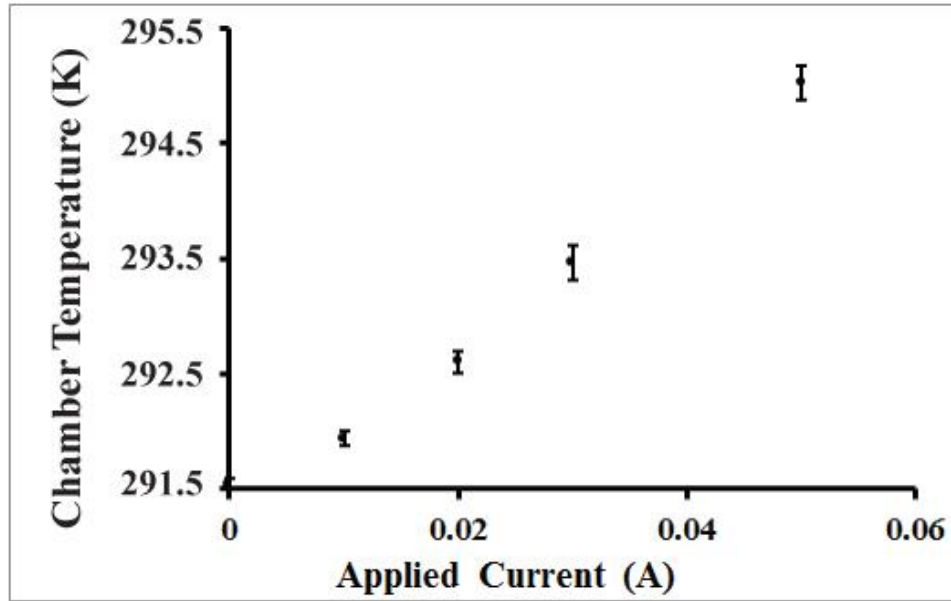


**Figure 3.16** Experimentally determined relationship between the applied current and chamber temperature in a device with flowing PF127 solution

In addition to tightly controllable temperature, the heating has to remain localized to individual chambers, i.e insulation between chambers is important and minimizing cross talk between chambers is important. I performed a COMSOL simulation to model the temperature profile in a chamber and its immediate vicinity. The model consisted of a single quadrant of the microfluidic device with accurate dimensions. The chamber used has 1 mm diameter. The boundary conditions on all external surfaces were set to heat transfer, with the coefficient of heat transfer values corresponding to forced air flow ( $100 \text{ W/m}^2 \cdot \text{K}$ ). The quadrant external surfaces corresponding to faces sectioned from PDMS were set at symmetry boundary conditions. The general equation solved was  $\nabla \cdot (k \nabla T) = Q$ . The heat source for in the domain corresponding to an electrode was calculated via  $Q = I^2 \cdot R$ . The materials used were glass, PDMS, water and ITO. The water was modeled as static, as this case would lead to greatest cross-talk between the chambers as a “worst-case” scenario.

The results show that the temperature increase is centered on the chamber of interest, with only a 0.47 °C increase in neighboring chambers and 0.33 °C increase in diagonal chambers per 1 °C increase in the target chamber. Though this ratio decreases with increasing current, at 0.3% the effect is for all practical purposes minimal.

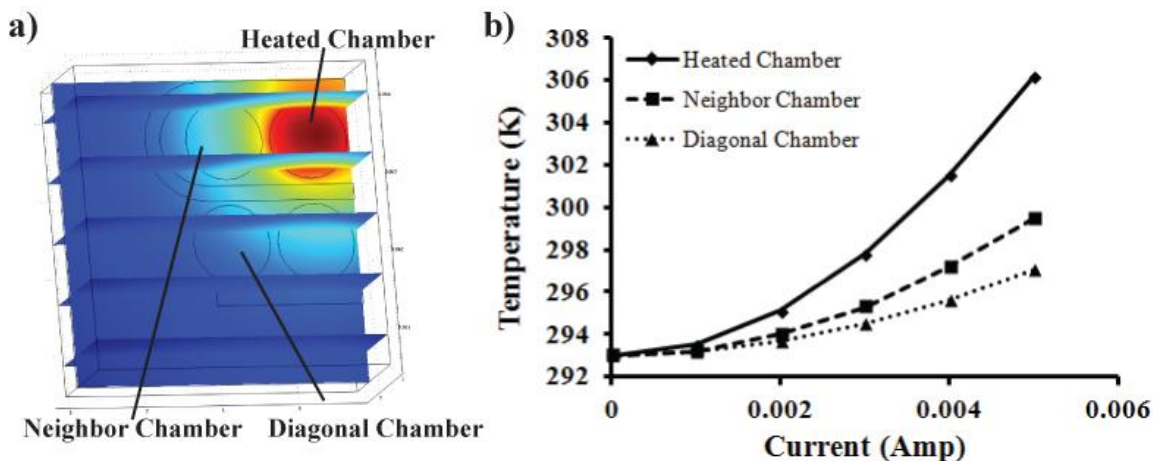


**Figure 3.17** COMSOL Simulation of device temperature profile from heating a single chamber. a) Schematic of the model used to simulate device chamber distribution. b) Temperature vs. current relationship for the target heated, the direct neighbor, and the diagonal neighbor chambers.

With such targetable and precise temperature control, many applications can be tackled, such as thermotaxis assays, induction of thermal stress, or immobilization of animals for imaging. I tested the application of the method developed in Chapter 2 for immobilizing animals with Pluronic solution for high resolution and high magnification repeatable imaging.[89] In this case, solution of 20% w/v of Pluronic F127 was first loaded into the device. Once the exchange across the array was completed (~15 seconds), current was applied to target chambers until the sol-gel transition was reached and the animals were immobilized. Figure 3.18 shows a time lapse of an immobilization cycle, which starts after Pluronic solution has been loaded into the device. Heat was turned on to trigger the gelation and immediately turned off once the transition began. As can be seen, the animal is immobilized for a period of at least 5 seconds. This length of time is more than sufficient to take a stack of images of various z-planes across the animal body.

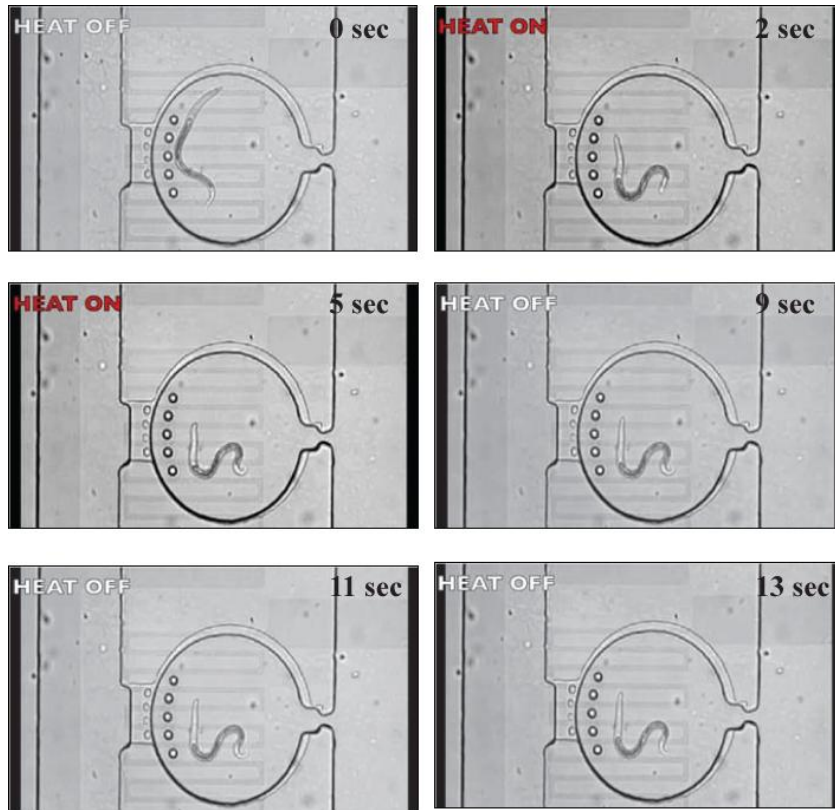


**Figure 3.18** Time-lapse of *C. elegans* immobilization for imaging via Pluronic F127, showing the animal becoming fully immobilized after a heat pulse. The immobilization occurs via the sol-gel transition of the solution of PF127 triggered via heating from the transparent ITO electrodes.

### 3.6.3 Rapid Fluid Exchange

To ensure the design of the array facilitates rapid and uniform response, I measured the fluorescent intensity of Rhodamine 110 Chloride dye inside culture chambers as the dye solution was pulse-injected into the device. The chambers imaged were at the beginning of the array, the middle, and by the outlet. As shown in Figure 3.19, the exchange is highly uniform between the chambers and reaches completion after 8 seconds. This rise time and the corresponding fall time are determined by two factors. First, measurement of rise time (and fall time) started from the point of externally switching flow. Therefore, the rise time includes the time required for the dye liquid (or buffer during fall time) to get to the array from the inlet of the device, which takes approximately ~1 second. The

second factor is the time it takes to exchange the fluids inside a culture chamber, since the fluid within the sinusoidal delivery channel is exchanged within ~1 second. The exchange of fluid in the culture chambers is the dominant factor affecting the fall and rise time.

Despite the rise and fall times, the exchange is rapid and highly controllable. This is critical if embryos need to be exposed to a series of external stimuli in a rapid and controlled fashion for example. If developing animals were to be treated with pheromones for monitoring behavioral response after embryonic treatment, the delivery of said pheromones has to be uniform and rapid. This is because behavioral response occurs immediately after exposure.

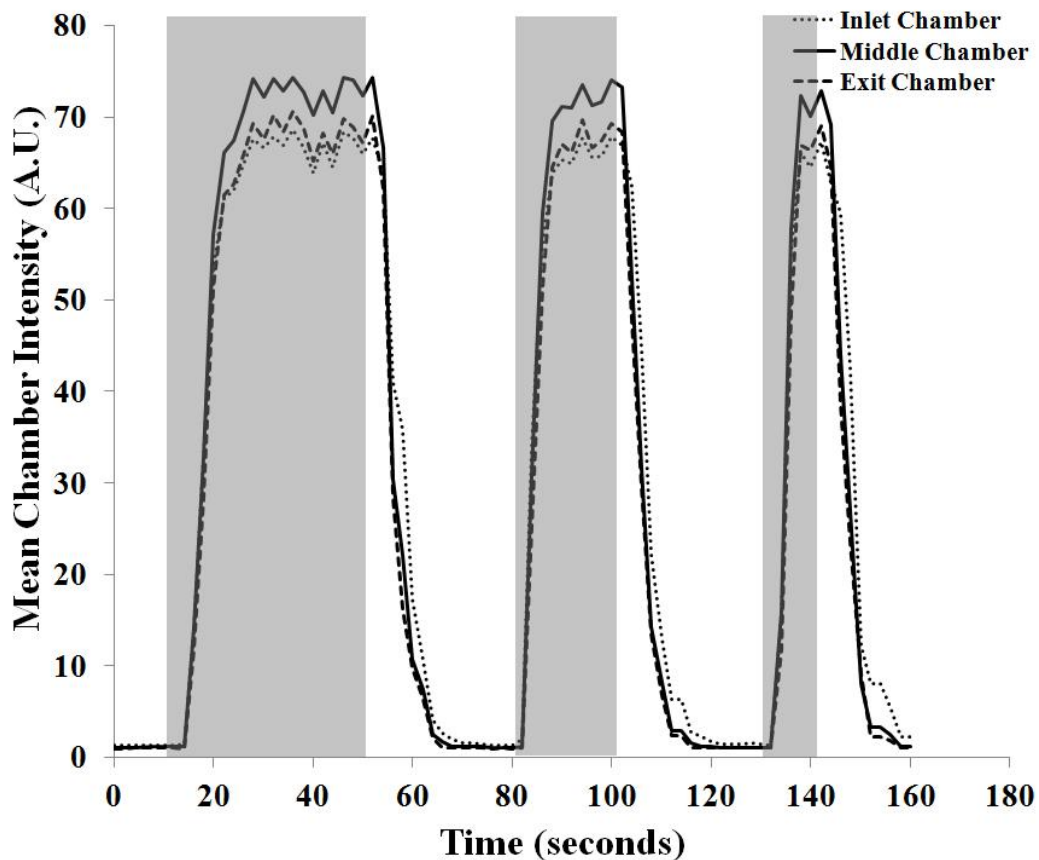


**Figure 3.19** Average fluorescent intensity inside culture chambers after a pulse of dye solution (grey). The exchange of fluids is rapid following the introduction of a dye pulse of 40, 20 and 10 seconds.

### 3.6.4 Culture of *C. elegans* on Device

The ability to culture *C. elegans* on device after hatching is critical if developmental effects are to be studied after exposing embryos to external stimulation or stress. This requires continuous perfusion of nutrients through the device and the creation of benign conditions. Nutrients are perfused through the device in the form of OP50 *E. coli* bacterial suspension in nematode buffer. This solution continuously delivers bacteria to the culture chamber for animals to consume. Additionally, the expansion and resulting slowing of flow inside the chamber decreases the shear rate experienced by animals and increases the residence time of bacteria. This further increases the animals' ability to feed. Lastly, the resistive heating technique increases the temperature uniformly across the whole chamber, instead of directly heating the animals as is the case when laser heating is used. [150] Since laser heating is used to ablate cells in certain applications, it is difficult to rule out any negative effects from such direct and focused exposure. As can be seen from Figure 3.20, the system can successfully trap embryos, which then hatch and develop through the standard L1, L2, L3 and early L4 stage at 20 °C.

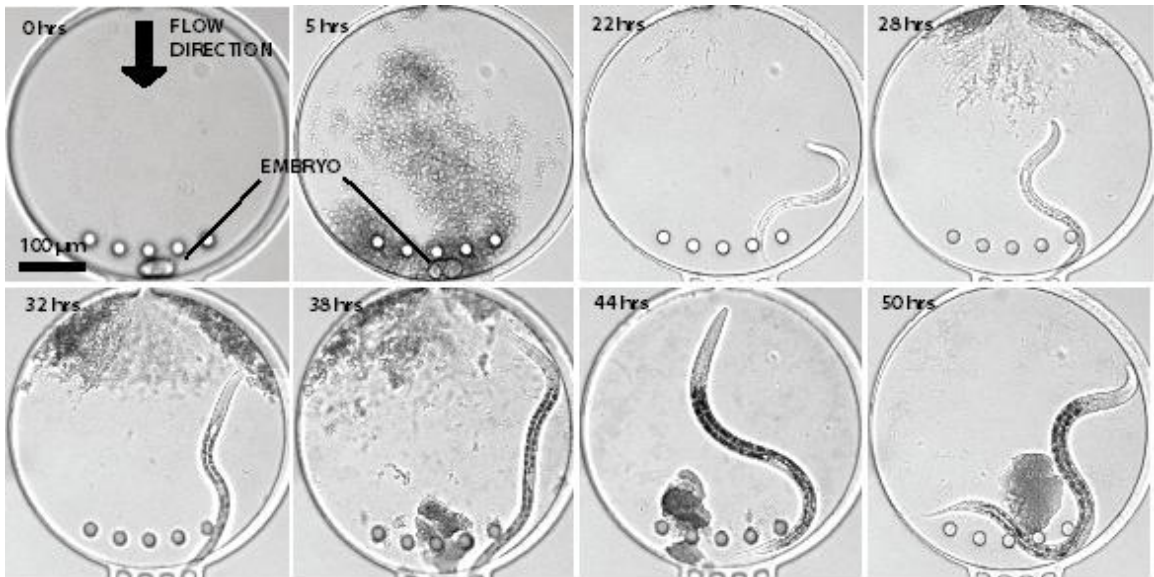


**Figure 3.20** Hatching of trapped embryo and subsequent development of the hatched animal inside the culture chamber of the microfluidic array. At 50 hours, the animal has reached early L4 larval stage.

The expansion of flow is beneficial to the animals, but the increased bacterial residence time can also contribute to the formation of bio-films and clogging of the device. This is the case because the bacteria delivered to the animals' is live to maintain maximum nutritional value, and has not been treated with antibiotics. To limit the formation of biofilms, I followed the established approach of pre-treating the surface of PDMS with Pluronic polymers to decrease protein and cell adhesion. [151-153] Solution of 1% Pluronic F127 circulated through the device overnight. The solution was then replaced with nematode buffer prior to the experiment. Only the Pluronic polymer absorbed to the surface remains after washing. As can be seen in Figure 3.21, the treated device exhibited a significant decrease in formation of bacterial films. However, this treatment is not permanent and thus cannot be used for experiments to last longer than ~72 hours.

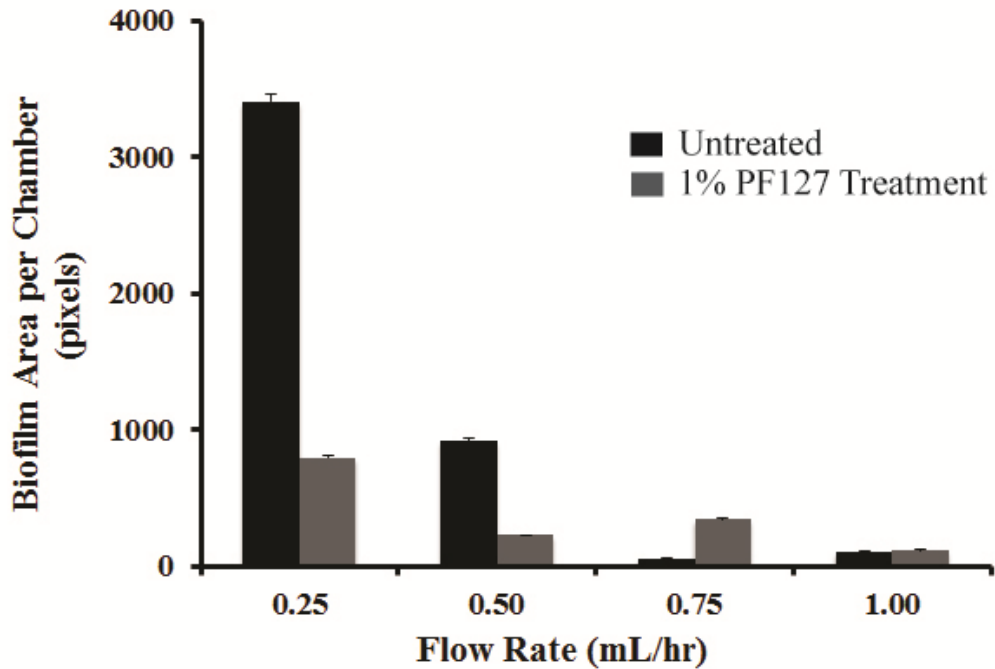


**Figure 3.21** Comparison of biofilm formation between untreated devices and devices treated with 1% solution of Pluronic F127.



### 3.6.5 Observing Developmental Events on Device

To confirm that difficult to observe developmental effects can be studied on the device, we monitored the synaptic re-arrangement of synapses of the DD class motor neurons between the L1 and L2 larval stages. [58] The synapses of these neurons in the L1 larval stage innervate muscles on the dorsal side of *C. elegans*. After the development of VD motor neurons, the DD motor neurons begin innervating the muscles on the dorsal side. This process is completed during the L2 larval stage. We studied animals of the CZ456 strain containing *juls-1 (Punc-25-snb-1::gfp)*. The protein produced is SNB-1::GFP, which is a fusion of synaptobrevin and GFP. Synaptobrevin is a protein that associates with synaptic vesicles and becomes part of the vesicle docking mechanism at a synapse as a member of the SNARE complex.[154] Thus, this fusion protein allows for observation of localization of synaptic vesicles and the location of synapses.

We observed individual animals trapped inside culture chambers over time. As shown in Figure 3.22, we were able to observe the synaptic re-arrangement between the L1 and L2 larval stages. This validates the ability of our system to facilitate normal development and to observe developmental processes.

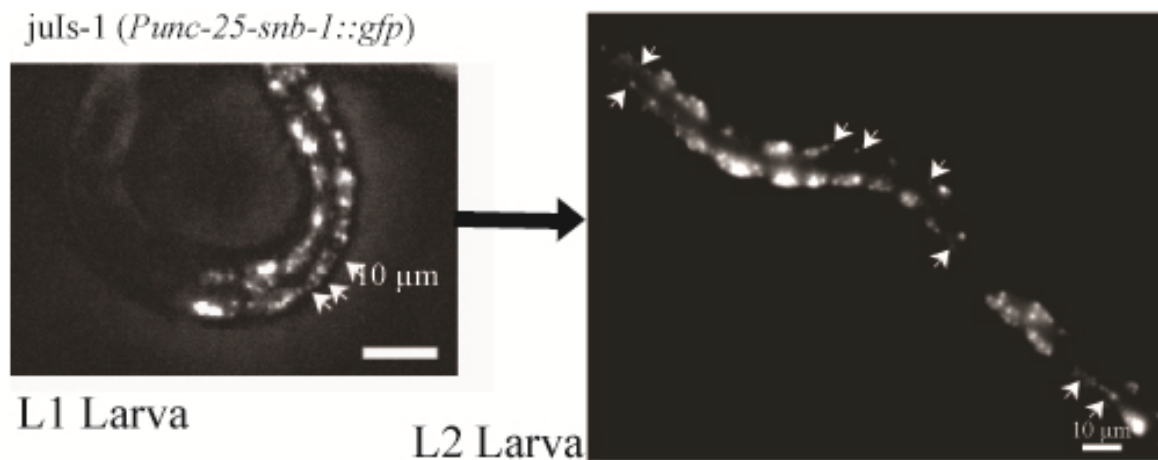


**Figure 3.22** Synaptic rearrangement of DD motor neuron synapses from the dorsal to the ventral side. Arrows point to synapses.



### 3.7 Conclusions

In this work, I have presented a technology for high throughput trapping and chemical and thermal manipulation of *C. elegans* embryos with the ability to follow their development after treatment. The technology consists of a highly scalable microfluidic array designed to trap and manipulate embryos without active components or direct user input and of a microelectrode array for temperature control. Both components are assembled in a simple and robust way designed for re-usability of expensive and difficult to make components to maintain low costs in large scale experimentation. I have demonstrated the ability of the system to efficiently trap single embryos in chambers for culture after treatment. I have also shown that temperature control is robust and can be applied to a range of applications, such as immobilization of animals using Pluornic F127 for imaging. Additionally, fluid exchange in the array is rapid and even across chambers in different positions. Lastly, I have show that it is possible to observe complex developmental events in the device in hatched animals. This technology potentiates a broad range of studies including the understanding of how early development affects biological function, how stress during early development may be damaging or induce future resistance and how various stimuli such as drugs or common chemicals impact natural developmental processes and functions.

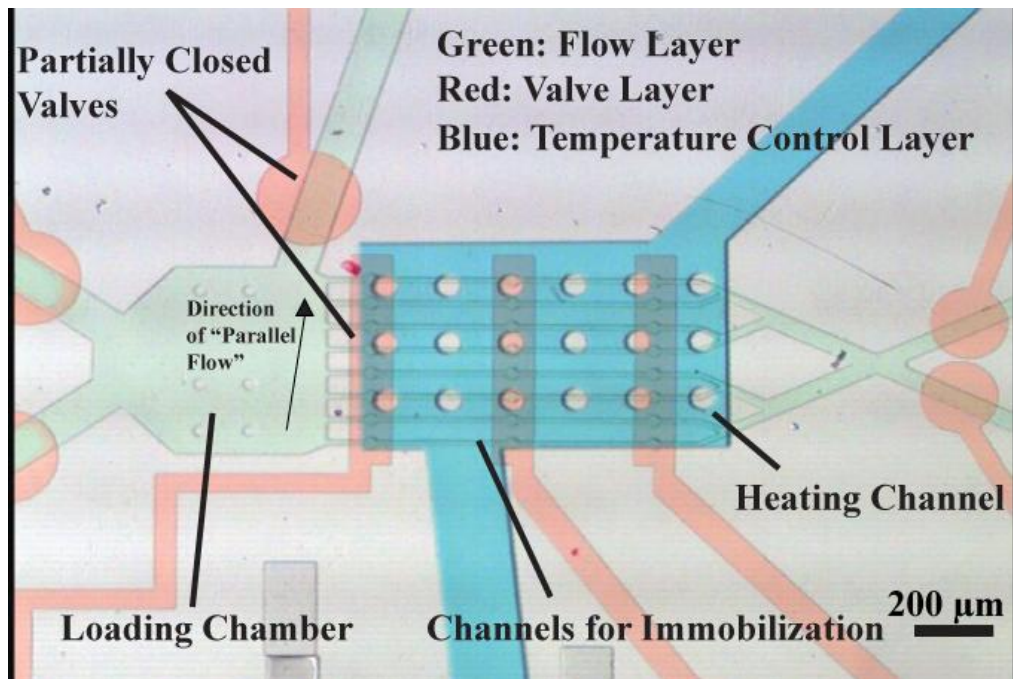
## **CHAPTER 4 C.L.I.P – CONTINUOUS LIVE IMAGING PLATFORM FOR DIRECT OBSERVATION OF *C. ELEGANS* PHYSIOLOGICAL PROCESSES**

This chapter describes the development and sample implementation of a system for live observation. Direct observation of developmental and physiological changes in certain model organisms over time has been technically challenging. In the model organism *C. elegans*, these studies require frequent or continuous imaging at physiologically benign conditions. However, standard methods use anaesthetics, glue, or microbeads, which prevent animals from feeding during the experiment. Thus, animals' normal physiological function may be affected over time. Here I present a platform designed for live imaging of *C. elegans*. The system is capable of immobilizing only animals' bodies under benign conditions and without physical deformation. Simultaneously, animals' heads remain free to move and feed for the duration of the experiment. This allows for high-resolution and high-magnification fluorescent imaging of immobilized and feeding animals. The system is easy to fabricate, set up, and operate, and should be widely applicable to a wide range of problems development and physiology. This work was completed with help from Yan Hao from the laboratory of Dr. Ho Yi Mak of Stowers Medical Institute, Kansas City. The content of this chapter has been adapted from reference [155], "C.L.I.P.–continuous live imaging platform for direct observation of *C. elegans* physiological processes."

### **4.1 System Design Process**



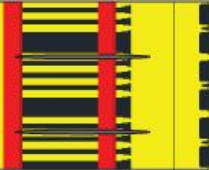
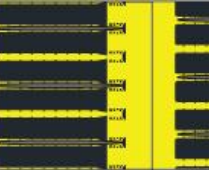
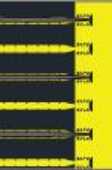
The purpose of this system is to facilitate live observation of *C. elegans*. As such, the design has to conform to the previously stated criteria of immobilizing animals for imaging while the animals are simultaneously i) allowed to feed as they normally would, ii) while they remain within their physiological temperature range of 15-25 °C, and iii)

while their physiological processes are not otherwise affected. The technical inspiration for such a design came from early testing of a device originally intended for long term developmental studies, depicted in Figure 3.1. The principle of this three-layer PDMS device was to trap animals in channels by using partially closed valves. Nutrients were to be delivered in form of bacterial suspension in buffer. Immobilization for imaging would be achieved using Pluronic F127, which would be heated past the sol-gel transition temperature. Although this design was ultimately discarded for its impracticality in three layer fabrication and for the high pressure drop required to deliver nutrients to filled channels, it provided inspirational insights. First, because of the mentioned high pressure drop, flow would preferentially exit the chamber via the channel on top. This led to bacteria flowing primarily in parallel to the trapping channel inlets. It also caused Pluronic gel to be eroded in the chamber prior to returning to the sol state, while not eroding the gel inside the channels as fast. Lastly, it caused animals to try and crawl back towards the inlet, where the concentration of bacteria was highest.



**Figure 4.1** Early long term developmental study testing design, which was used as a technical inspiration for the C.L.I.P platform.

Based on this design, a series of adaptations was tested. The goal was to develop a design capable of properly trapping and positioning animals inside channels, so that only their heads would protrude out. As before, Pluronic gel would be used to immobilize bodies, while the gel around their heads would be eroded by flow. Additionally, the same flow would deliver nutrients in form of *E. coli* suspended in solution. The designs tested were i) a straight channel with partially closed valves used for positioning, ii) a channel with a tapered outlet to stop animals, iii) a channel with a tapered outlet in combination with partially closed valves, iv) a channel with bumps to prevent motion and a pillar array at the outlet to stop and properly position animals, v) the same design, but using a chrome mask for master fabrication to ensure high feature fidelity.

Design Features					
Type	Straigh Channel Partially Closed Valves for Stopping and Positioning	Straigh Channel Tapered Channel Outlet for Stopping and Positioning	Straigh Channel Tapered Channel Outlet + Valves for Stopping and Positioning	Straigh Channel with Protrusions Tapered Channel + Pillar Array for Stopping and Positioning	Chrome Mask Fabrication Process
Loading Efficiency (% of Animals Stopped)	~ 0 %	< 20%	< 60%	< 70%	~ 95%
Proper Head Positioning Of Loaded Animals	~ 0 %	< 10%	< 10%	~ 80%	~ 95%
# of Layers	2	1	2	1	1
Equipment Required	Pressure source Control Valves Syringe Pump	Syringe Pump	Pressure source Control Valves Syringe Pump	Syringe Pump	Syringe Pump
Preparation Time	1 hour	25 min	1 hour	25 min	25 min

**Table 4.1** Description of the various features of the different designs tested.

## 4.2 Final System Design

The final design is microfluidic platform capable of immobilizing just the animal body while leaving the head free to move, and doing so for a prolonged period while I

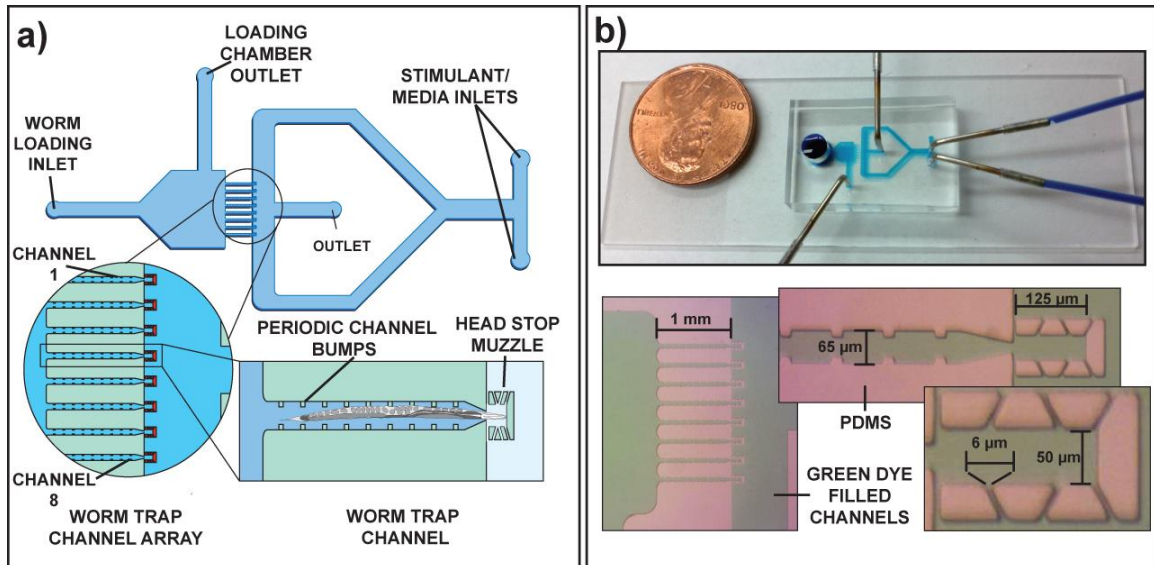


**Figure 4.2** Microfluidic device component of the platform. a) The device is a simple array of trapping channels. Animals and solutions are loaded through the worm loading inlet. From here animals are moved to the 8-channel array. Bodies are immobilized inside the channels with the immobilizing agent, Pluronic F127 solution (or Sodium alginate/Gelatin mixture) and microbeads. Animals heads are free to move and feed inside the head stop muzzle. Nutrients are delivered to the muzzle through media inlets via symmetric bifurcated flow. b) The device is extremely simple and only has 5 inlets/outlets. Positioning of animals is done passively via geometry design. The muzzle is sized to only allow the head of an animal to enter. Spacing between pillars prevents animals' escape. Bumps in the trapping channel help prevent sinusoidal body movement of animals.

observe physiology in vivo. The worm body is immobilized at physiologically benign conditions without any physical deformation. At the same time, the animals are fed via their freely moving heads. This approach ensures proper physiological function during the experiment. The platform combines a microfluidic device and an immobilization agent. The microfluidic component is an array of channels used to properly position animals (Figure 4.2). The second component is an immobilization agent for the portion of animals' bodies in the trapping channels. The combination allows us to observe dynamic processes without artifacts and changes caused by alteration of normal physiological function. The platform is designed to be extremely simple to prepare for experiments and

to not require user manipulation after initial preparation. It also requires minimal use of external peripheral devices to work and can be easily applied in any laboratory.

#### **4.2.1 System Design Principles and Operation**

To design a platform that is easy to use for a variety of applications in any laboratory, I placed emphasis on simple fabrication, an extremely simple experimental setup, and minimal requirements for external peripherals, while maintaining all the necessary functionality.

The device is a single-layer PDMS-based device and has no active components such valves. After initial setup, the device does not require any additional input from the researchers. It consists of a loading chamber (Figure 4.2), which is used to load all liquids and animals. The inlet to this chamber is cut with a 7 gauge cutter. The inlet is cut to this size to serve as a liquid pseudo-reservoir on device. From this chamber, animals are loaded into the array of trapping channels (Figure 4.2) by withdrawing liquid through the main outlet (Figure 4.3). In these channels, their bodies are immobilized with our immobilizing agent. However, the animals' heads protrude into an array of pillars, or the "muzzle" (Figure 4.2). The array width and length dimensions are designed to accommodate the head of the animals to the second pharyngeal bulb. The pillars are spaced 6  $\mu\text{m}$  apart to prevent animals from escaping. This array serves multiple purposes. First, it stops the forward motion of the animals. This leads to proper positioning; bodies remain inside the channel, and heads are positioned in the muzzle. Second, it allows flow to enter the muzzle area. This facilitates delivery of nutrients and stimulants to the animals' heads. These are delivered to the muzzle from the nutrient and stimuli inlets via a symmetric, bifurcated flow (Figure 4.2, 4.3).

While the microfluidic chip places the animal in position, I use an immobilization agent to suppress the body movement. The immobilizing agent is either a solution of Pluronic F12740 or a solution of sodium alginate with gelatin. Both of these

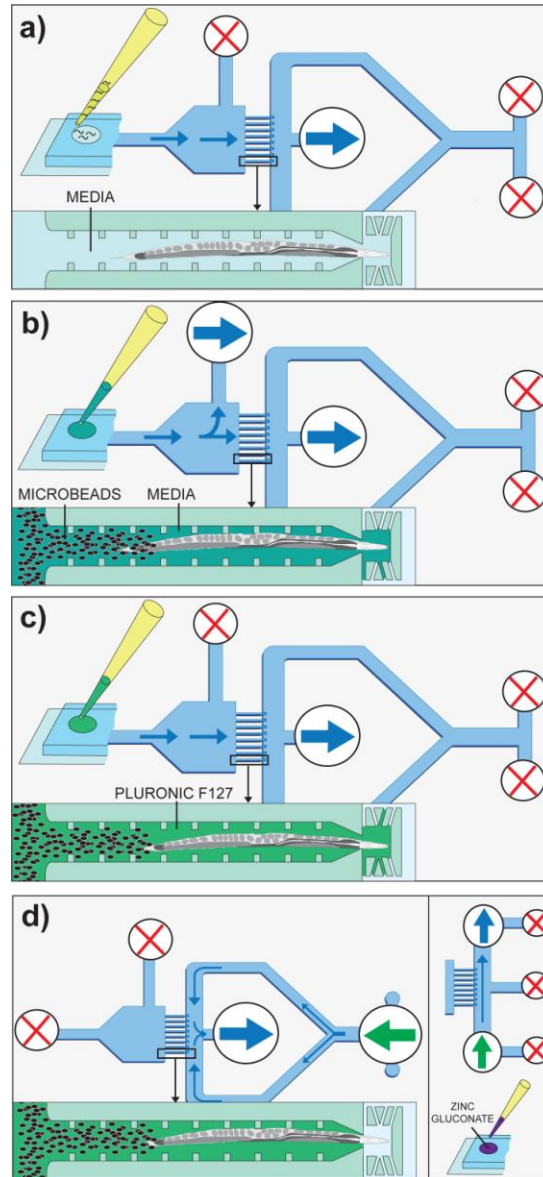


**Figure 4.3** Simple loading procedure. a) Animals are loaded into the device via the chamber inlet. They are pulled into and positioned in the trapping channels by withdrawing liquid from the outlet. b) Next, solution containing 10  $\mu\text{m}$  microbeads is loaded. This solution is used to remove excess animals from the loading chamber. Also, the microbeads accumulate at the tail and physically immobilize it. c) Then, the immobilizing solution of Pluronic F127 (or alternatively mixture of sodium alginate and gelatin) is applied while cooled to 0  $^{\circ}\text{C}$  (sodium alginate/gelatin is applied at 25  $^{\circ}\text{C}$ ). The solution warms to ambient temperature. During this time it crosses through the sol-gel transition temperature of 17  $^{\circ}\text{C}$  and forms the immobilizing gel. d) Lastly, nutrients are delivered to the animals for feeding through the media inlets via the symmetrical bifurcated flow. (Insert) If the alternative immobilizing agent is used, the inlet and outlet used are positioned as shown. Additionally, zinc gluconate is applied through the loading inlet to trigger the gelation of sodium alginate component

are used in combination with microbeads. I chose the Pluronic F127 solution because it undergoes a thermo-reversible sol-gel transition. This transition is rapid, requires a very small temperature change ( $<1$  °C), and the desired transition temperature can be easily tuned with concentration. Additionally, the formed gel does not affect animal physiology and does not cause physical deformation. The ideal ambient temperature for using this solution is between 18 to 20 °C. Sodium alginate/gelatin solution can be used as an alternative when ambient temperature control is either difficult, or the temperature is too high (such that it is not feasible to handle PF127). The microbeads are used to physically immobilize animals' tails and prevent backwards movement. This is especially critical during the loading procedure when animals need to be kept in proper position for the gels to set. The only alternative would be pneumatic valves, which would complicate the device design and its operation.

The platform is prepared for experimentation by following a simple loading procedure (Figure 4.3). Briefly, after connecting tubing via metal pins and de-gassing the device, approximately 20 animals in 30  $\mu$ L of solution are loaded into the chamber inlet/reservoir. Animals are pulled into the trapping channels and properly positioned by withdrawing liquid through the outlet at 2 mL/hr (Figure 4.3a). Next, solution containing 10  $\mu$ m diameter microbeads is applied into the reservoir. This solution is used to flush out excess animals from the loading chamber. It is also used to deliver microbeads into the trapping channels (Figure 4.3b). Here, the microbeads accumulate at the animals' tails. The beads physically prevent backward motion and aid in immobilizing the tail.

Then, the immobilization solution is loaded into the device. In case of the PF127, 40  $\mu$ L of 25 w/v % solution chilled to 0 °C is loaded into the inlet reservoir. The procedure relies on passive warming to ambient room temperature. While the solution warms to room temperature, it passes the sol-gel transition temperature at  $\sim 17$  °C. This leads to the formation of the gel. I chose to not include active temperature control components to keep the system as simple as possible. Active temperature control makes



fabrication more complicated and requires external equipment. This would make using the platform in other laboratories difficult and potentially costly. Instead, I designed the system and loading procedure to be functional, simple, and inexpensive. However, in environments where ambient temperature is not steady or is too warm, the solution may gel prematurely. In this scenario, a solution of sodium alginate/gelatin can be used. The same volume of a 0.75% w/v sodium alginate/15% w/v gelatin is loaded at 25°C.

In the last step, loading is finalized. Nutrient and stimuli inlets are opened, so that these may be delivered to the trapped animals. In case of the sodium alginate/gelatin solution, an additional action is required. Here, a 5% w/v zinc gluconate solution is applied to the loading reservoir. This provides the Zn<sup>2+</sup> ions required to cross link the alginate. This procedure from start to finish takes approximately 20 minutes. It is easy to follow and the platform can be set up in any laboratory with a syringe pump capable of withdrawing liquid.

## **4.3 Materials and Methods**

### **4.3.1 Device Fabrication and Setup**

We fabricated all microfluidic devices using a combination of microfabrication and soft lithography techniques. [65, 68] In short, the design was prepared in AutoCAD 2012; photolithography chrome masks were prepared by Elvsys (Paris, France). Chrome masks were required, because the feature fidelity of transparency printed masks was not sufficient to fabricate molds with pillars fully capable of stopping animals from escaping (Figure 4.4). The mask pattern was transferred to masters of SU8-2025 photoresist (Microchem) spun to 60 μm on Si wafers following standard protocol by the

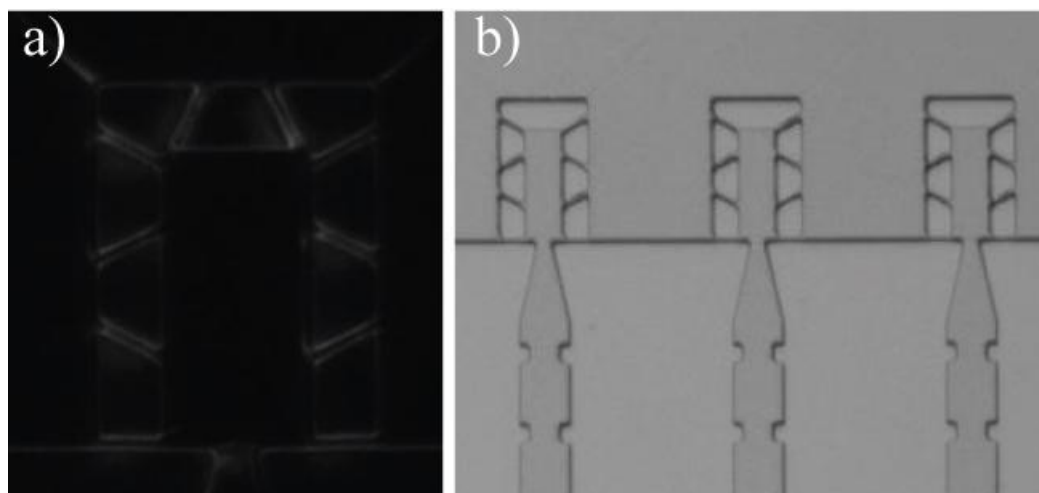


**Figure 4.4** High feature fidelity of the SU-8 master (a) and corresponding PDMS mold (b) could only be achieved using a chrome mask over a conventional transparency printed mask used for rapid prototyping. This feature fidelity is required to fabricate device capable of stopping and positioning animals.

manufacturer. After developing the resist, the finished master was treated with tridecafluoro-(1,1,2,2-tetrahydrooctyl)-1-trichlorosilane silane (UCT Specialties, LLC).

The microfluidic chips were molded from the masters into PDMS. A 5:1 mix of pre-polymer to cross-linker mixture was poured over the master to a depth of 4 mm, degassed in a desiccator for 2 hours to allow the PDMS to enter into the small features, and cured for two hours at 70 °C. Afterwards, the individual chips were cut out and fluid interconnect holes were cut. Seven holes are required to operate the device - a 7 gauge hole into the device loading chamber, and a total of six 21 gauge holes. The 21 gauge holes are cut at the loading chamber flushing outlet, at the device liquid withdrawal outlet, in the media delivery channel (x2), at the media inlet, and at the stimulant inlet each (Fig 1). The 7 gauge hole is cut at the loading chamber inlet. The whole chip was then cleaned with clear tape and compressed air, followed by bonding to a glass slide or cover slip via oxygen plasma treatment for 20 sec (PDC-32G plasma cleaner).

The 21 gauge holes are connected to PE-60 tubing (Micro Medical Tubing, Scientific Commodities, Inc.) via metal pins for fluid delivery. All liquid manipulation was

performed via syringe pump (NE-1000, New Era Pump Systems). Liquids were loaded into the 7 gauge hole directly via micropipeter. The hole serves as an open liquid pseudo-reservoir.

#### **4.3.2 Materials**

Solution of sodium alginate (Sigma Aldrich) with gelatin in water was prepared at 0.75% w/v sodium alginate and 15% w/v gelatin. Prior to the experiment, the solution was boiled for proper mixing and rapidly cooled to 40 °C prior to loading. It was applied to the device at 25 °C. Solution of Pluronic F127 was prepared at 25% w/v. All solutions were filtered through a 0.2 µm nylon membrane filter (MF-75, Nalgene) to remove particulates. Standard nematode buffer solution containing OP50 bacteria was prepared by centrifuging OP50 bacteria suspended in LB medium, removing the supernatant, and re-suspending the bacteria in M9 buffer at  $OD_{600}=1.0$ .

#### **4.3.3 *C. elegans* Culture, Experimental Procedure, and Microscopy**

*C. elegans* were cultured at 20 °C on standard nematode culture plates with OP50 bacterial lawns, and were suspended in standard nematode buffer<sup>43</sup> for experiments. I used the N2 strain for all experiments where fluorescence was not required. The *hjSi3*; *hjSi112* (carrying *R01B10.6::GFP* and *mRuby::DGAT-2*) strain was used for all fluorescence studies.

To measure the ability of animals to feed during the experiment, I measured the pharyngeal pumping rate of animals trapped on device and animals on standard plates. The rate was quantified by counting the number of bulb contractions in the pharynx over a period of 2 minutes.

Temperature calibration and measurement in device was performed by measuring fluorescent intensity of Rhodamine B (Rho B) and Rhodamine 110 (Rho 110). [156] Calibration was performed using a thermocouple suspended in a large reservoir. The reservoir was filled with Pluronic F127 solution containing Rho B/Rho 110 at a 1:1 ratio.

It was cooled to 4 °C and then placed on the microscope. The fluorescent intensity of each dye was recorded at 0.5 °C intervals. The Rho B/Rho 110 intensity ratio data was then used to calculate a correlation between temperature and intensity ratio. Temperature measurement on a microfluidic device was then performed using the standard loading procedure. A movie was recorded starting immediately after the cooled PF127 solution was loaded into the device to measure temperature changes in the device as they would occur during an experiment. Frames were extracted at each time point of interest to measure intensities of each dye and processed using ImageJ. I measured the temperature at the inlet to each trapping channel. Measurement of sodium alginate/gelatin solution temperature was performed with a standard thermocouple prior to use.

Gel behavior on chip was observed via recordings of PF127 solution dyed with Rhodamine B. Movies were recorded at each stage of the setup and experimental process, frames were extracted at time-points of interest, and thresholded to determine the gel-media boundary in the immobilization channels and the media delivery channel.

## **4.4 Results**

### **4.4.1 Loading and Analysis of Gel Behavior**

The goal of the loading procedure is to provide as many single head-first animals loaded per channel as possible. The device is scaled for L4 larvae/young adults. I observed the frequency of single head-first animal loading over 27 experiments. On average, the array is loaded with more than 4 animals (median = 5 animals per experiment) at the prescribed loading flow rate of 2 mL/hr (Figure 4.5). At higher flow rates, the fraction of head-first animals decreases significantly. For instance, at 3 mL/hr, the number of properly loaded animals decreases to below 2 on average. This is because there is a tendency of animals to orient and swim against the flow. If moderate flow rates are used, the loading procedure provides a sufficient number of animals per experiment, since typically high

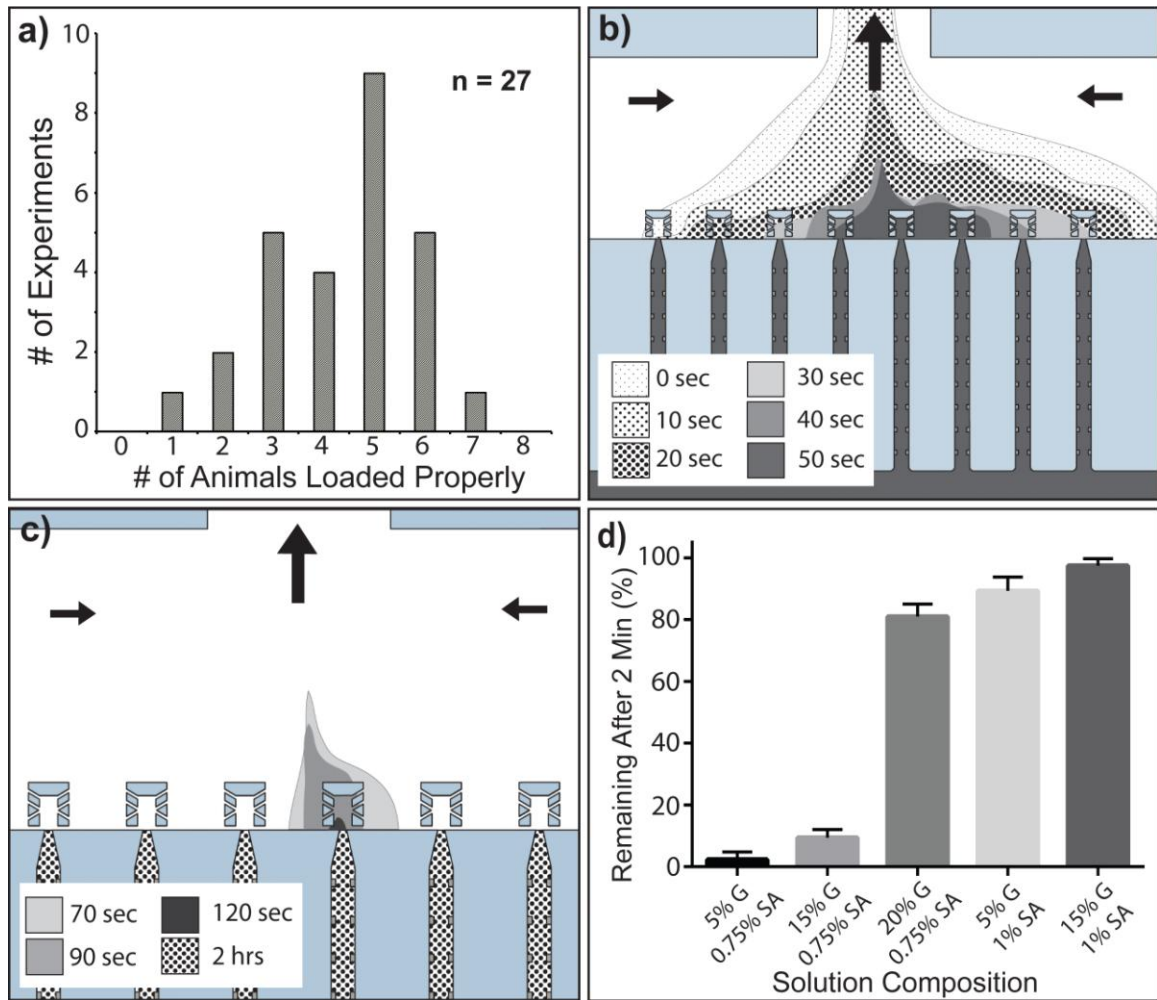


**Figure 4.5** Device functional characterization. a) Single head-first animals per channel are loaded efficiently. The average number of properly loaded animals per experiment out of 27 experiments is 4. b-c) Snapshots of the extent of the presence of the Pluronic F127 gel after formation at different times. At  $t = 0$  sec, the gel is present in the bulk of the channel and muzzle area. Within 2 minutes, the gel is completely eroded. It remains stable inside the trapping channels. The gel remains stable inside the channels because the streamlines of the bifurcated symmetric flow do not enter the channels. d) The alternative immobilizing solution of sodium alginate/gelatin cannot be eroded once gel has formed. It has to be removed prior to gellation. Alginate and gelatin solutions are viscous and are difficult to remove from the muzzle. The mixture of 15% w/v and 0.75% w/v gelatin and sodium alginate respectively is the highest concentration which can be removed efficiently prior to gellation. Also, the solution is removed fast enough to limit ingestion by the animals.

resolution imaging limits the field of view to just one animal. However, if more are necessary, the array can be expanded and the loading process can be optimized.

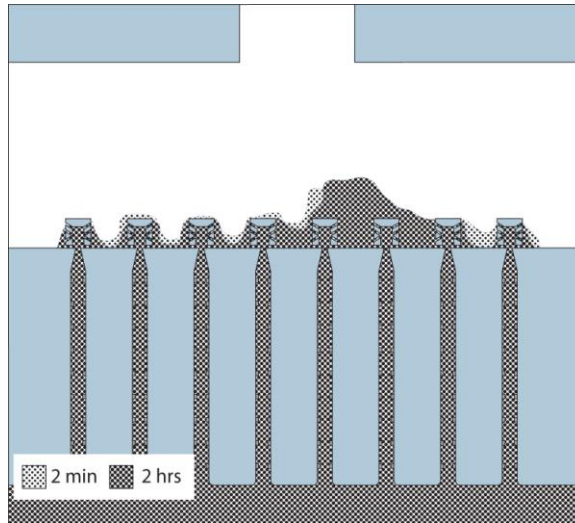


**Figure 4.6** Sample gel behavior of the sodium alginate/gelatin mixtures. Once the gel is formed, it is extremely difficult to erode and remove the gel from the bulk and the muzzle area. I thresholded images taken at different time-points to show the extent of the gel in the device. Between 2 minutes and 2 hours after gelation (15% gelatin solution), there is minimal removal from the bulk of the channel and no removal from the muzzles themselves. This would completely prevent animals from feeding. Therefore, it is necessary to remove the sodium alginate/gelatin mixture from the delivery channels and the muzzles prior to gelation.

The critical step following efficient loading is proper immobilization. Animals' bodies have to be immobilized, while their heads are free to move. However, both immobilization solutions are allowed to flow through the device simply until they gel for the sake of simple loading. In the case of PF127, the gel forms everywhere the solution is present (Figure 4.5). This includes the area of the muzzle and the bulk of the delivery channel. However, after flow of nutrients is turned on, the gel is eroded rapidly. Within 2 minutes (Figure 4.5), the muzzle and channel areas are both clear of PF127 gels. Gel inside the trapping channels remains stable and does not get eroded. This is because the bifurcated symmetrical flow stream lines do not dip into the channels themselves.

Gelation of sodium alginate/gelatin solution follows different mechanics. Sodium alginate polymers are cross-linked via binding to  $Zn^{2+}$  ions. These ions diffuse from the loading reservoir through the loading chamber all the way into the trapping channels. This process takes approximately 15 minutes. The sodium alginate component provides

stiffness and rigidity. The gelatin component settles over time as individual gelatin polymers intertwine. At 15% w/v, this process also takes approximately 15 minutes. The gelatin gel component provides elasticity and shape retention properties. However, gelatin cannot be eroded by flow after gelation (Figure 4.6). Thus, it is critical to remove it from the muzzle prior. This cannot be achieved with reasonable flow rates using the symmetrical flow because of the high viscosity of the solution. Instead, direct cross flow from the extra inlet and outlet in the nutrient delivery channel is used. With this side to side flow, over 90% of the gel solution is removed from the muzzle within 2 minutes (Figure 4.5). I chose this specific combination of concentrations for two reasons. First, the similar gelation times lead to more uniform immobilization. Second, higher concentration and thus higher viscosity solutions are more difficult to wash away from the muzzle area. This concentration is the highest, where a timely removal can be achieved.

#### **4.4.2 Temperature Characterization**

The goal of the platform is immobilization without altering physiology. *C. elegans* is generally cultured at 15-25 °C. Because the immobilization solutions are loaded either chilled (PF127) or prepared by heating (sodium alginate/gelatin) for the sake of simple setup. I therefore verified that the animals remain within the physiological range or are exposed to temperatures outside that range only for a very short time.

We used a previously reported fluorescent intensity temperature measurement technique<sup>44</sup>. I focused at the inlets of the trapping channels, as once the solution passed this point it can only get warmer from the surrounding material. It is also difficult to measure temperature inside the channels because of accumulation of dye in the PDMS and presence of animals. The average lowest temperature at the channel inlet is 12 °C (Figure 4.7). However, the immobilization occurs within 20 seconds. This means that the transition temperature of 17 °C has been reached. I can conclude that animals are

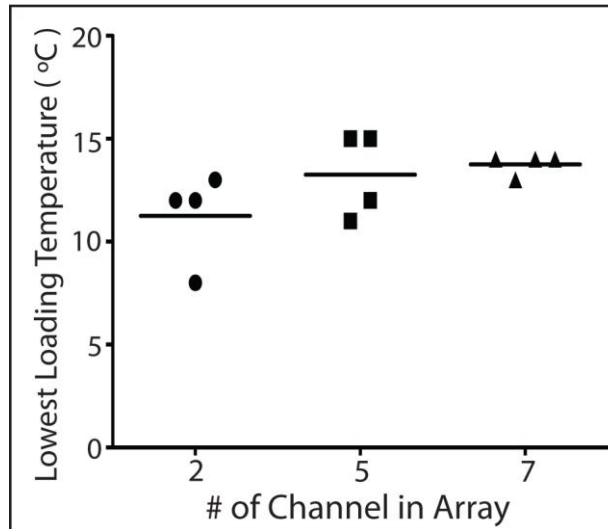


**Figure 4.7** The temperature of Pluronic F127 solution as measured at the inlet to trapping channels using a fluorescent intensity measurement technique. On average, animals are not exposed to temperatures lower than 12 °C. The lowest temperature occurs in the channels closest to the outlet of the loading chamber, where fluid exchange is the most rapid.

exposed to temperature outside their physiological range (15-25 °C) for less than 20 seconds.

We measured the temperature of the sodium alginate/gelatin solution using a standard thermocouple. First, the bulk of the solution has to be rapidly cooled to 40 °C. After this, 40  $\mu$ L of the solution can be withdrawn with a standard micropipeter. This process further cools the solution to 27 °C on average. The solution rapidly equilibrates to ambient temperature after loading because of the small thermal mass and the very high surface to volume ratio. This means that animals are not exposed to temperatures outside their physiological range during the experiment.

#### 4.4.3 Characterization of Nutrient Delivery and Animal Feeding

Once animals are loaded and immobilized, the device has to facilitate proper feeding. The ability to properly feed the animals is critical for experiments lasting over a period of several hours. Additionally, animals should not be exposed to high shear within the muzzles. I qualitatively observed the conditions in the bulk of the delivery channel and



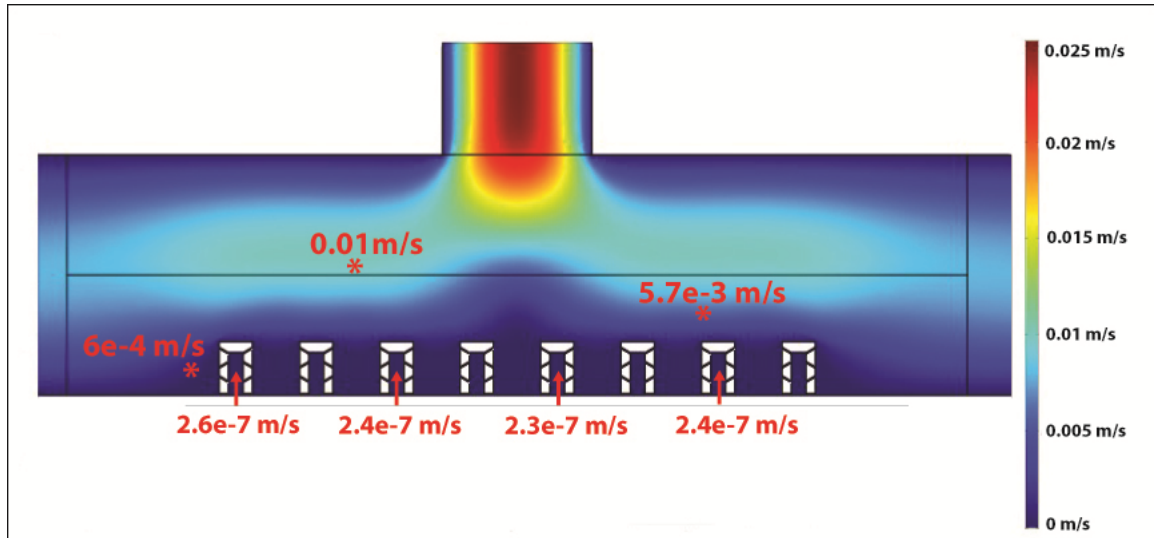


**Figure 4.8** COMSOL model of the velocity field surrounding the muzzle area. The results of the simulation show a five orders of magnitude decrease in velocity inside the muzzles when compared to the bulk of the nutrient delivery channel. The system was modeled as steady state using the Incompressible Navier-Stokes module. Inlet and outlet velocities were specified based on the flow rate used and the cross-sectional channel area.

in the muzzle area using fluorescent microbeads. As shown in Figure 4.9, the speed of the microbeads is much higher in the bulk than around and inside the muzzle traps. This leads to lower shear and higher residence time of bacteria. I verified this observation by performing a computation fluid dynamic simulation in COMSOL (COMSOL, Inc., Burlington, MA) (Figure 4.8). The model shows that the flow rate in the bulk of the channel is five orders of magnitude greater than the flow rate inside the muzzles, which is consistent with our observation.

A possible downside of lower shear and higher bacterial residence time is clogging from buildup of bacteria and formation of biofilms. I measured the rate buildup of bacteria inside the device without animals consuming them. For the period of the first 4 hours, the buildup, as measured by the average percentage of the surface area inside the muzzles and the total area in the bulk of the channel covered by bacteria, remains negligibly low (Figure 4.9). After 16 hours, the buildup is significantly increased. However, this device is intended for experiments up to approximately 4-6

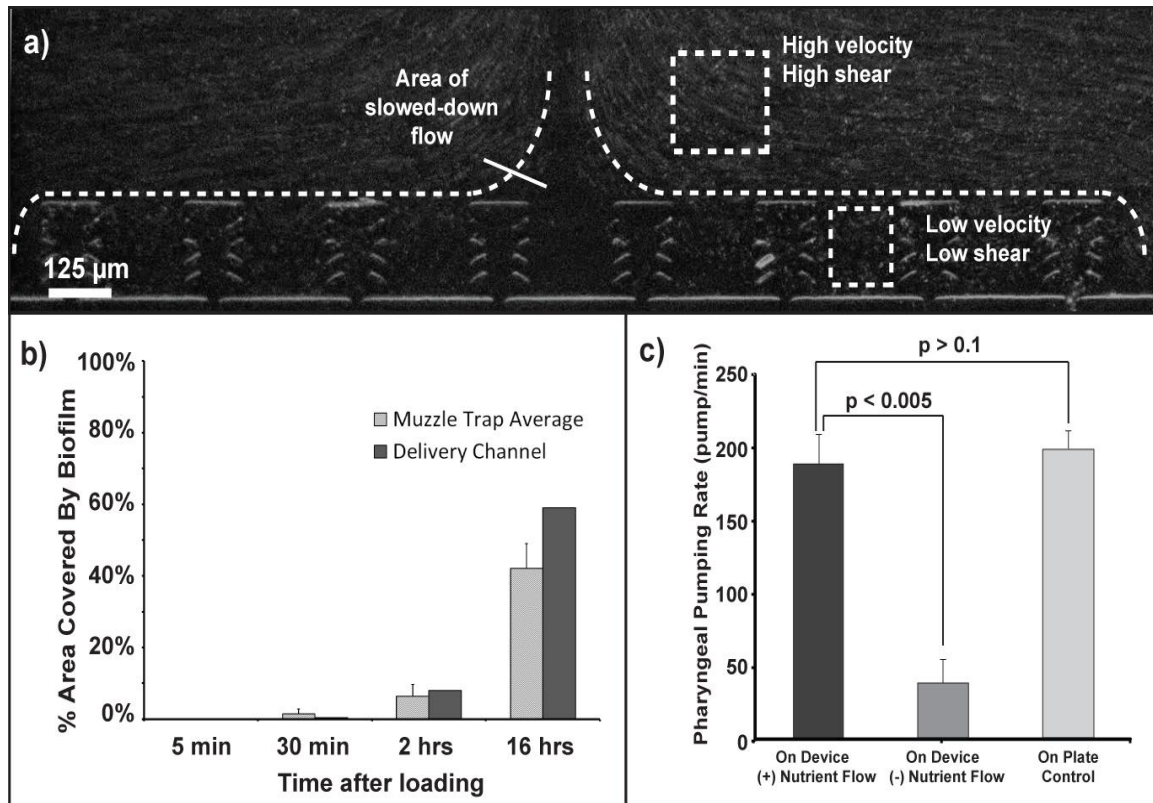


**Figure 4.9** Characterization of animals' environment and feeding on device. a) The muzzle design facilitates delivery of nutrients by allowing perfusion of bacteria. The design also slows flow inside and around the muzzle. I observed this effect qualitatively using fluorescent beads. In the bulk of the channel during long exposure the beads leave streaks. In the area of the muzzle I can see individual beads. This indicates much lower flow rate, leading to lower shear and higher residence time of bacteria. b) Lower shear and higher bacterial residence time can lead to build-up of bacteria and potential clogging. I measured the percentage of the area covered by biofilm in the muzzle and bulk of the channel. Over 2 hours (approximate period of a standard experiment), this effect is negligible. c) Pharyngeal pumping is an excellent indicator of animals feeding properly. Compared to animals feeding on standard nematode growth plates, the difference is statistically not significant ( $p > 0.1$ ). However, when animals on device are not being provided with nutrients or are improperly immobilized, the pumping rate is significantly lower.

hours, as most processes which require this type of imaging do not last longer. As such, the buildup over such a long period does not pose a problem.

Next I tested whether the animals themselves actually feed while immobilized. Non-starved animals show a significant decrease in pumping rate when they do not sense bacteria in the environment. [157, 158] Therefore, normal pumping rates suggest

sufficient amounts of nutrients in the animals' environment. I observed the pharyngeal pumping rate of animals immobilized on the device as compared to pumping on plates in normal culture conditions. Immobilized animals were recorded 30 minutes after loading over a period of 2 minutes. The comparison between animals trapped in the device and animals on standard nematode growth plate with a bacterial lawn showed no statistical difference (Welch's t-test) (Figure 4.9). However, when nutrient flow was turned off or animals could not feed properly due to incorrect positioning, the pumping rate was significantly lower ( $p < 0.005$ , Welch's t-test). This indicates that proper loading and nutrient delivery are critical for animals' continuing development on-chip.

#### **4.4.4 Immobilization of the Animal Body to Facilitate Long-term Imaging**

The last critical aspect for complete functionality of the device is the ability to image properly immobilized animals. I evaluated the positional shift of the body of animals immobilized within the gel while exposed to blue fluorescent light (as animals would be during experimental conditions). This is relevant because *C. elegans* is normally excited by blue light that causes increased body movement. [159] For the purpose of this experiment I imaged animals continuously over a period of 1 minute (Figure 4.10). Over this period, when frames from 0 seconds, 20 seconds, and 40 seconds are overlaid on top of each other, it is clear that the body remains perfectly immobilized, while the head is free to move inside the muzzle. This result shows the applicability for analysis of cell-wide fluorescent signals, such as calcium signaling, and for analysis of signals from networks of neurons. I were able to maintain animals immobilized in this fashion for up to 16 hours (Figure 4.10). At this point I were still able to observe expression of fluorescent markers, indicating normal physiological processes were not affected.

Next, I imaged animals over a period of 3 hours and observed the change in size of fluorescently labeled lipid droplets. *C. elegans* has lipid droplets in the intestinal cells for fat storage. It is known that genetics and diet have an effect on droplet morphology

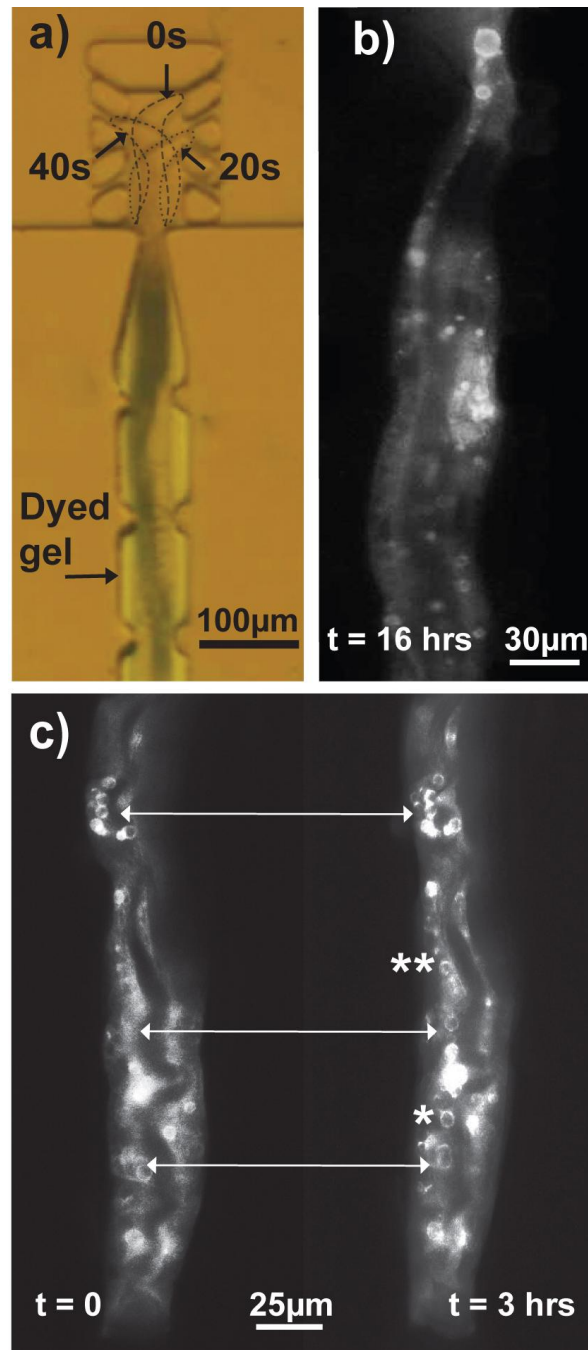


**Figure 4.10** Dynamic studies of *C. elegans* using C.L.I.P. a) While the animals heads are free to move, the body remains perfectly immobilized. In this figure, images from three time points are overlaid on top of each other. The animal's head is in a different position at each time point. Meanwhile, the body remains immobile. b) I have maintained animals trapped on device for up to 16 hours. After 16 hours I were still able to observe expression of fluorescent markers, indicating that physiology has not been affected. c) I were able to monitor animals over time. I observed the formation and development of lipid droplets labeled with R01B10.6:GFP over a period of 3 hours.

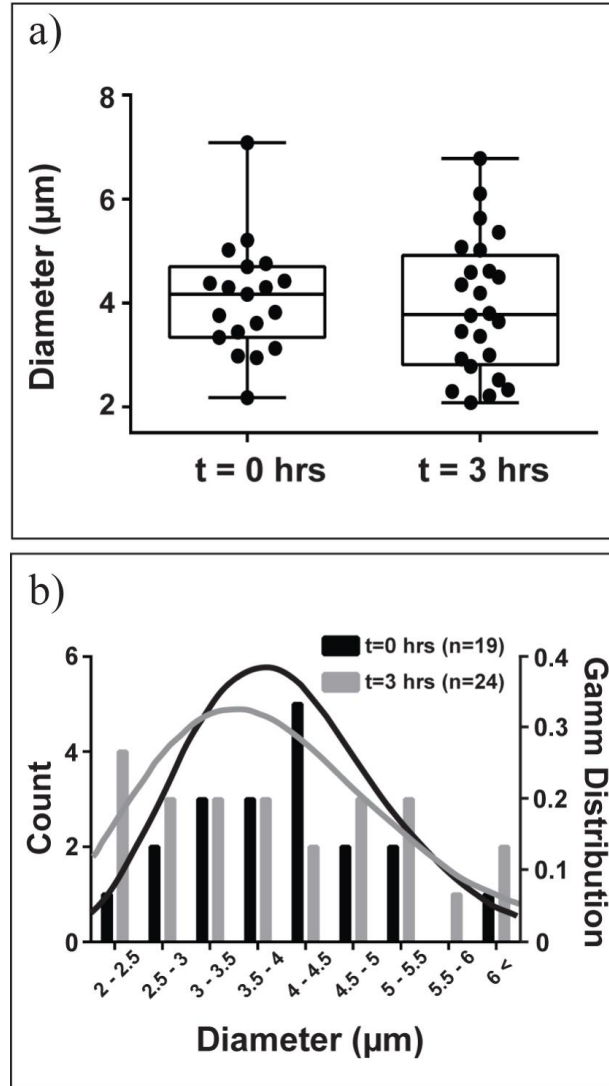


**Figure 4.11** Statistical analysis of dynamic changes. a) After three hours, the number of droplets with a large diameter ( $> 4.5 \mu\text{m}$ ) as well as very small diameter droplets ( $2 - 2.5 \mu\text{m}$ ) has increased. This is consistent with growth of existing droplets and formation of new small droplets. The box bottom and top represent the 25th and 75th percentile respectively, the center line is the median, and whiskers represent the min and max values. b) Over the period of the experiment, the distribution shifts to indicate appearance of new lipid droplets. Left y-axis corresponds to the histogram data, while the right y-axis corresponds to the fitted gamma distribution.

and size. [160-163] I imaged animals expressing R01B10.6:GFP, which labels a subset of lipid droplets (Y. Hao and H.Y. Mak, unpublished data) when observed at 40x magnification. I recorded images spaced at  $0.5 \mu\text{m}$  in the z-direction over a thickness of  $40 \mu\text{m}$ , which takes approximately 3 seconds. The images were then projected to a single

plane using maximum pixel intensity. If the animals were moving during the imaging, the projection would be smeared in the xy plane. Since this is not the case, I conclude that the animals are properly immobilized while simultaneously feeding.

We measured the diameter of the lipid droplets at the start of the experimental period and at the end of 3 hours. At this magnification on an epifluorescence microscope, I were only able to detect droplets larger than 2  $\mu\text{m}$ , while confocal microscopy may allow resolution of smaller droplets. [164] While the population did not show statistically significant changes in droplet size over the 3 hours of continuous feeding on-chip ( $p < 0.05$ , Welch's t-test), I observed an increase in the number of large droplets ( $> 4.5 \mu\text{m}$ ), and also detected an increased number of small droplets (2 - 2.5  $\mu\text{m}$ ) (Figure 4.11). The data suggest that growth of existing droplets and formation of new small-sized droplets is occurring over the 3-hour period, which is presumed the case but not observable in standard protocols (since anesthetics are usually used and feeding is not possible).

## 4.5 Conclusions

In this work, I have demonstrated a technique to immobilize *C. elegans* animals for continuous live imaging at physiological conditions. I verified that animals can be loaded and immobilized for experiments and that immobilized animals feed on a continuous flow of nutrients provided for them for the duration of experiments. If necessary, the channel array can be expanded to accommodate a larger number of trapped animals and improve the speed of data acquisition. Most importantly, this technology allowed us to observe the type of dynamic change which could previously be observed only statically. This can contribute to elucidating the true nature of this and many other processes, such as understanding the effect of learning on synaptic physiology, mapping of functional network connections of the nervous system, and better understanding of neuronal regeneration.

## CHAPTER 5      *C. ELEGANS* LIFE-SPAN ON CHIP WITH INTEGRATED TEMPERATURE CONTROL AND HIGH CONTENT STUDIES

This chapter describes the development of a bench-top system for performing large scale *C. elegans* life-span experiments in a highly controlled fashion. Studies of life-span in *C. elegans* are aiming to explain the genetic regulation of ageing, the various pathways involved in the process, and how environmental and somatic signaling is integrated into the regulation process. Several major pathways, the critical components, and their effect on ageing have been identified, such as the DAF-2 insulin like receptor and DAF-16 fork head transcription factor pathway [165-169], the *clk-1* pathway [170-173], and various somatic signals involved in modulation of development and metabolism [174-178].

Practically performing these studies is extremely labor intensive. Large numbers of animals are required for each run; up to 200 animals may be required at the start to account for loss during the experiment and to get statistically significant data. Additionally if individual tracking is necessary, each animal needs a separate agar plate. If animals need to be moved between plates for removal from progeny or because of dietary restriction, loss from physical damage may occur. The issue of progeny removal can be eliminated by treating animals with RNAi or including the drug FUdR in the culture to induce parental sterility [179], but the drug itself may cause artifacts in life-span analysis of non-wild type animals. [180-182]

Environmental manipulation during experiments adds further complication. Temperature control of hundreds of agar plates requires incubator space, and bacterial lawns used in diet restriction protocols [183] may form with uneven thickness. Liquid culture based dietary restriction protocols eliminate this problem by providing a more uniform environment [179, 184-186], but do not eliminate the difficulty of handling animals. Performing other assays such as behavior analysis during ageing experiments is

practically extremely difficult due to animals handling and tracking requirements, yet could prove very useful. This is because many of the insulin-like-peptide signaling molecules are also involved in modulation of behavior. [187-191]. As discussed in Chapter 1, Hulme *et al.* in 2010 [87] and Xian *et al.* in 2013 [88] both presented microfluidic systems for life-span analysis on chip, but neither combines the full set of features to tackle the presented difficulties.

The system described in this chapter aims to be a comprehensive tool for life-span on chip studies. It takes advantage of microfluidics for handling, trapping, and culturing of *C. elegans* without loss due to manual handling during the experiment. The microfluidic device provides precisely controlled liquid dietary restriction conditions via liquid DR protocols, with the ability to expose animals to chemical agents with high temporal resolutions, and with individual tracking of animals for gathering data content such as metabolic rate indicators, behavior response change with age, and potentially even measurement of neuronal activity via calcium imaging. This data would typically not be obtainable during standard life-span experiments.

In addition, a bench-top temperature controller has been designed to eliminate the need for incubators during these experiments. High heat conductivity construction materials are used for the platform of a Peltier-based temperature control stage. This allows for achieving of even temperature within microfluidic devices placed on this bench-top controller throughout the full height of the channels and chambers containing animals. Lastly, a fluid delivery system based on a peristaltic pump fluid recirculation method can be used to connect multiple devices to the same source of nutrient solution and perform experiments in parallel. The main circuit recirculates fluids at a high flow rate to keep bacteria mixed. Each device can be connected to this circuit at any time without disrupting the main flow or flow to already connected devices and while maintaining even flow rates across all connected devices. In combination, the bench-top temperature controller and the fluid delivery system allow for parallel running of up to 14 devices for



highly scalable high throughput experimentation without the need for incubators. This work was completed in partial collaboration with Michael Youmans.

## 5.1 General System Overview

The basic operating principle of this system is depicted in Figure 5.1a. The system operates two stages. The first stage is initial loading; a suspension of *C. elegans* age synchronized to the L4 larval stage in nematode buffer is loaded into the device for trapping. Trapping occurs passively without any direct researcher involvement via flow dynamics and feature design. The direction of flow is from the device inlet to the outlet and liquid flow is set at a constant rate via withdrawal by a syringe pump. From the animal traps, animals are moved to culture chambers by pressuring the device and opening a path between the trap and its corresponding chamber.

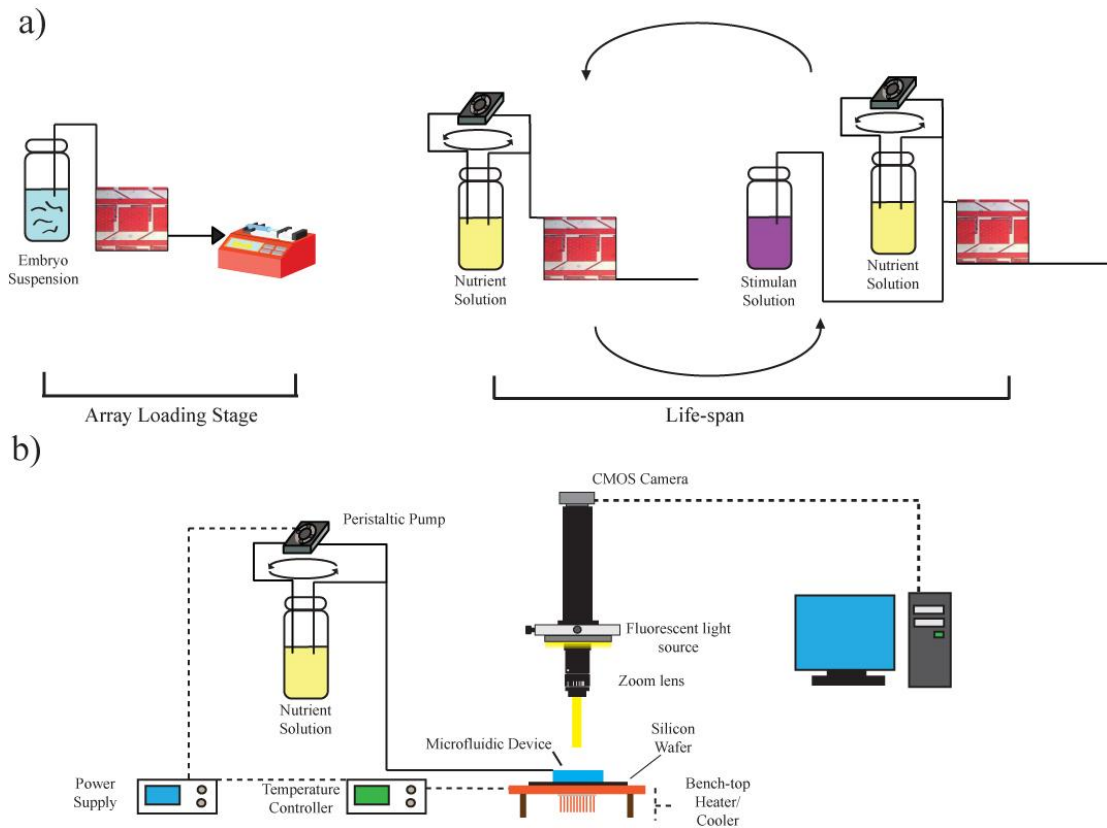


**Figure 5.1** Life-span system overview. a) General system operation overview. b) Main system components

The second stage is the culture stage; OP50 *E. coli* suspended in nematode buffer are delivered to the device and flow through the culture chambers containing *C. elegans*. During this stage, the device is connected to a peristaltic pump based fluid delivery system and the direction of flow inside the device is reversed from outlet to inlet. Additionally, the flow is periodically reversed. Both flow modes serve to prevent chamber clogging with bacteria and help remove progeny.

The whole system consists of the microfluidic chip placed on a bench-top temperature controller, and of the peristaltic pump fluid delivery system (Figure 5.1b). A video zoom lens in combination with a CMOS camera, fluorescent light source, and silicon wafer below the microfluidic chip serving as a mirror is used to image animals during life-span experiments in a pseudo dark-field mode.

## **5.2 Adaptation of Existing Designs for Life-Span on Chip**

In this thesis I have presented systems for loading and trapping of *C. elegans* or their embryos in individual culture chambers for developmental studies. Isolation in individual chambers has many advantages, such as per-animal tracking, precise and uniform environmental control and targeted exposure to stimulants. This principle has thus been applied in the design of a life-span chip as well. However, there are certain differences in functional needs arising from the different time scales for developmental and life-span studies.

First, developmental studies focus primarily on the period from embryonic to young adult stage. This necessitates trapping of single animals inside the chamber of all developmental stages and sizes; not even the earliest L1 larvae may escape. However, life-span experiments begin at the L4 stage and progress until death, which means trapped animals lay embryos from which L1 larvae hatch. For life-span studies, this progeny has to be removed and only the original animal retained. Obviously, the passive chamber trapping mechanism thus has to be adapted to fit this requirement.

Second, developmental studies occur over a period of several days, with generally 3-4 days of length being the upper limit. During this time, nutrients have to be delivered to the animals with minimal bio-fouling and clogging of chamber inlets. Fouling and clogging can be alleviated with surface treatments, but with increasing time the risk of clogging is ever increasing. Life-span studies occur over a period of several weeks to several months and thus the chips used for such studies are very likely to clog. Because of this, the chamber inlets have to be adapted to trap animals, yet not be vulnerable to clogging and stopping of flow into culture chambers. Lastly, since L4 larvae are used as the starting point for these life-span experiments, passive loading has to be adjusted for these animals.

In our laboratory, Kwanghun Chung and Mei Zhan have developed a microfluidic device for on-chip behavioral studies, which uses passive loading of adult *C. elegans* into individual chambers. [85]. Passive loading relies on trapping animals in appropriately dimensioned channels branching off a main fluid delivery channel. These channels are connected to a culture chamber by a narrow restriction channel, similarly to that in the embryo trap from Chapter 3. Also similarly, the narrow restriction channel has a two layer design, with the first 5-10  $\mu\text{m}$  in the z-direction being wide (25+  $\mu\text{m}$ ), and the remaining height of the restriction channel being only 10  $\mu\text{m}$  wide. This design stops the loaded adult animals in the channels, and allows them to enter the culture chamber only upon pressurization of the device, which opens the restriction. The outlets of their circular chambers are formed by an array of closely spaced pillars. This design became the basis for the development of a life-span on a chip.

The modifications made to the device are depicted in Figure 5.2. The first iteration was a reproduction of the design by K. Chung and M. Zhan in the form of square chambers to achieve higher chamber density on chip. The pillars forming the chamber outlet were round. This outlet design had very poor trapping design, although the loading results were satisfactory (Table 5.1). In the next set of iterations, the pillars were changed to

square, rectangular, and rectangular with smaller spacing – each change increased the trapping efficiency. Then, two sides of the square chamber were turned into outlets instead of one. This did not have an effect on trapping, but provided for more hedging against the risk of clogging. In the last iteration, the loading “pinch” restriction channel design was changed with the goal of improving the loading efficiency. Because the animals used in this device are smaller (late L3/early L4), animals were slipping through the restriction and causing double loading.

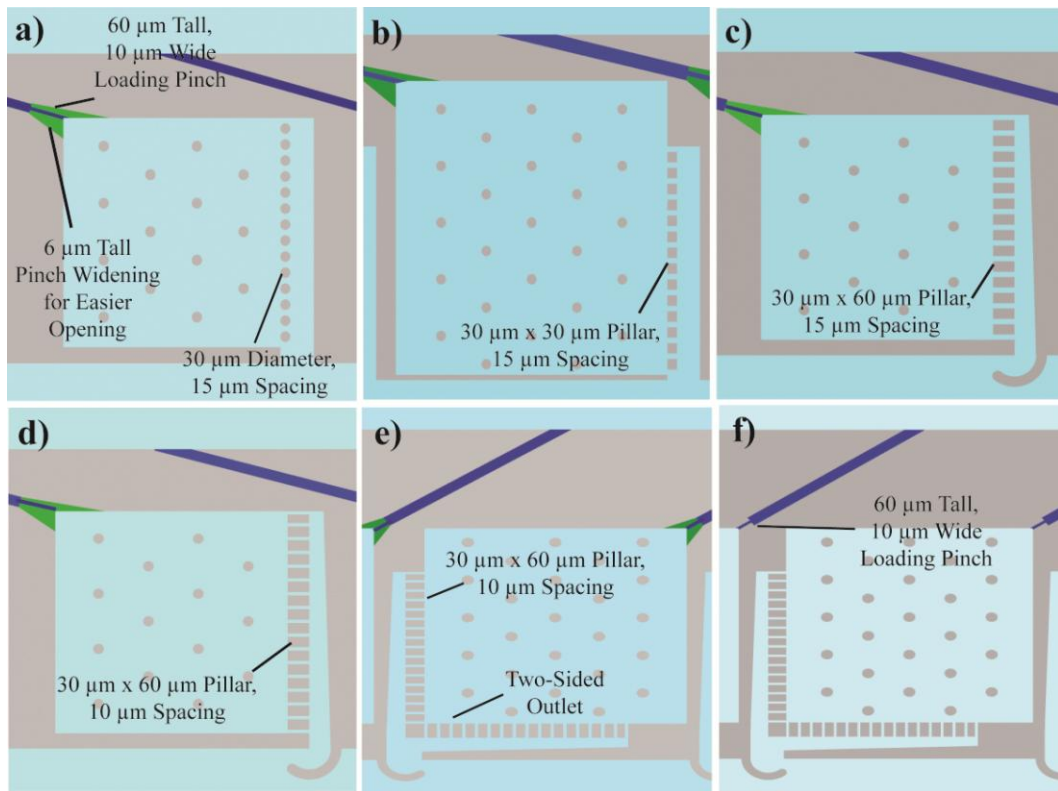


**Figure 5.2** Design iterations for efficient loading and trapping of L4 *C. elegans* larvae. a) Design reproduced from [85]. b) Outlet pillars change to squares. c) Outlet pillars changed to rectangles. d) Spacing between pillars decreased. e) Two sides of a culture chamber used as outlets. f) Loading channel restriction changed to single width across the whole height.

**Table 5.1** Loading and trapping efficiency of design iterations.

	Design A	Design B	Design C	Design D	Design E	Design F
L4 Loading Efficiency	~ 70%	~ 70%	~ 70%	~ 70%	~ 70%	85%
L4 Trapping Efficiency	< 10%	< 10%	~45%	87%	90%	90%

An additional change made is not to the design of the chambers, but to which features are used as inlets and outlets and the direction of flow. During loading inlets chamber inlets and outlets are used as described. However, during culturing, the direction of flow is reversed. This way, the outlet pillar arrays become a large row of inlets. The inlet restriction becomes the chamber outlet. This is done to simply increase the number of inlets and eliminate the risk of clogging from bacteria. Lastly, the flow direction may be periodically alternated to help with the removal of progeny.

### 5.3 Final Design

#### 5.3.1 Microfluidic Device

The final microfluidic design is an array of culture chambers as shown in Figure 5.3. These chambers are loaded passively via the previously described restriction channel mechanism, and contain trapped animals via an outlet pillar array, also as described. The easily scalable array offers individual culturing of animals during life-span experiments in a crawl-like environment while simultaneously taking advantage of the benefits of liquid dietary restriction methods. It also allows for highly controlled chemical stimulation and studies of behavior during aging. The features of the microfluidic device are 70  $\mu\text{m}$  tall to accommodate adult sized animals.

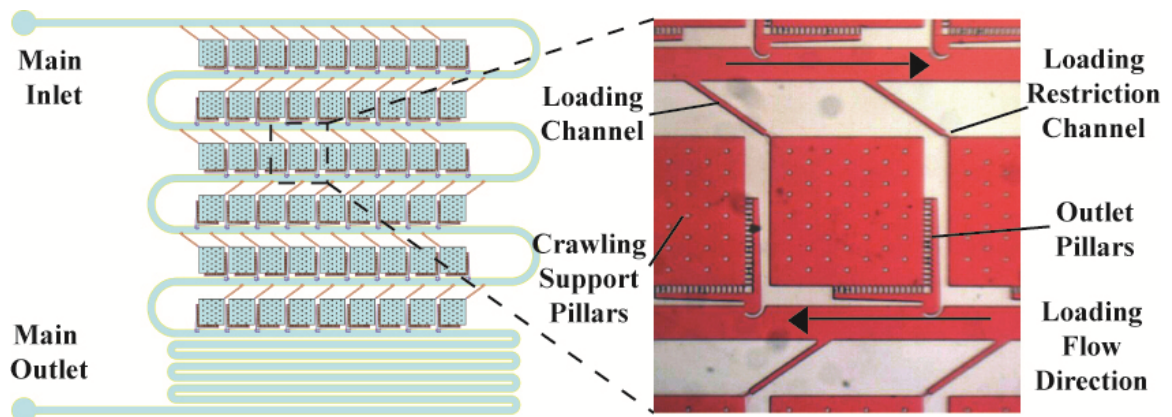


**Figure 5.3** Design of the microfluidic chamber array and the individual chamber features.

The microfluidic device is prepared in a simple loading procedure described in Figure 5.4. Three interconnects are used in the procedure, two 24 gauge holes and with metal pins to connect to tubing, and one 14 gauge hole as a loading reservoir. For loading, the outlet of the device is connected to a syringe pump capable of withdrawing fluid via one of the 24 gauge pins; the other pin is connected to a fluid filled syringe. This syringe is used for rapid pressurization of the device. The 14 gauge hole is left open as a reservoir for loading solution. First, the device is pressurized via the syringe pump while holding the other interconnects closed. Next, the 14 gauge hole is opened until completely filled with fluid, at which point the syringe pump is set to withdraw fluid at 2 mL/hr. Solution of L4 *C. elegans* larvae is loaded into the reservoir and the animals are pulled through the device and passively loaded into the loading channels. After the array has been filled, the reservoir and outlet are closed and the device is rapidly pressurized via the attached syringe to open the restriction and push larvae into their respective chambers.

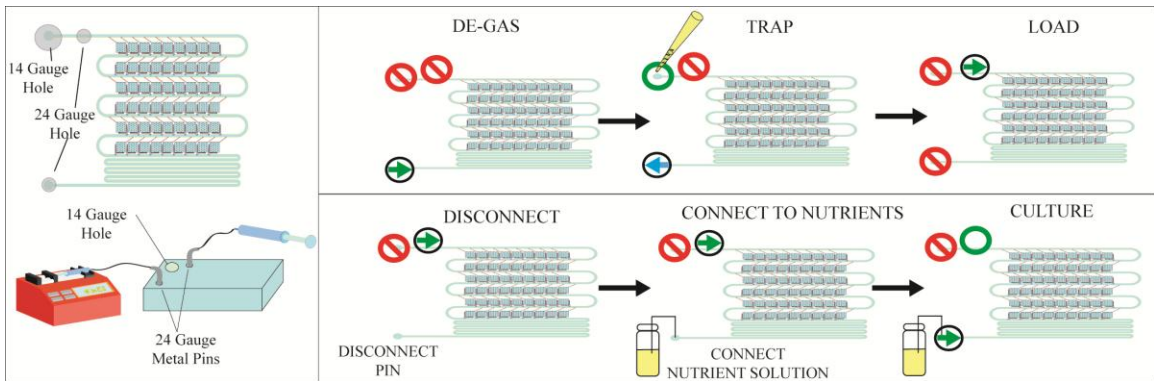


**Figure 5.4** Step-by-step preparation, loading, and re-connection procedure.

After this, the device is re-connected for culturing. First, the syringe pump connection is removed while the device is mildly pressurized by the syringe to not allow for back flow or introduction of gas bubbles. The outlet is then connected to a nutrient solution fluid delivery system for large scale parallel experimentation. The syringe is disconnected and the tubing connected to a waste collection reservoir, allowing the solution to flow through the device. The flow is opposite in direction to that during loading. This turns the

chamber outlets into a large number of inlets to minimize the risk of clogging. If only a single experiment is being run, the syringe pump may be used to drive fluid through the device. In this case, a syringe pump is connected to the inlet 24 gauge pin, while the outlet is connected to a nutrient solution reservoir. The syringe pump then withdraws liquid, to maintain the correct direction of flow.

### 5.3.2 Fluid Delivery System

The fluid delivery system is designed to deliver nutrient solution to multiple devices simultaneously with consistent flow rates. The devices can be connected or disconnected at any time without disturbing the flow to the remaining connected devices. The principle of the system depends on peristaltic pump fluid delivery. A Watson-Marlow 400/A peristaltic 300RPM pump drives fluid through a main re-circulation loop. The flow rate through this loop is approximately 15 mL/min. The high flow rate prevents bacteria from settling and keeps the main nutrient solution reservoir well mixed. Connection of devices to this loop is facilitated by 4-way switches. The flow to each device is negligible in comparison to the flow in the main loop due to the fluid flow resistance across the device, but sufficient to provide the necessary fluid exchange in each connected device.

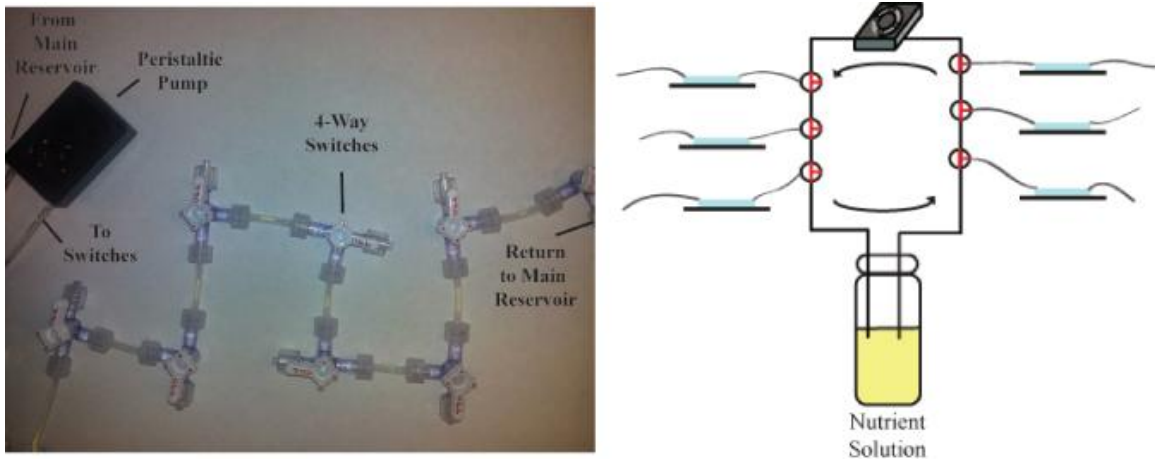


**Figure 5.5** The simple fluid delivery system used to provide even flow rates to multiple devices running in parallel.

### **5.3.3 Bench-Top Temperature Control**

The purpose of the bench-top temperature controller is to eliminate the need for incubators. Temperature control is critical for life-span experiments since temperature variation has significant effect on *C. elegans* metabolism, development, and life-span. In standard plate assays, incubators must be used. Microfluidic systems are no exception; the complete system would have to be placed inside an incubator for the duration of the experiment. The bench-top temperature controller is designed to maintain proper temperature on devices anywhere in the laboratory. The controller is a copper plate insulated on all surfaces except the top surface, on which microfluidic devices are placed (Figure 5.6). The temperature of the plate is regulated by a Peltier temperature controller. A copper heat spreader is attached to the Peltier unit for heat exchange. The heat spreader is ventilated by a pair of fans working in a push-pull setup within an air tunnel. Microfluidic devices mounted on silicon for better heat exchange are placed on the surface of the copper plate during an experiment. Even though the temperature in the devices themselves is not even, close to the silicon to a height sufficient to reach past the microfluidic features it matches the temperature of the silicon extremely well. Thus, by using the silicon mounting pieces for temperature measurement for a feedback control loop, temperature inside culture chambers of the microfluidic device can be precisely controlled.

### **5.3.4 Imaging of Animals on Chip**

Since the microfluidic devices are mounted on silicon for improved heat exchange, direct bright field imaging cannot be used. Instead, a technique previously developed in our laboratory by Jeffrey Stirman is used. By shining white light from a fluorescent bulb at the microfluidic device mounted on silicon square, the animals can be observed in a pseudo-darkfield mode instead. Because this mode of imaging relies on reflection off of the silicon surface, a stereo microscope cannot be used. This would lead to appearance of



ghost images. Instead, a single video zoom lens is used to record movies and images for data analysis.

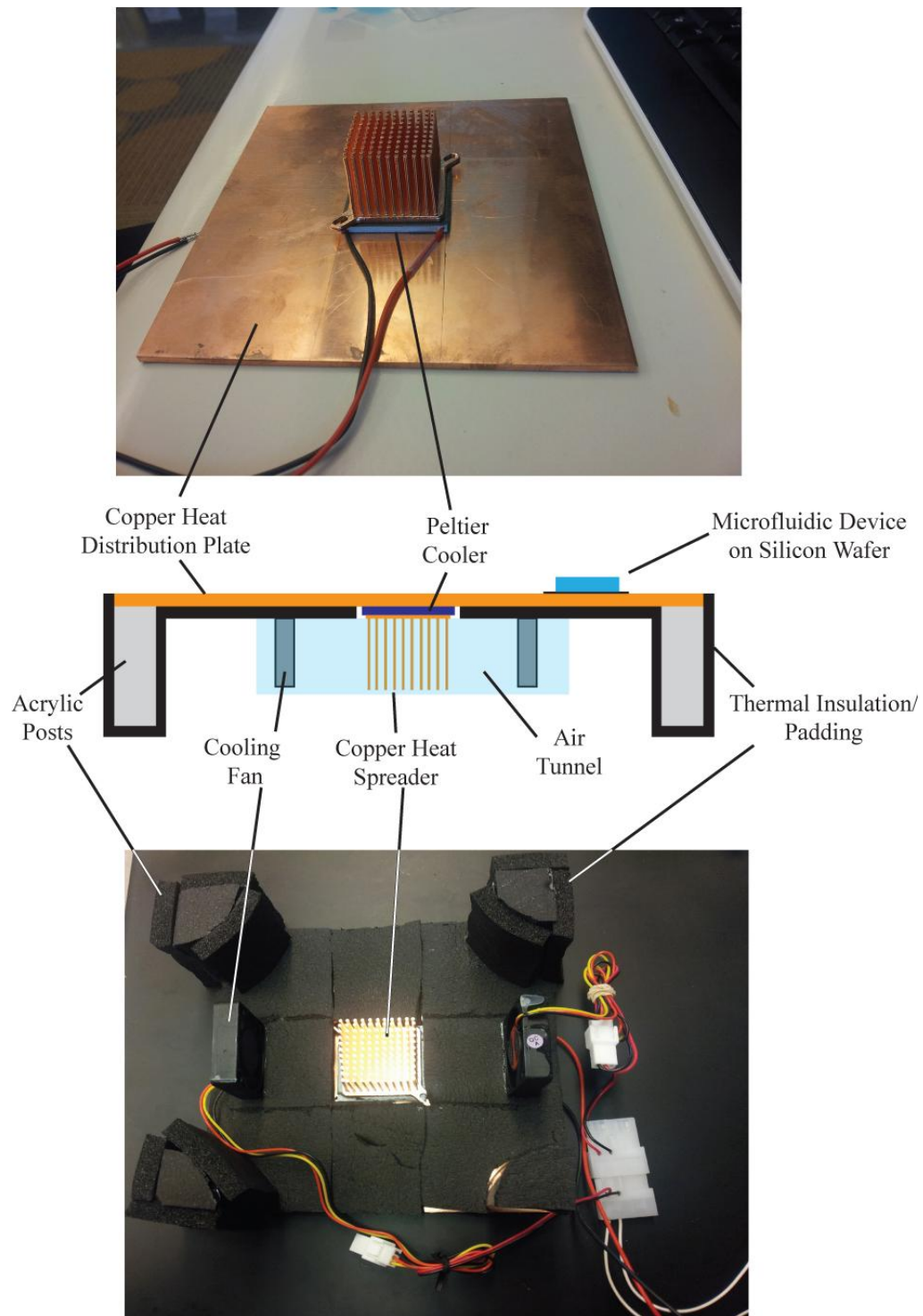


**Figure 5.6** Schematic of the bench-top temperature controller for microfluidic devices.

## 5.4 Methods

### 5.4.1 Fabrication

We fabricated all microfluidic devices in poly(dimethylsiloxane) using the method described in the previous chapters. The PDMS devices were then bonded to silicon wafer squares via oxygen plasma treatment for 20 seconds (PDC-32G plasma cleaner).

### 5.4.2 Solutions

Nutrient solution of standard nematode buffer with *E. coli* suspended in solution was prepared in the following fashion. 200 mL of autoclaved LB media was seeded with Streptomycin and Carbenicilin resistant *E. coli* and left to grow overnight at 37 °C. Then it was spiked with Streptomycin to a final concentration of 50 mcg/mL and continued to incubate for 30 minutes. Following, the solution was distributed into falcon tubes and chilled in ice water for 10 minutes. Then the solution was centrifuged at 4 °C for 5 minutes at 4000RPM, followed by the removal of the supernatant and re-suspension in M9 to the chosen concentration as determined by optical density measurements. Streptomycin and Carbenicilin were then added to a final concentration of 50mcg/mL each. Solution of repellent was prepared by diluting Nonanone in M9 by a ratio of 1:1000. Green dye was included to allow for determining the.

### 5.4.3 *C. elegans* Culture, Experimental Procedure, and Image Processing

#### 5.4.3.1 *C. elegans* Culture and Animal Preparation

*C. elegans* were cultured at 25 °C on standard nematode culture plates with OP50 without dietary restriction for at least two generations prior to the experiment. The animals were then placed allowed to lay embryos for 3 hours and removed from the plate. The age synchronized embryos remaining on plate were allowed to hatch and grow to the L4 larval stage, at which point they were loaded into the microfluidic device.

#### 5.4.3.2 Temperature Measurement

Temperature measurement to characterize the current-temperature response of the bench-top temperature controller was performed using a standard thermocouple and a custom designed thermistor probe. The probe consisted of a 10k, 3435, 1.6mm diameter thermistor (Digikey) mounted on a silicon square with thermal tape (VWR) and covered by thermal insulation foam.

#### 5.4.3.3 Flow Rate and Open Inlets Measurement

Measurements of flow rate through microfluidic devices connected to the fluid delivery system was performed by collecting fluid from the outlet for a period of 5 minutes and using micro-pipettors to exactly measure the volume collected from each device. Measurement of open inlets was performed by counting the number of inlets in each chamber containing animals at 1,2,6 and 14 days.

#### 5.4.3.4 Loading and Trapping Statistics

Loading statistics were recorded for each experiment. L4 larvae loading efficiency was recorded immediately upon loading. The trapping efficiency of L4 larvae was determined by measuring the number of L4 animals remaining trapped after 1 day. The L1 larvae removal efficiency was measured on day 5 by counting the number of chambers still containing L1 larvae. The actual percentage was determined in relationship to the number of chambers still occupied with single L4 animals 1 day after loading.

#### 5.4.3.5 Life-Span Experiment

The life-span experiment was performed at 23 °C using a syringe pump for fluid delivery with wild-type animals (N2 strain). Animals were loaded at L4 stage and the device was checked daily for remaining alive animals. The live-dead assay was performed by observing movement and exposing animals to blue light. Animals, which responded to stimulus after being labeled dead prior were re-labeled as alive.

## 5.5 Results

### 5.5.1 Microfluidic Device

#### 5.5.1.1 Loading

The device has been designed to optimize loading of L4 larvae; the loading channel length, width, and the channel restriction dimensions fit the average length and width of early L4 larvae. To achieve highest possible efficiency, animals loaded into channels have to hold loaded without squeezing into the chamber themselves and cannot be pushed into the chamber by a second animal loading into the channel. As shown in Figure 5.7a, L4 animals will 99.9% of the time hold loaded without squeezing in or getting pushed in. However, it is critical to use an age synchronized population, since L4 animals will push previously loaded earlier stage animals into the culture chamber over 60% of the time (Figure 5.7b).

The overall loading efficiency of the device after pressurization to push animals into their chambers is 85% (Figure 5.7c). The desired loading is one animal trapped inside a culture chamber. This is dependent not only on proper positioning of animals in loading channels, but also on the successful pressurization and pushing of animals into chambers. Errors in this process can lead to double loading or an animal only partially or not at all moving into the chamber.

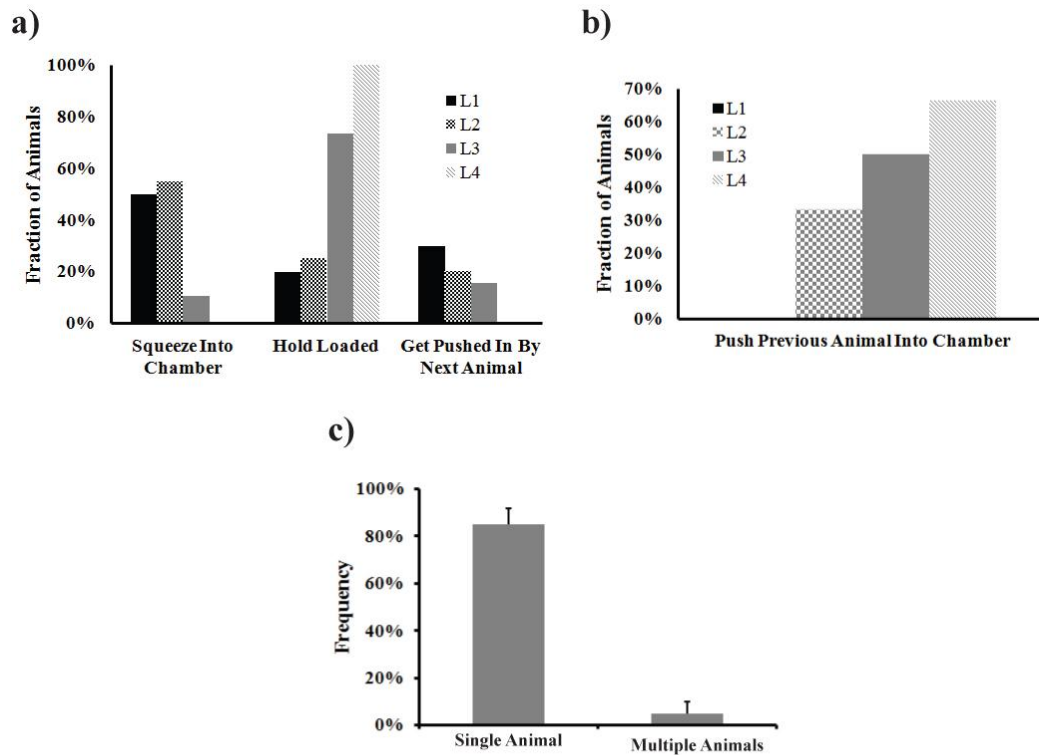


**Figure 5.7** Life-span on chip loading efficiency. a) Fraction of animals remaining properly positioned in loading channels during loading. b) Frequency of pushing previously loaded animals into culture chamber by a second animal loading into loading channels. c) Overall loading efficiency of L4 animals in the chip.

### 5.5.1.2 Trapping

The trapping of animals inside chambers once loaded has to be sufficient to prevent L4 larvae and older animals from escaping, while allowing progeny to be removed from the chamber. The ratio of the pillar spacing and the height of the chamber appear critical for this as shown in Figure 5.8. At a height of 45  $\mu\text{m}$  and 10  $\mu\text{m}$  pillar spacing, over 95% of L4 larvae are retained. However, only 18% of chambers with an originally single L4 animal loaded remain progeny free 5 days after egg-laying. An increase in spacing of pillars improves progeny removal, but decreases the trapping ability of chambers. At a chamber height of 65  $\mu\text{m}$ , a change in spacing from 10 to 15  $\mu\text{m}$  decreases the efficiency by over 30% with only a minor increase in progeny removal (2%). For the life-span chip,

the height of 65  $\mu\text{m}$  is critical to accommodate adult animals; the 10  $\mu\text{m}$  pillar spacing thus leads to the greatest final device loading efficiency. This final device efficiency is a multiple of the loading, trapping, and progeny removal efficiencies and is 74.9% for the device. Thus, on average 40 of those chambers will retain one animal per chamber without any progeny.

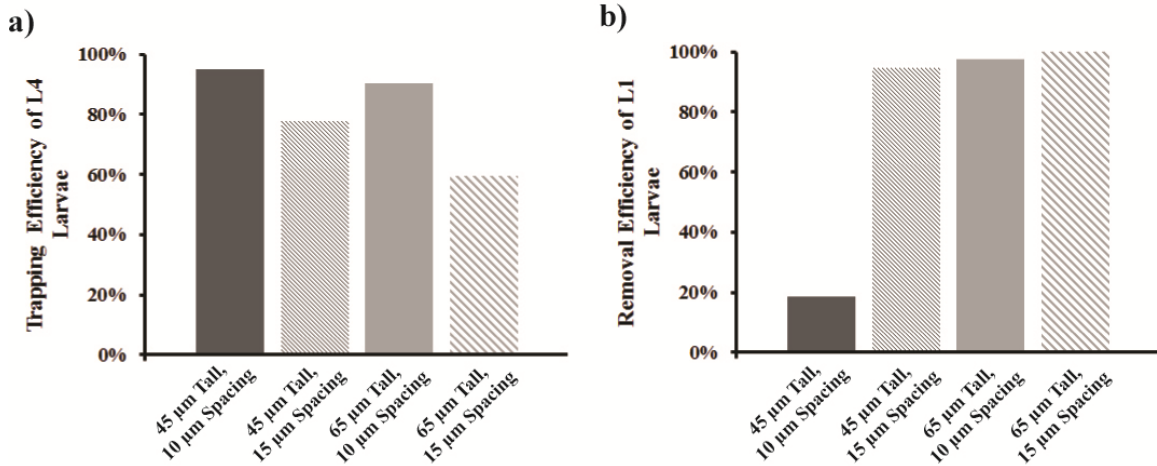


**Figure 5.8** Trapping efficiency on chip. a) Trapping efficiency of L4 larvae inside culture chambers. b) Removal efficiency of L1 larvae/progeny.

### 5.5.1.3 Reversal of Flow Direction During Culture Stage as Clogging Prevention

The reversing of the direction of flow is used to turn chamber outlets into an increased number of inlets. This serves to decrease the chance of complete chamber clogging by bacteria in the solution. As can be seen from Figure 5.9, this is indeed necessary as the average number of unblocked inlets during the experiment is approximately 25 per chamber containing *C. elegans*, indicating that several inlets clog on average for each chamber. However, a sufficient number of inlets always remains open to continue flow of nutrients to the animals.

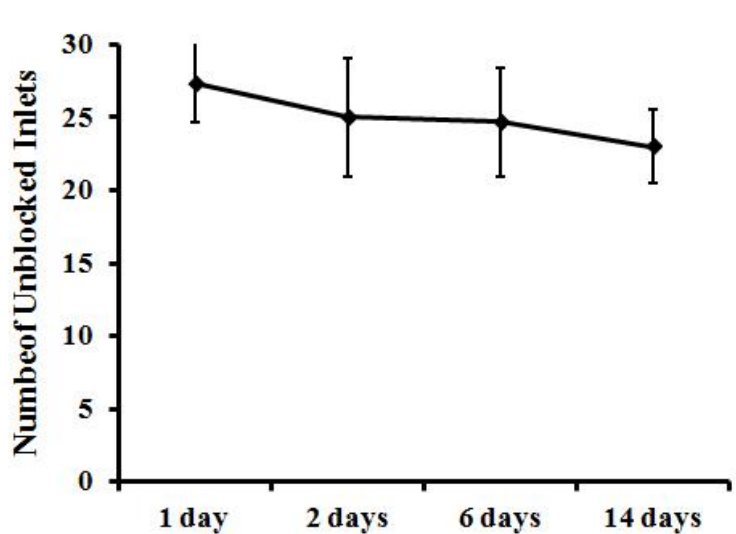


**Figure 5.9** Average number of inlets remaining unblocked during an experiment.

### 5.5.2 Temperature Control

The principle the bench-top temperature controller depends on is the matching of temperatures between the silicon substrate and the PDMS device to a minimum required height. This height is represented by the height of the microfluidic features housing *C. elegans*. As long as the channels and culture chambers are at a temperature matching that of the silicon substrate, the silicon itself can be used for temperature measurement for a closed-loop thermal control system.

I performed a COMSOL simulation of microfluidic devices being cooled or heated on the bench-top controller as they would be during a regular experiment (Figure 5.10). Devices were placed in the model as they would be on the physical controller. Such an arrangement leads to centered and corner devices (Figure 5.10a). The model was performed with accurate dimensions and for steady state heat transfer. The boundary conditions at insulated surfaces (all except the top), the top of the plate and the devices were set to heat transfer. The heat transfer coefficient values used corresponded to natural convection of a flat plate (range 2-20 W/m<sup>2</sup>·K). The materials used were copper, silicon

and PDMS. The general equation solved was  $\nabla \cdot (\cdot k \nabla T) = Q$  . The total number of elements was  $6.2^{e6}$  with mesh quality set to extra fine.

I compared the resulting temperature at the center of a device and at the corner of a device (Figure 5.10a). I modeled cooling from room 25 °C ambient temperature (Figure 5.10b-c) and heating from 15 °C ambient temperature (Figure 5.10d-e). All case scenarios showed temperature gradients within the bulk of the PDMS microfluidic device (light blue). However, the temperature in the silicon (grey) and the region of interest within microfluidic devices (dark blue band) for any situation matched very closely independent from the heating/cooling or the temperature difference between device and ambient temperature.

Since only natural heat convection is assumed, I modeled the effects of across a range of natural convection heat transfer coefficients for a flat surface. The coefficient did have an effect on the shape of the gradient in the bulk of the PDMS of the microfluidic devices. However, again in the area of interest the temperatures remained even and matched the silicon temperature independently of the coefficient value (Figure 5.11a). Figure 5.11b shows a summary of all the individual cases and the corresponding height within the PDMS devices, within which the temperature matches the silicon temperature to within  $\pm 0.3$  °C. The line indicates the height of the microfluidic features. For all cases, either matches or significantly exceeds the minimum height requirement. The only insufficient case is the extreme case of heating a device to 25 °C from 15 °C ambient at a natural convection heat transfer coefficient of  $20 \text{ W}/(\text{m}^2 \text{ K})$  and only at the extreme corner of the device.



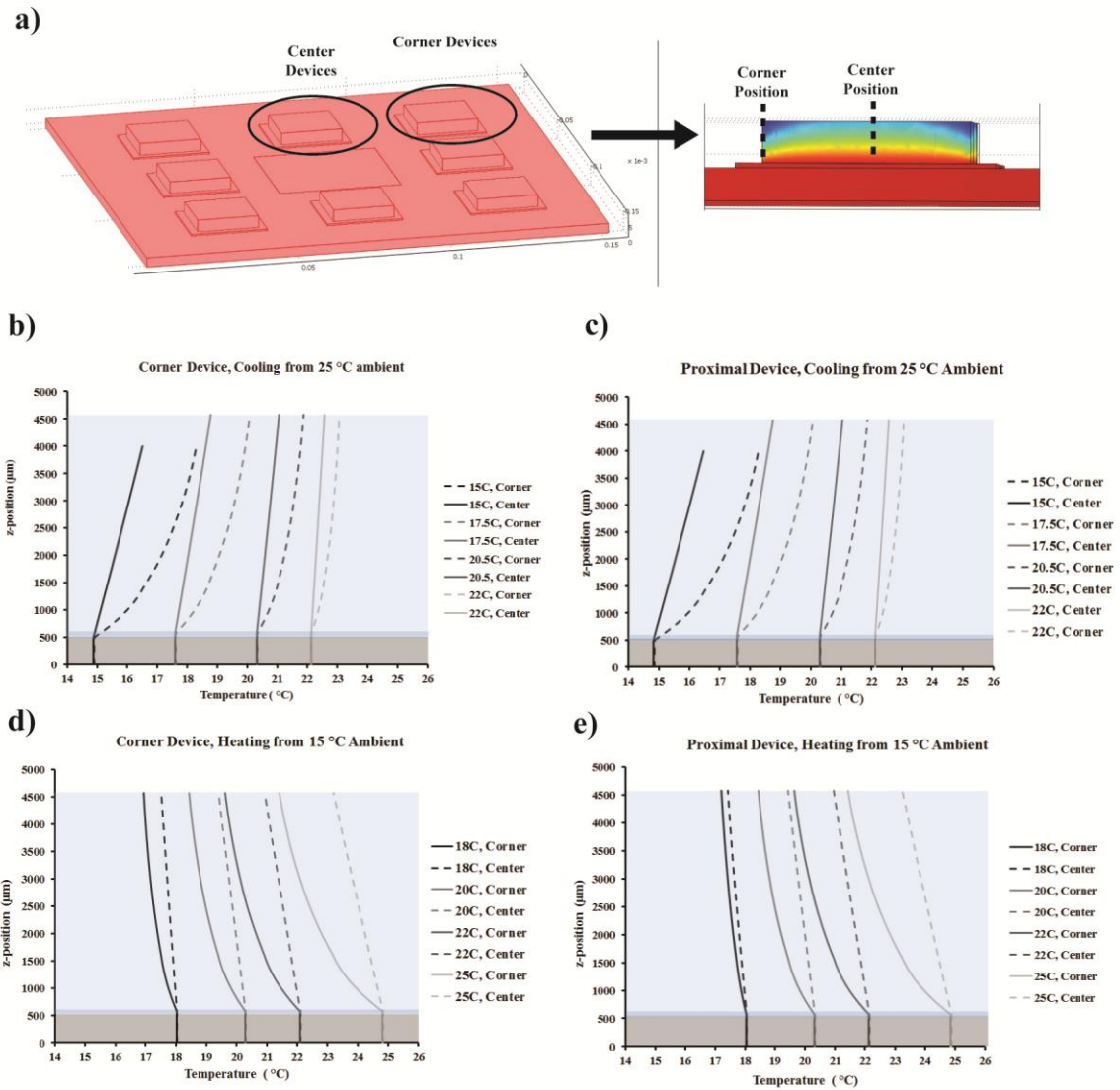


**Figure 5.10** Results of the temperature distribution simulation. a) Arrangement of the COMSOL simulation and the location of temperature data gathering within the microfluidic devices. b-e) Simulation of different case scenarios. Light blue background indicates PDMS bulk, grey indicates silicon, and the dark blue band indicates the area of interest within the microfluidic device. b-c) Cooling from 25 °C ambient. d-e) Heating from 15 °C ambient.

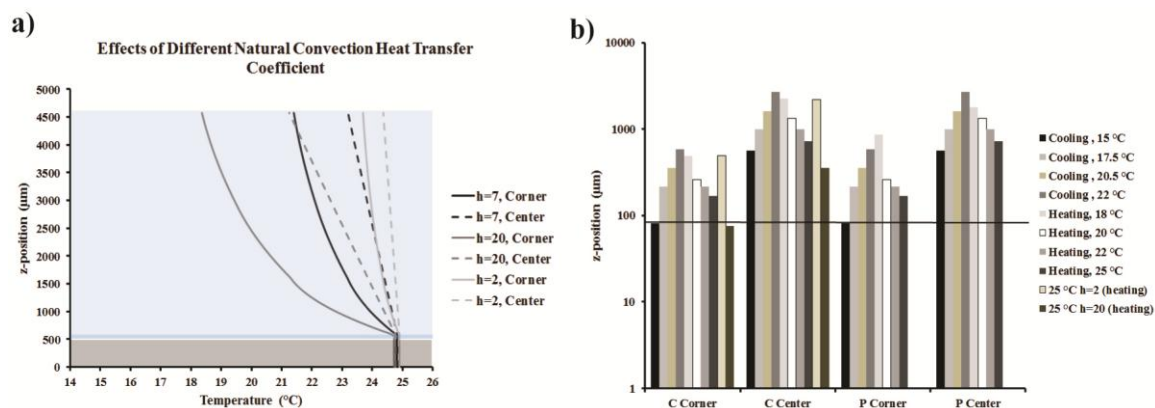


**Figure 5.11** Summary of simulation results. a) Effect of varying the natural convection heat transfer coefficient on the temperature gradient. b) Summary of all cases. The z-positions indicate the height up to which the PDMS temperature matches that of the silicon to  $\pm 0.3$  °C. The line indicates the height of microfluidic features within the PDMS.

I measured the temperature at the interface between the silicon and the PDMS of a sample device placed on the temperature controller and compared this value to the set point of the temperature regulator and to the reading provided by a custom made thermistor probe. The probe consists of a thermistor mounted on a silicon square via thermal tape. The 1.6mm-diameter thermistor is covered by thermal tape as well and a piece of insulating padding is attached over the whole assembly. The silicon square is placed on the temperature controller as a device would be.

Figure 5.12 shows the difference between the set point, the thermistor probe reading, and temperature measurement via a micro-thermocouple is minimal. The difference is at most 0.2 °C across the whole range of steadily maintained temperatures, whether the system was cooling or heating from the 23.5 °C room temperature. This shows the temperature controller truly is applicable to maintaining desired temperature on microfluidic devices in the laboratory without the need for incubators.

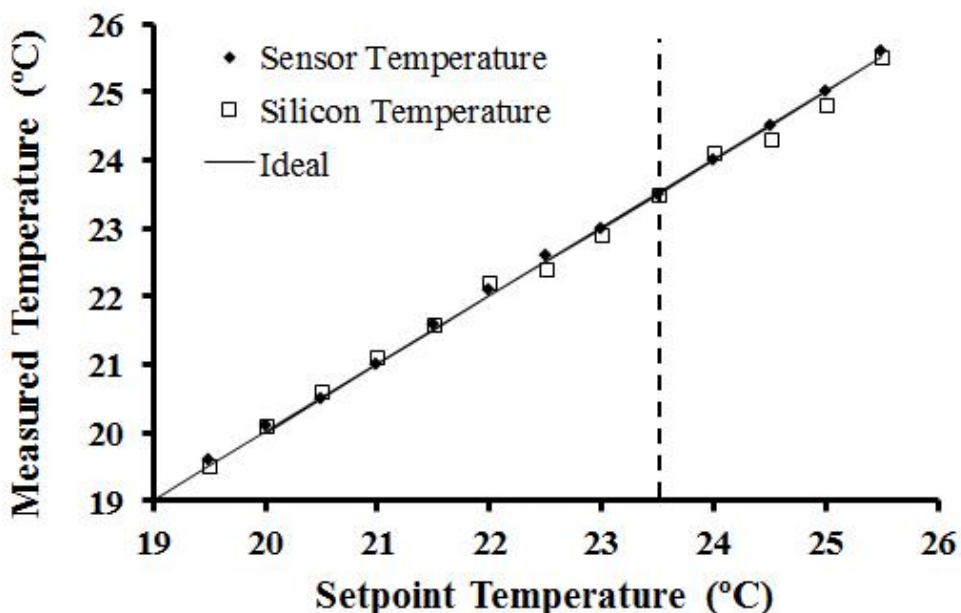


**Figure 5.12** Results of temperature measurement of devices placed on bench-top temperature controller. The custom thermistor sensor, the temperature of silicon at the silicon-PDMS interface, and the desired temperature match up closely across the range of temperatures. The dashed line indicates the ambient temperature during the experiment, 23.5 °C.

### 5.5.3 Fluid Delivery

The goal of the peristaltic fluid delivery system is to be able to connect devices at will without significantly affecting flow rates in other devices, such as would be the case with a direct flow splitter for example. This is enabled by the high ratio of flow rates in the main loop compared to flow rates across a device. The flow rate in the main loop is ~15 mL/min, or 900 mL/hr, which compares to less at most 0.6 mL/hr through an individual connected device (Table 5.2). Thus, each device draws at most 0.07% of the flow through the main loop. I analyzed the effect of connecting multiple devices on the average device flow rates. As can be seen in Table 5.2, connecting additional devices tends to decrease the flow rate across each device. This effect however is less dependent of the position where the device is connected, and depends more on the total number of devices. Additionally, the larger the resistance to flow across a device (i.e. larger arrays have greater resistance), the low the effect of adding devices is on flow rates. Thus, the larger

the array, the steadier the flow delivered to each array will be. This is critical for large-scale parallel experimentation and scaling of arrays to accommodate more animals. Lastly, the lowest flow rates measured were still sufficient to exchange the total volume of liquid in a large array in less than 40 seconds.

**Table 5.2** Results of flow rate measurement through devices connected to the peristaltic fluid delivery system.

Flowrate (mL/hr) Through Devices Connected to the Fluid Delivery System												
Array Size:	Large	Small	Large	Small	Large	Small						
# of Connected Devices	Device 1	Device 2	Device 3	Device 4	Device 5	Device 6	All Device Mean	StDev	Large Array Mean	StDev	Small Array Mean	StDev
	1	0.42						0.42	0	0.42		
2	0.42	0.59					0.50	0.119	0.42		0.59	
3	0.43	0.60	0.41				0.48	0.105	0.42	0.017	0.60	
4	0.35	0.49	0.37	0.47			0.42	0.071	0.36	0.017	0.48	0.017
5	0.35	0.48	0.35	0.43	0.35		0.39	0.062	0.35	0.000	0.46	0.034
6	0.35	0.41	0.37	0.44	0.32	0.34	0.37	0.046	0.35	0.024	0.40	0.055
All Runs Device Average	0.39	0.51	0.38	0.45	0.34	0.34						
StDev	0.042	0.080	0.025	0.018	0.017	N/A						

#### 5.5.4 Life-Span On Chip

To verify the ability of the device to perform full life-span experiments, I performed a pilot study using wild type N2 animals (Figure 5.12). In this particular experiment, fluid was driven via a syringe pump. Nutrient solution at an  $OD_{600}=2.5$  was delivered to the animals. The number of remaining live animals was recorded daily (except between day 10 and 12) via observing movement and response to blue light exposure for stationary animals, which normally triggers an evasive response [159]. Each chamber was tracked individually, which enabled re-classification of a “dead” animal into “live” after responding to stimulus two days after being classified as “dead” (animal #16 between days 6 and 8).

I compared the results to data previously reported by Houthoofd *et al.* in 2003 [179], data which was obtained by culturing animals on standard plates with a spread bacterial lawn. The life span curve does show a shorter maximum life span, but the experimental results

are highly comparable. This indicates the system is a viable alternative for performing life-span on chip studies.

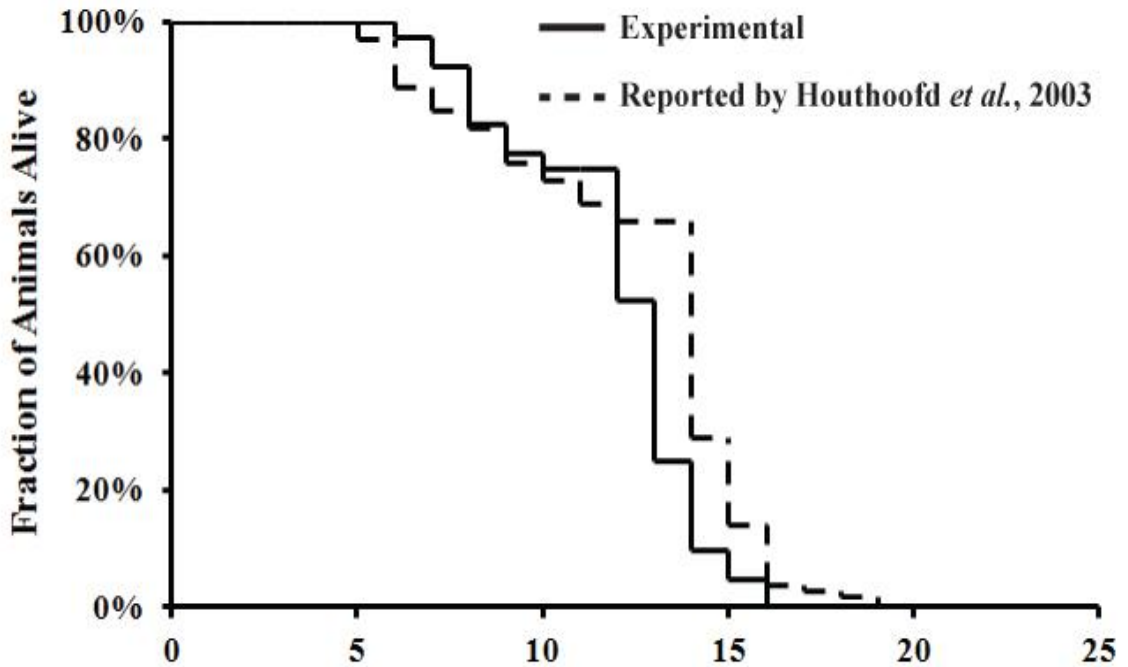


**Figure 5.13** Comparison of life-span data for wild type N2 animals obtained experimentally on the life-span chip to previously reported data from Houthoofd *et al.*, *Experimental Gerontology*, 2003 [179] (Resuse permission license: 3161501375891).

In addition to monitoring the life-span of the animals on chip I recorded their pharyngeal pumping rate as an indicator of normal activity and as an example of additional information obtainable from using this system. As shown in Figure 5.14, the pharyngeal pumping rate is lowest immediately upon loading, but returns to the range of normal values for *C. elegans* 24 hours and 48 hours after loading [157, 158] while the animals are feeding of a solution of bacteria at  $OD_{600}=1.0$ . Normal pharyngeal pumping is an important indicator of the animals perceiving sufficient food and physiological functions continuing normally. [157, 158]

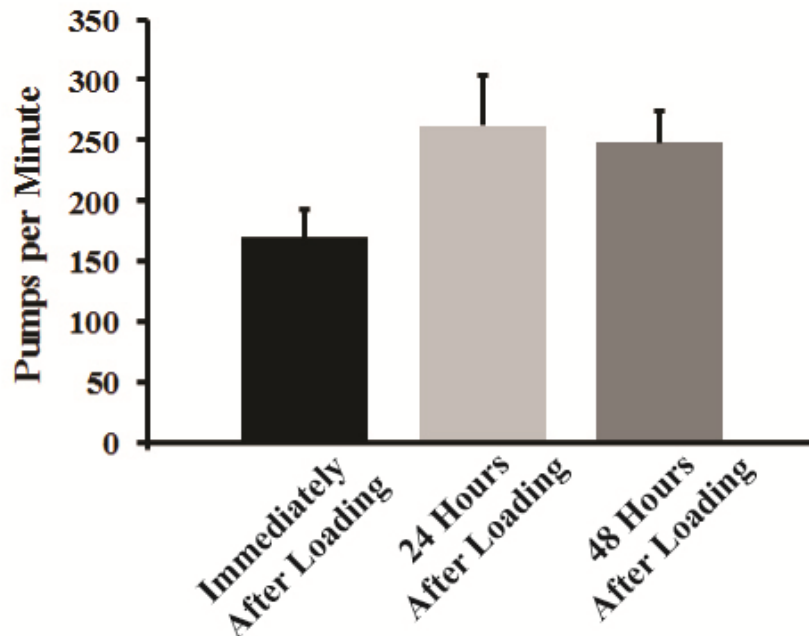


**Figure 5.14** Measurement of pharyngeal pumping rate of *C. elegans* on device. The rate is lowest immediate after loading, but returns to the range of normal values 24 and 48 hours after loading.

48 hours after loading, I exposed the animals to a pulse buffer solution containing 2-nonanone, a chemical repellant. Prior to the pulse, animals were exposed to pure buffer instead of nutrient solution for 30 minutes. I recorded animal responses 15 seconds prior to the 2-nonanone pulse, during the 120 seconds exposure, and for 40 seconds after removal of the repellant. A response was recorded if an animal exhibited a reversal (change of direction) or when the head touched the tail followed by movement in this new direction. Figure 5.15 plots the incidence of animal responses prior, during and after 2-nonanone stimulation for each individual animal. As can be seen, the incidence of responses increases after the chemical is introduced and gradually wears off, with some animals performing reversals and head-tail touches upon removal of the repellant. This shows that behavioral response can be studied during an ongoing life-span experiment.

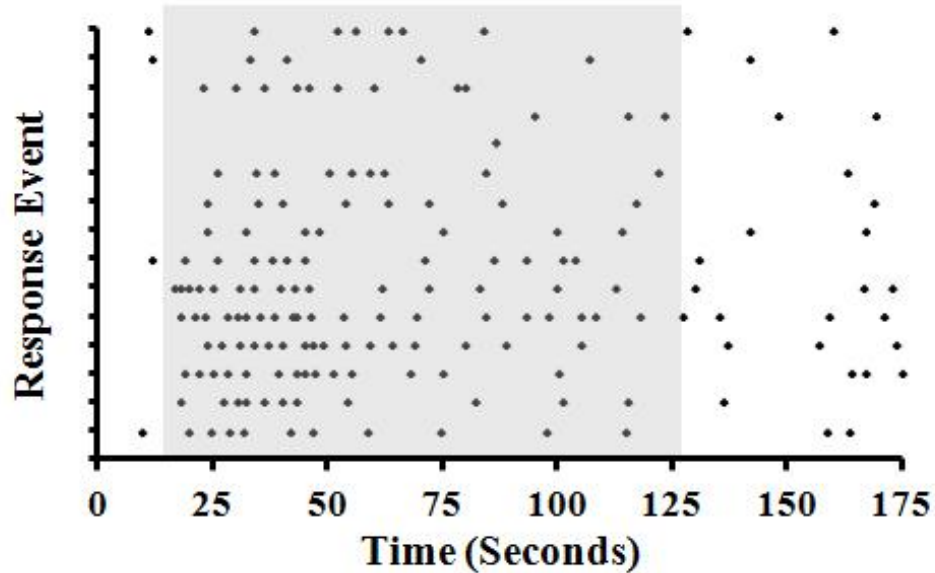


**Figure 5.15** Incidence of reversals and head-tail touches before, during, and after exposure to the repellant 2-nonanone.

## 5.6 Conclusions

In this work, I have presented a system for high content life-span studies with precise dietary, chemical exposure, and temperature of *C. elegans* without the need for using incubators. The technology consists of a highly scalable microfluidic array designed to load, trap and culture *C. elegans* over their life-span while removing progeny, providing highly controlled liquid dietary restriction conditions and allowing for studying behavior with aging. The off-chip components provide the option of large-scale parallel experimentation via a peristaltic pump fluid delivery system and eliminate the need for incubators via a custom designed bench-top temperature controller. This technology potentiates a increase in the throughput of life-span studies with a significant decrease in manual labor and need for equipment requirements in the form of incubator space for hundreds of nematode growth plates. In addition, the potential to combine aging and learning assays opens up the path to a broader understanding of signaling in *C. elegans*.

## THESIS CONTRIBUTIONS AND FUTURE DIRECTIONS

### 5.7 Thesis Contributions

The work in this dissertation has focused on adapting technologies from the field of microfluidics and developing novel methods for enabling dynamic studies of *C. elegans*. The goal was to provide a toolkit to cover the full range of dynamic studies time-scales. For this purpose, a system was developed for short term live imaging over minutes to hours, for dynamic studies of development over hours to days, and for life-span studies with high content experimentation over days to weeks. Prior to this work, no technology was available to perform live imaging with feeding or dynamic developmental studies on an individual animal basis. The technology to facilitate life-span experiments has surfaced, but has lacked the full set of features necessary, such as capability of controlled chemical stimulation, individual animal tracking, controlled dietary conditions, and temperature control without the need for an incubator. Achieving the thesis goal required developing a novel immobilization method, designing temperature control systems integrated in device, developing novel designs to trap embryos or passively position animals for immobilization, designing peripheral systems such as a bench-top temperature controller and fluid re-circulation and delivery system, and integrating these components.

This thesis presents the first system designed for studying *C. elegans* development dynamically on a per-animal basis. It is the first technology capable of repeatedly and reversibly immobilizing animals for high resolution and high magnification imaging at physiological conditions. The immobilization is facilitated by the solution of Pluronic F127. The solution of this polymer undergoes a thermo-reversible sol-gel transition and has found uses in drug delivery mechanisms, cell encapsulation systems, and has via this work been introduced as a *C. elegans* immobilization agent. The thesis establishes the ability of the gel formed after a transition to immobilize animals at physiological



conditions without any harm as well as the compatibility of the solution with *C. elegans* physiology. To complement the Pluronic F127 component, a microfluidic system was developed to culture developing *C. elegans* in individual chambers and to facilitate their development. Larvae are trapped inside these chambers via partially closed valves, which prevent animals from escaping while allowing flow of bacteria through the chambers to deliver nutrients. The system also includes a liquid based temperature control mechanism to trigger the Pluronic F127 sol-gel transition for periodic immobilization for imaging. As a whole, this technology represents a completely novel approach to studying *C. elegans* development and potentiates dynamic studies of developmental processes to replace traditional population composite based studies.

As an extension of the principles from this design, this thesis presented the first microfluidic system for high throughput and efficient manipulation of *C. elegans* embryos. This technology is the first to facilitate trapping of embryos for highly controlled chemical and thermal stimulation, while allowing for subsequent dynamic observation of animals hatched from these embryos. Trapping occurs passively; flow directs embryos into empty traps and trapped embryos redirect flow into those traps which remain empty. Afterwards, embryos are kept in individual chambers which also passively prevent embryo and animal escape and enable studying development after stimulation. Because of the passive nature, the user is only responsible for loading solutions into the device and no active microfluidic components such as valves are necessary, thereby cutting down on peripheral equipment requirements. The device also facilitates cross-flow across the device to increase the rate of fluid exchange for precise timing of chemical stimulation of embryos. Additionally, this work presents a novel approach to controlling temperature on chip in the form of individually addressable transparent electrodes, which serve as resistive heaters. Because of transparency, the electrodes can be placed directly under the chambers in which *C. elegans* are being cultured, without preventing fluorescent microscopy. The ability to individually actuate

each electrode also lends to targeting of heating to single chambers. Furthermore, the design presented can be fabricated using pre-coated commercially purchased slides with surface un-evenness instead of requiring custom deposition by focusing maximum resistance into a small footprint. Lastly, the electrodes are integrated into the system via an assembly method which leads to re-usability of the electrodes. Such a system of temperature control can be used for a myriad of applications from inducing thermal stress, to studying thermotaxis behavior, to immobilizing animals using the method developed in this thesis. This technology presents the first platform for studying thermal stress and chemical agent exposure on a broad range of developmental processes in a highly controlled and high throughput fashion.

The system presented in this thesis for live observation of *C. elegans* physiological processes is the first capable of such observation via selectively immobilizing only the animals bodies, while leaving the head free to move and feed. The ability to feed is critical for continuous immobilization for live imaging; if animals do not feed, their natural physiological processes may be altered. The technology is again based on a passive design, which properly positions the animals' bodies and heads in trapping channels via an array of pillars. In this position, only the bodies are immobilized via immobilizing agents. These include Pluronic F127 or a mixture of sodium alginate and gelatin; the choice of agent depends on application and environmental conditions. Animals immobilized in this fashion can then feed on nutrient solution, while they bodies remain immobile even during exposure to blue light during fluorescent imaging, which normally triggers an escape response. This technology is critical to studying events which occur continuously such as trafficking of synaptic vesicles or over a time scale requiring very frequent imaging. This work showed the applicability of the system to studying morphological changes in lipid droplets, but the range of applications extends to any dynamic physiological process or function.

Lastly, this thesis presented a system for life-span studies of *C. elegans*. Other options and designs have been previously made available to the *C. elegans* community, but each only has a subset of features required for large scale experimentation. The platform presented here is capable of culturing animals in individual chambers for per-animal tracking, leading to high content per-animal data gathering. This includes but is not limited to measurement of growth rates, pharyngeal pumping rates, and other metabolic indicators, periodic exposure to stimulants while correlating behavioral response change to aging, and improved life-span tracking. The design of the life-span culture chambers combined with flow in alternating directions leads to elimination of all progeny, thereby eliminating the need for using sterile strain or sterilizing animals via RNAi exposure. It also provides a more natural, crawl-like environment. The peripheral equipment designed for this system facilitates parallel experimentation and eliminates the need for incubators. First, each microfluidic device can be connected to a fluid distribution system driven by a peristaltic pump via flow splitters, which doesn't interrupt the operation of the delivery system or the flow of nutrients to already connected devices. Second, a custom designed peltier-based bench-top temperature controller is used to maintain steady temperature on-chip. The controller can hold up to ~15 individual microfluidic devices and completely eliminates the need for incubators. This feature is very critical, as temperature variation significantly affects *C. elegans* life span, and can also be applied to a broad range of applications requiring temperature control. By combining these features, the whole system aims to become the standard microfluidic platform for life-span analysis studies.

## 5.8 Future Directions

The goal of this thesis was to develop technologies to enable dynamic studies of *C. elegans* across the full range of time-scales during which a process of interest may occur. As such, the primary focus was design of microfluidic and MEMS components, design of peripheral equipment, and the introduction of a novel immobilization method. Since these

technologies are the first of their kind (or first to integrate a full set of features required), the majority of work centered on obtaining a functioning design and the validation of principles used in the development. The designs have the functionality required, but can be further improved to include functionality such as orienting animals in tandem with positioning for example. Also, peripheral equipment such as pumps, electrodes, valves, and bench-top heaters are all individually controlled and could benefit from a unified computer control interface. Additionally, actual biological applications were only used for validation. However, the technologies described potentiate an extremely broad range of experiments and studies of genetic regulation of development and other physiological processes, the understanding of which can be applied to a broad range of organisms including human. Thus, the suggestions for future work include optimizations of designs to include additional functionality of benefit to the *C. elegans* research community, integration of peripheral component control into a single interface for easier adaptation by biologists and the possibility of fully automated operation, and the use application of systems to answer pertinent questions in developmental biology and neuroscience. Last but not least, a possible strategy to drive acceptance by the biological community is also outlined.

Optimizing the designs for additional functionality can increase the range of applications. For example, the live imaging device trapping channels are straight channels. Although animals are positioned properly, their rotation along their central axis is arbitrary. The animals may thus not orient with their dorsal-ventral axis parallel to the glass, but the axis may be perpendicular or at an arbitrary angle. However, orientation along this axis is critical for some applications such as imaging synapses, because different orientations lead to different apparent object sizes. In our laboratory, curved channels and straight channels with bumps have been developed to orient animals with the dorsal-ventral axis either perpendicular or parallel to the glass slide. Integration of these features into the live imaging device can thus potentially increase its usefulness to broader range of problems.

The systems have been designed with simplicity in mind and thus have the least number of external components possible. However, syringe or peristaltic pumps, digital I/O controllers, and peltier temperature controllers are still used for example. Although these can be easily controlled individually, a unified computer control interface may make adaptation by non-engineers more rapid. This way, the systems could be distributed as a complete plug-and-play package. Additionally, a unified interface lends itself well to automation. This could be useful in dynamic developmental studies for example, where at predetermined time intervals the system would automatically replace culture solution with the immobilization agent, actuate temperature in culture chambers to immobilize animals, and automatically acquire images of each chamber. This would further minimize user involvement and increase experiment multiplexing capabilities.

The technologies presented here potentiate and should be utilized for a broad range of biological applications in *C. elegans*. Live observation of neuronal growth cone development and axonal regeneration, of trafficking of synaptic vesicles, of rearrangement of synaptic connections, maintenance of germ cells, and structural changes to lipid droplets all become possible. Studies of protein polarity distributions in embryos, of localization of protein rich germ granules during embryonic and later developmental stages, of exposure to alcohol and other chemical agents such as drugs and their effects on genetic expression and development can also be pursued. High throughput and controlled life-span experiments in combination with age-related behavior studies should also be investigated. With appropriate imaging equipment, these can further be expanded to include measurement of changes to behavior generating neuronal activity with age. Also, the principles used to design these systems can be extended to applications on other model organisms or platforms such as other nematodes, zebra fish embryos, or embryoid bodies.

To drive the dissemination of these systems and accelerate research into relevant applications, acceptance by the biological community is required. The passive nature of

the systems developed in this thesis with focus on simplicity and functionality without user interaction is one key aspect in this process; the easier the devices are to use, the more likely they will be adapted. Simplification of the external components and a simple unified GUI will also aid in the process. The third aspect lies in convincing the biological community that the systems can accurately reproduce published experiments and simultaneously provide data or information not obtainable using standard established methods. In the case of the Lifespan-on-Chip system for example, the results needed to show the community that the system is capable of lifespan experiments include i) the established relationships between lifespan and dietary restriction in form of bacterial concentration, ii) the established lifespan differences between long-lived and short-lived mutants and wild type animals, and iii) the temperature dependence of *C. elegans* lifespan. In tandem, the argument has to be made that using the microfluidic system allows researchers to gather data not possible to obtain using standard methods and thereby provides a significant advantage. For example, the ability to observe behavior along aging and the changes to behavioral responses is unique to the microfluidic system while the combination is extremely difficult or impossible to implement with on-plate assays. By additionally incorporating techniques such as calcium imaging to measure neural activity as well the functional advantage increases even more. The microfluidic system can thus lead to a depth of analysis impossible with standard techniques. This argument has to be the focus of convincing the biological community and should drive the acceptance of the microfluidic systems developed in this thesis.

## APPENDIX

### A.1. Publications and Other Scientific Activity

#### A.1.1. Journal and Book Publications

Edward Park, Jan Krajniak, and Hang Lu. “Packaging for BioMicro-Electro-Mechanical Systems (BioMEMS) and Microfluidic Chips.” Nano-Bio-Electronic, Photonic and MEMS Packaging, Springer Science+Business Media, 2010, New York, NY, USA

Jan Krajniak and Hang Lu. “Long-term High-Resolution Imaging and Culture of *C. elegans* in Chip-Gel Hybrid Microfluidic Device for Developmental Studies.” Lab on a Chip. 2010, Issue 14, Page 1862-1868

Jan Krajniak, Yan Hao, Ho Yi Mak, and Hang Lu. “Continuous Live Imaging for Direct Observation of *C. elegans* Physiological Processes.” Lab on a Chip. 2013. doi 10.1039/C3LC50300C

Jan Krajniak, Iva Franjkic, and Hang Lu. “Microfluidic trap array for chemical and thermal manipulation of *C. elegans* embryos with subsequent observation of development.”. Lab on a Chip. In Preparation

#### A.1.2. Conference Talks

Jan Krajniak and Hang Lu. “Repeated High-Resolution Long-Term Imaging without Anesthetics Using Microfluidics and Thermally Controllable Gels”. Oral Presentation. Neuronal Development, Synaptic Function & Behavior *C. elegans* Topic Meeting. June 2010, Madison, WI

Jan Krajniak and Hang Lu. “C.L.I.P – Continuous Live Imaging Platform for *C. elegans* at Physiological Conditions”. Oral presentation.  $\mu$ TAS 2012, October 2012, Okinawa, Japan

### **A.1.3. Poster Presentations**

Jan Krajniak, Iva Frankjic, and Hang Lu. “Use of Integrated Electrodes and Embryo Traps for Individually Addressable Loading, Culturing and Monitoring of *C. elegans*.” Poster presentation.  $\mu$ TAS 2010, October 2010, Groningen, The Netherlands

Jan Krajniak, Michael Warner, and Hang Lu. “Integrated Electrodes and Embryo Traps for Developmental Studies of *C. elegans*.” Poster presentation. Worm Club Symposium. January 2012, Emory University, Atlanta, GA

### **A.2. Image Reuse Permissions and Licenses**

Figure 1.1: WORMATLAS.ORG provides general permission for non-profit use with proper citation

Figure 1.2a: Mun et al., *Journal of Cellular Physiology*, 2010, License Number 3161420755282

Figure 1.2b: Hutter et al., *Developmental Biology*, 2005, License Number 3161430923941

Figure 1.2c: Nonet, *Journal of Neuroscience Methods*, 1999, License Number 3161430466403

Figure 1.2d: Hendricks et al., *Nature*, 2012, License Number 3161431163024

Figure 1.3a: Sieburth et al., *Nature*, 2010, License Number 3157751282231

Figure 1.3b: Avery, *Genetics*, 1998, Email permission received

Figure 1.4a: Klassen et al., *Neuron*, 2010, License Number 3157760787685

Figure 1.4b: Hallam et al., *Nature*, 1998 License Number 3157760958706

Figure 1.4c: Albrecht et al., *Nature*, 2011 License Number 3157761282059



Figure 1.6a: Allen et al., Journal of Neuroscience Methods, 2008, License Number 3158251120582

Figure 1.6b: Rohde et al., PNAS, 2007, General permission with proper citation (Email request sent)

Figure 1.6c: Chung et al., Nature Methods, 2007, License Number 3161470996206

Figure 1.7a: Gray et al., Nature, 2004, License Number 3161480925107

Figure 1.7b: Zhang et al., Nature, 2005, License Number 3161481271215

Figure 1.7c: Chronis et al., Nature Methods, 2007, License Number 3161481433129

Figure 1.7d: Lockery et al., Journal of Neurophysiology, 2008. Permission Not Required

Figure 1.7e: Albrecht et al., Nature Methods, 2011, License Number 3161490491141

Figure 1.8: Rhode et al., Nature Communications, 2011, License Number 3161491152952

Figure 1.9: Xian et al., Aging Cell, 2013, License Number 3161500139097

Figure 2.4a: Wanka *et al.*, Colloid and Polymer Science, 1990, License Number 3161500986408

Figure 2.4b: Wanka *et al.*, Colloid and Polymer Science, 1990, License Number 3161500986408

Figure 5.12: Houthoofd *et al.*, Experimental Gerontology, 2003, License Number 3161501375891

## REFERENCES

1. Brenner, S., *The genetics of Caenorhabditis elegans*. Genetics, 1974. **77**(1): p. 71-94.
2. Sulston, J.E. and S. Brenner, *The DNA of Caenorhabditis elegans*. Genetics, 1974. **77**(1): p. 95-104.
3. Ward, S., et al., *Electron microscopical reconstruction of the anterior sensory anatomy of the nematode Caenorhabditis elegans.* J Comp Neurol, 1975. **160**(3): p. 313-37.
4. White, J.G., et al., *The structure of the ventral nerve cord of Caenorhabditis elegans*. Philos Trans R Soc Lond B Biol Sci, 1976. **275**(938): p. 327-48.
5. Bargmann, C.I., *Neurobiology of the Caenorhabditis elegans genome*. Science, 1998. **282**(5396): p. 2028-33.
6. Kuwabara, P.E. and N. O'Neil, *The use of functional genomics in C-elegans for studying human development and disease*. Journal of Inherited Metabolic Disease, 2001. **24**(2): p. 127-138.
7. Lai, C.H., et al., *Identification of novel human genes evolutionarily conserved in Caenorhabditis elegans by comparative proteomics*. Genome Res, 2000. **10**(5): p. 703-13.
8. Fraser, A.G., et al., *Caenorhabditis elegans inhibitor of apoptosis protein (IAP) homologue BIR-1 plays a conserved role in cytokinesis*. Curr Biol, 1999. **9**(6): p. 292-301.

9. Hengartner, M.O. and H.R. Horvitz, *C. elegans cell survival gene ced-9 encodes a functional homolog of the mammalian proto-oncogene bcl-2*. Cell, 1994. **76**(4): p. 665-676.
10. Koelle, M.R. and H.R. Horvitz, *EGL-10 regulates G protein signaling in the C. elegans nervous system and shares a conserved domain with many mammalian proteins*. Cell, 1996. **84**(1): p. 115-25.
11. Hall, D.H. and R.L. Russell, *The posterior nervous system of the nematode Caenorhabditis elegans: serial reconstruction of identified neurons and complete pattern of synaptic interactions*. J Neurosci, 1991. **11**(1): p. 1-22.
12. Himmelhoch, S. and B.M. Zuckerman, *Xiphinema index and Caenorhabditis elegans: preparation and molecular labeling of ultrathin frozen sections*. Exp Parasitol, 1982. **54**(2): p. 250-9.
13. White, J.G., et al., *The structure of the nervous system of the nematode Caenorhabditis elegans*. Philos Trans R Soc Lond B Biol Sci, 1986. **314**(1165): p. 1-340.
14. Sulston, J.E. and H.R. Horvitz, *Post-embryonic cell lineages of the nematode, Caenorhabditis elegans*. Dev Biol, 1977. **56**(1): p. 110-56.
15. Fire, A., et al., *Potent and specific genetic interference by double-stranded RNA in Caenorhabditis elegans*. Nature, 1998. **391**(6669): p. 806-11.
16. Chalfie, M., et al., *Green fluorescent protein as a marker for gene expression*. Science, 1994. **263**(5148): p. 802-805.
17. Altun, Z.F.a.H., D.H., *Introduction*. WormAtlas, 2009.
18. Thomas, J.H., *The mind of a worm*. Science, 1994. **264**(5166): p. 1698-9.

19. Bargmann, C.I., E. Hartweg, and H.R. Horvitz, *Odorant-selective genes and neurons mediate olfaction in C. elegans*. Cell, 1993. **74**(3): p. 515-27.
20. de Bono, M., et al., *Social feeding in Caenorhabditis elegans is induced by neurons that detect aversive stimuli*. Nature, 2002. **419**(6910): p. 899-903.
21. Liu, K.S. and P.W. Sternberg, *Sensory regulation of male mating behavior in Caenorhabditis elegans*. Neuron, 1995. **14**(1): p. 79-89.
22. Wicks, S.R. and C.H. Rankin, *Integration of mechanosensory stimuli in Caenorhabditis elegans*. J Neurosci, 1995. **15**(3 Pt 2): p. 2434-44.
23. Mun, J.Y., et al., *Caenorhabditis elegans mitofilin homologs control the morphology of mitochondrial cristae and influence reproduction and physiology*. J Cell Physiol, 2010. **224**(3): p. 748-56.
24. Hutter, H., et al., *Novel genes controlling ventral cord asymmetry and navigation of pioneer axons in C. elegans*. Dev Biol, 2005. **284**(1): p. 260-72.
25. Nonet, M.L., *Visualization of synaptic specializations in live C. elegans with synaptic vesicle protein-GFP fusions*. J Neurosci Methods, 1999. **89**(1): p. 33-40.
26. Hendricks, M., et al., *Compartmentalized calcium dynamics in a C. elegans interneuron encode head movement*. Nature, 2012. **487**(7405): p. 99-103.
27. Akerboom, J., et al., *Optimization of a GCaMP calcium indicator for neural activity imaging*. J Neurosci, 2012. **32**(40): p. 13819-40.
28. Mao, T., et al., *Characterization and subcellular targeting of GCaMP-type genetically-encoded calcium indicators*. PLoS One, 2008. **3**(3): p. e1796.

29. Pologruto, T.A., R. Yasuda, and K. Svoboda, *Monitoring neural activity and [Ca<sup>2+</sup>] with genetically encoded Ca<sup>2+</sup> indicators*. J Neurosci, 2004. **24**(43): p. 9572-9.
30. Tian, L., et al., *Imaging neural activity in worms, flies and mice with improved GCaMP calcium indicators*. Nat Methods, 2009. **6**(12): p. 875-81.
31. Breusegem, S.Y., et al., *In vivo visualization of protein-protein interactions in C. elegans muscle attachment structures by FRET microscopy*. Biophysical Journal, 2003. **84**(2): p. 22A-23A.
32. Meng, F., et al., *Real Time FRET Based Detection of Mechanical Stress in Cytoskeletal and Extracellular Matrix Proteins*. Cell Mol Bioeng, 2011. **4**(2): p. 148-159.
33. Shyu, Y.J., et al., *Visualization of protein interactions in living Caenorhabditis elegans using bimolecular fluorescence complementation analysis*. Nat Protoc, 2008. **3**(4): p. 588-96.
34. Wagner, O.I., et al., *Synaptic scaffolding protein SYD-2 clusters and activates kinesin-3 UNC-104 in C. elegans*. Proc Natl Acad Sci U S A, 2009. **106**(46): p. 19605-10.
35. Schultheis, C., et al., *Optogenetic analysis of GABAB receptor signaling in Caenorhabditis elegans motor neurons*. J Neurophysiol, 2011. **106**(2): p. 817-27.
36. Stirman, J.N., et al., *Real-time multimodal optical control of neurons and muscles in freely behaving Caenorhabditis elegans*. Nat Methods, 2011. **8**(2): p. 153-8.

37. Abrams, B., et al., *Cellular and molecular determinants targeting the Caenorhabditis elegans PHR protein RPM-1 to perisynaptic regions*. Developmental Dynamics, 2008. **237**(3): p. 630-639.
38. Dai, Y., et al., *SYD-2 Liprin-alpha organizes presynaptic active zone formation through ELKS*. Nat Neurosci, 2006. **9**(12): p. 1479-87.
39. Grill, B., et al., *C. elegans RPM-1 regulates axon termination and synaptogenesis through the Rab GEF GLO-4 and the Rab GTPase GLO-1*. Neuron, 2007. **55**(4): p. 587-601.
40. Poon, V.Y., M.P. Klassen, and K. Shen, *UNC-6/netrin and its receptor UNC-5 locally exclude presynaptic components from dendrites*. Nature, 2008. **455**(7213): p. 669-73.
41. Sieburth, D., et al., *Systematic analysis of genes required for synapse structure and function*. Nature, 2005. **436**(7050): p. 510-7.
42. Zhen, M. and Y.S. Jin, *Presynaptic terminal differentiation: transport and assembly*. Current Opinion in Neurobiology, 2004. **14**(3): p. 280-287.
43. Altun-Gultekin, Z., et al., *A regulatory cascade of three homeobox genes, ceh-10, ttx-3 and ceh-23, controls cell fate specification of a defined interneuron class in C. elegans*. Development, 2001. **128**(11): p. 1951-69.
44. Avery, L., *The genetics of feeding in Caenorhabditis elegans*. Genetics, 1993. **133**(4): p. 897-917.
45. Bargmann, C.I. and H.R. Horvitz, *Control of larval development by chemosensory neurons in Caenorhabditis elegans*. Science, 1991. **251**(4998): p. 1243-6.

46. Zallen, J.A., S.A. Kirch, and C.I. Bargmann, *Genes required for axon pathfinding and extension in the C-elegans nerve ring*. *Development*, 1999. **126**(16): p. 3679-3692.
47. Bargmann, C.I., J.H. Thomas, and H.R. Horvitz, *Chemosensory cell function in the behavior and development of Caenorhabditis elegans*. *Cold Spring Harb Symp Quant Biol*, 1990. **55**: p. 529-38.
48. Chalasani, S.H., et al., *Dissecting a circuit for olfactory behaviour in Caenorhabditis elegans*. *Nature*, 2007. **450**(7166): p. 63-70.
49. Chalfie, M. and J. Sulston, *Developmental genetics of the mechanosensory neurons of Caenorhabditis elegans*. *Dev Biol*, 1981. **82**(2): p. 358-70.
50. Gray, J.M., J.J. Hill, and C.I. Bargmann, *A circuit for navigation in Caenorhabditis elegans*. *Proc Natl Acad Sci U S A*, 2005. **102**(9): p. 3184-91.
51. Gray, J.M., et al., *Oxygen sensation and social feeding mediated by a C. elegans guanylate cyclase homologue*. *Nature*, 2004. **430**(6997): p. 317-22.
52. Hobert, O., et al., *Regulation of interneuron function in the C. elegans thermoregulatory pathway by the ttx-3 LIM homeobox gene*. *Neuron*, 1997. **19**(2): p. 345-57.
53. Kaplan, J.M. and H.R. Horvitz, *A dual mechanosensory and chemosensory neuron in Caenorhabditis elegans*. *Proc Natl Acad Sci U S A*, 1993. **90**(6): p. 2227-31.
54. Mori, I. and Y. Ohshima, *Neural regulation of thermotaxis in Caenorhabditis elegans*. *Nature*, 1995. **376**(6538): p. 344-8.

55. Shtonda, B.B. and L. Avery, *Dietary choice behavior in Caenorhabditis elegans*. J Exp Biol, 2006. **209**(Pt 1): p. 89-102.
56. Waggoner, L.E., et al., *Control of alternative behavioral states by serotonin in Caenorhabditis elegans*. Neuron, 1998. **21**(1): p. 203-14.
57. Klassen, M.P., et al., *An Arf-like small G protein, ARL-8, promotes the axonal transport of presynaptic cargoes by suppressing vesicle aggregation*. Neuron, 2010. **66**(5): p. 710-23.
58. Hallam, S.J. and Y. Jin, *lin-14 regulates the timing of synaptic remodelling in Caenorhabditis elegans*. Nature, 1998. **395**(6697): p. 78-82.
59. Albrecht, D.R. and C.I. Bargmann, *High-content behavioral analysis of Caenorhabditis elegans in precise spatiotemporal chemical environments*. Nat Methods, 2011. **8**(7): p. 599-605.
60. Kenyon, C., et al., *A C. elegans mutant that lives twice as long as wild type*. Nature, 1993. **366**(6454): p. 461-4.
61. Kimura, K.D., *daf-2, an Insulin Receptor-Like Gene That Regulates Longevity and Diapause in Caenorhabditis elegans*. Science, 1997. **277**(5328): p. 942-946.
62. Lin, K., *daf-16: An HNF-3/forkhead Family Member That Can Function to Double the Life-Span of Caenorhabditis elegans*. Science, 1997. **278**(5341): p. 1319-1322.
63. Stiernangle, T., *Maintenance of C. elegans*, WormBook. The C. elegans Research Community, WormBook.
64. El-Ali, J., P.K. Sorger, and K.F. Jensen, *Cells on chips*. Nature, 2006. **442**(7101): p. 403-11.



65. Whitesides, G.M., *The origins and the future of microfluidics*. Nature, 2006. **442**(7101): p. 368-373.
66. Duffy, D.C., et al., *Rapid Prototyping of Microfluidic Systems in Poly(dimethylsiloxane)*. Anal Chem, 1998. **70**(23): p. 4974-84.
67. Jackman, R.J., et al., *Using Elastomeric Membranes as Dry Resists and for Dry Lift-Off*. Langmuir, 1999. **15**(8): p. 2973-2984.
68. Unger, M.A., et al., *Monolithic microfabricated valves and pumps by multilayer soft lithography*. Science, 2000. **288**(5463): p. 113-6.
69. Xia, Y.N. and G.M. Whitesides, *Soft lithography*. Angewandte Chemie-International Edition, 1998. **37**(5): p. 551-575.
70. Hulme, S.E., et al., *A microfabricated array of clamps for immobilizing and imaging C. elegans*. Lab Chip, 2007. **7**(11): p. 1515-23.
71. Allen, P.B., et al., *Single-synapse ablation and long-term imaging in live C. elegans*. J Neurosci Methods, 2008. **173**(1): p. 20-6.
72. Rohde, C.B., et al., *Microfluidic system for on-chip high-throughput whole-animal sorting and screening at subcellular resolution*. Proc Natl Acad Sci U S A, 2007. **104**(35): p. 13891-5.
73. Zeng, F., C.B. Rohde, and M.F. Yanik, *Sub-cellular precision on-chip small-animal immobilization, multi-photon imaging and femtosecond-laser manipulation*. Lab on a Chip, 2008. **8**(5): p. 653-656.
74. Chung, K.H., M.M. Crane, and H. Lu, *Automated on-chip rapid microscopy, phenotyping and sorting of C. elegans*. Nature Methods, 2008. **5**(7): p. 637-643.

75. Chokshi, T.V., A. Ben-Yakar, and N. Chronis, *CO2 and compressive immobilization of C. elegans on-chip*. Lab on a Chip, 2009. **9**(1): p. 151-157.
76. Chung, K. and H. Lu, *Automated high-throughput cell microsurgery on-chip*. Lab on a Chip, 2009. **9**(19): p. 2764-2766.
77. Crane, M.M., K. Chung, and H. Lu, *Computer-enhanced high-throughput genetic screens of C. elegans in a microfluidic system*. Lab on a Chip, 2009. **9**(1): p. 38-40.
78. Crane, M.M., et al., *Microfluidics-enabled phenotyping, imaging, and screening of multicellular organisms*. Lab on a Chip, 2010. **10**(12): p. 1509-1517.
79. Zhang, Y., H. Lu, and C.I. Bargmann, *Pathogenic bacteria induce aversive olfactory learning in Caenorhabditis elegans*. Nature, 2005. **438**(7065): p. 179-184.
80. Chronis, N., M. Zimmer, and C.I. Bargmann, *Microfluidics for in vivo imaging of neuronal and behavioral activity in Caenorhabditis elegans*. Nature Methods, 2007. **4**(9): p. 727-731.
81. Lockery, S.R., et al., *Artificial dirt: microfluidic substrates for nematode neurobiology and behavior*. J Neurophysiol, 2008. **99**(6): p. 3136-43.
82. Baek, J.-H., et al., *Using machine vision to analyze and classify Caenorhabditis elegans behavioral phenotypes quantitatively*. Journal of Neuroscience Methods, 2002. **118**(1): p. 9-21.
83. Ramot, D., et al., *The Parallel Worm Tracker: a platform for measuring average speed and drug-induced paralysis in nematodes*. PLoS One, 2008. **3**(5): p. e2208.

84. Swierczek, N.A., et al., *High-throughput behavioral analysis in C. elegans*. Nat Methods, 2011. **8**(7): p. 592-8.
85. Chung, K., et al., *Microfluidic chamber arrays for whole-organism behavior-based chemical screening*. Lab on a Chip, 2011. **11**(21): p. 3689-3697.
86. Rohde, C.B. and M.F. Yanik, *Subcellular in vivo time-lapse imaging and optical manipulation of Caenorhabditis elegans in standard multiwell plates*. Nat Commun, 2011. **2**: p. 271.
87. Hulme, S.E., et al., *Lifespan-on-a-chip: microfluidic chambers for performing lifelong observation of C. elegans*. Lab Chip, 2010. **10**(5): p. 589-97.
88. Xian B, S.J., Chen W, Sun N, Qiao N, Jiang D, Yu T, Men Y, Han Z, Pang Y, Kaeberlein M, Huang Y, Han JD, *WormFarm: a quantitative control and measurement device toward automated Caenorhabditis elegans aging analysis*. Aging Cell, 2013.
89. Krajniak, J. and H. Lu, *Long-term high-resolution imaging and culture of C. elegans in chip-gel hybrid microfluidic device for developmental studies*. Lab Chip, 2010. **10**(14): p. 1862-8.
90. Alexandridis, P., J.F. Holzwarth, and T.A. Hatton, *Micellization of Poly(ethylene oxide)-Poly(propylene oxide)-Poly(ethylene oxide) Triblock Copolymers in Aqueous Solutions: Thermodynamics of Copolymer Association*. Macromolecules, 1994. **27**(9): p. 2414-2425.
91. Attwood, D., J. Collett, and C. Tait, *The micellar properties of the poly(oxyethylene) - poly(oxypropylene) copolymer Pluronic F127 in water and*

- electrolyte solution*. International Journal of Pharmaceutics, 1985. **26**(1-2): p. 25-33.
92. Jansson, J., et al., *The Interaction between PEO-PPO-PEO Triblock Copolymers and Ionic Surfactants in Aqueous Solution Studied Using Light Scattering and Calorimetry*. The Journal of Physical Chemistry B, 2004. **108**(1): p. 82-92.
93. Mortensen, K. and J.S. Pedersen, *Structural study on the micelle formation of poly(ethylene oxide)-poly(propylene oxide)-poly(ethylene oxide) triblock copolymer in aqueous solution*. Macromolecules, 1993. **26**(4): p. 805-812.
94. Wang, P. and T.P. Johnston, *Kinetics of sol-to-gel transition for poloxamer polyols*. Journal of Applied Polymer Science, 1991. **43**(2): p. 283-292.
95. Wanka, G., H. Hoffmann, and W. Ulbricht, *The aggregation behavior of poly-(oxyethylene)-poly-(oxypropylene)-poly-(oxyethylene)-block-copolymers in aqueous solution*. Colloid & Polymer Science, 1990. **268**(2): p. 101-117.
96. Rassing, J. and D. Attwood, *Ultrasonic velocity and light-scattering studies on the polyoxyethylene—polyoxypropylene copolymer Pluronic F127 in aqueous solution*. International Journal of Pharmaceutics, 1982. **13**(1): p. 47-55.
97. *BASF Performance Chemicals, FDA and EPA status, BASF Corporation, North Mount Oliver, New Jersey*.
98. Bromberg, L.E. and E.S. Ron, *Temperature-responsive gels and thermogelling polymer matrices for protein and peptide delivery*. Advanced Drug Delivery Reviews, 1998. **31**(3): p. 197-221.

99. Khattak, S.F., S.R. Bhatia, and S.C. Roberts, *Pluronic F127 as a cell encapsulation material: utilization of membrane-stabilizing agents*. Tissue Eng, 2005. **11**(5-6): p. 974-83.
100. Gong, C.Y., et al., *In vitro drug release behavior from a novel thermosensitive composite hydrogel based on Pluronic f127 and poly(ethylene glycol)-poly(epsilon-caprolactone)-poly(ethylene glycol) copolymer*. BMC Biotechnol, 2009. **9**: p. 8.
101. Johnston, T.P. and S.C. Miller, *Inulin disposition following intramuscular administration of an inulin/poloxamer gel matrix*. J Parenter Sci Technol, 1989. **43**(6): p. 279-86.
102. Ahringer, J., *Embryonic tissue differentiation in Caenorhabditis elegans requires dif-1, a gene homologous to mitochondrial solute carriers*. EMBO J, 1995. **14**(10): p. 2307-16.
103. Baugh, L.R., et al., *Composition and dynamics of the Caenorhabditis elegans early embryonic transcriptome*. Development, 2003. **130**(5): p. 889-900.
104. Benard, C., et al., *The C-elegans maternal-effect gene clk-2 is essential for embryonic development, encodes a protein homologous to yeast Tel2p and affects telomere length*. Development, 2001. **128**(20): p. 4045-4055.
105. Choi, B., et al., *A possible role for FRM-1, a C. elegans FERM family protein, in embryonic development*. Molecules and Cells, 2011. **31**(5): p. 455-459.
106. Hao, L., G. Aspöck, and T.R. Burglin, *The hedgehog-related gene wrt-5 is essential for hypodermal development in Caenorhabditis elegans*. Dev Biol, 2006. **290**(2): p. 323-36.

107. Kiehl, T.-R., H. Shibata, and S.-M. Pulst, *The Ortholog of Human Ataxin-2 is Essential for Early Embryonic Patterning in C. elegans*. Journal of Molecular Neuroscience, 2000. **15**(3): p. 231-242.
108. Molin, L. and A. Puisieux, *C. elegans homologue of the Caf1 gene, which encodes a subunit of the CCR4-NOT complex, is essential for embryonic and larval development and for meiotic progression*. Gene, 2005. **358**: p. 73-81.
109. Shim, J. and J. Lee, *The AP-3 clathrin-associated complex is essential for embryonic and larval development in Caenorhabditis elegans*. Molecules and Cells, 2005. **19**(3): p. 452-457.
110. Simeckova, K., et al., *Supplementary nuclear receptor NHR-60 is required for normal embryonic and early larval development of Caenorhabditis elegans*. Folia Biologica, 2007. **53**(3): p. 85-96.
111. Zipperlen, P., et al., *Roles for 147 embryonic lethal genes on C.elegans chromosome I identified by RNA interference and video microscopy*. Embo Journal, 2001. **20**(15): p. 3984-3992.
112. Carvalho, A., et al., *Acute Drug Treatment in the Early C. elegans Embryo*. Plos One, 2011. **6**(9).
113. Kawasaki, I., et al., *The PGL family proteins associate with germ granules and function redundantly in Caenorhabditis elegans germline development*. Genetics, 2004. **167**(2): p. 645-61.
114. Kumar, S., et al., *Anticancer drug 5-fluorouracil induces reproductive and developmental defects in Caenorhabditis elegans*. Reprod Toxicol, 2010. **29**(4): p. 415-20.

115. Richards, J.L., et al., *A quantitative model of normal Caenorhabditis elegans embryogenesis and its disruption after stress*. Dev Biol, 2013. **374**(1): p. 12-23.
116. Akagi, J., et al., *Miniaturized embryo array for automated trapping, immobilization and microperfusion of zebrafish embryos*. PLoS One, 2012. **7**(5): p. e36630.
117. Akagi, J., et al., *Fish on chips: Automated Microfluidic Living Embryo Arrays*, in *26th European Conference on Solid-State Transducers, Eurosensors 2012*, R. Walczak and J. Dziuban, Editors. 2012. p. 84-87.
118. Chung, K., et al., *A microfluidic array for large-scale ordering and orientation of embryos*. Nature Methods, 2011. **8**(2): p. 171-U103.
119. Gutierrez, E., et al., *Microfluidic devices for live imaging of gently immobilized C. elegans and for high-resolution imaging of early embryos during acute drug treatment*. Molecular Biology of the Cell, 2011. **22**.
120. Hwang, H. and H. Lu, *Microfluidic tools for developmental studies of small model organisms--nematodes, fruit flies, and zebrafish*. Biotechnol J, 2013. **8**(2): p. 192-205.
121. Levario, T.J., et al., *Microfluidic trap array for massively parallel imaging of Drosophila embryos*. Nat Protoc, 2013. **8**(4): p. 721-36.
122. Yang, F., et al., *An integrated microfluidic array system for evaluating toxicity and teratogenicity of drugs on embryonic zebrafish developmental dynamics*. Biomicrofluidics, 2011. **5**(2).
123. Gallo, C.M., et al., *Processing bodies and germ granules are distinct RNA granules that interact in C. elegans embryos*. Dev Biol, 2008. **323**(1): p. 76-87.

124. Hird, S.N., J.E. Paulsen, and S. Strome, *Segregation of germ granules in living Caenorhabditis elegans embryos: cell-type-specific mechanisms for cytoplasmic localisation*. Development, 1996. **122**(4): p. 1303-12.
125. Pitt, J.N., J.A. Schisa, and J.R. Priess, *P granules in the germ cells of Caenorhabditis elegans adults are associated with clusters of nuclear pores and contain RNA*. Dev Biol, 2000. **219**(2): p. 315-33.
126. Sheth, U., et al., *Perinuclear P granules are the principal sites of mRNA export in adult C. elegans germ cells*. Development, 2010. **137**(8): p. 1305-14.
127. Chiang, W.C., et al., *HSF-1 Regulators DDL-1/2 Link Insulin-like Signaling to Heat-Shock Responses and Modulation of Longevity*. Cell, 2012. **148**(1-2): p. 322-334.
128. Morton, E.A. and T. Lamitina, *Caenorhabditis elegans HSF-1 is an essential nuclear protein that forms stress granule-like structures following heat shock*. Aging Cell, 2013. **12**(1): p. 112-20.
129. Singh, V. and A. Aballay, *Heat-shock transcription factor (HSF)-1 pathway required for Caenorhabditis elegans immunity*. Proc Natl Acad Sci U S A, 2006. **103**(35): p. 13092-7.
130. Kumar, S., et al., *Anticancer drug 5-fluorouracil induces reproductive and developmental defects in Caenorhabditis elegans*. Reproductive Toxicology, 2010. **29**(4): p. 415-420.
131. Srivastava, D., et al., *Reserpine can confer stress tolerance and lifespan extension in the nematode C. elegans*. Biogerontology, 2008. **9**(5): p. 309-16.



132. Chang, Y.H., et al., *Integrated polymerase chain reaction chips utilizing digital microfluidics*. Biomedical Microdevices, 2006. **8**(3): p. 215-225.
133. Sung Kwon, C., M. Hyejin, and K. Chang-Jin, *Creating, transporting, cutting, and merging liquid droplets by electrowetting-based actuation for digital microfluidic circuits*. Journal of Microelectromechanical Systems, 2003. **12**(1): p. 70-80.
134. Gawad, S., L. Schild, and P.H. Renaud, *Micromachined impedance spectroscopy flow cytometer for cell analysis and particle sizing*. Lab Chip, 2001. **1**(1): p. 76-82.
135. Lagally, E.T., I. Medintz, and R.A. Mathies, *Single-molecule DNA amplification and analysis in an integrated microfluidic device*. Anal Chem, 2001. **73**(3): p. 565-70.
136. Lagally, E.T., P.C. Simpson, and R.A. Mathies, *Monolithic integrated microfluidic DNA amplification and capillary electrophoresis analysis system*. Sensors and Actuators B: Chemical, 2000. **63**(3): p. 138-146.
137. Liu, R.H., et al., *Self-contained, fully integrated biochip for sample preparation, polymerase chain reaction amplification, and DNA microarray detection*. Anal Chem, 2004. **76**(7): p. 1824-31.
138. Martin, R.S., A.J. Gawron, and S.M. Lunte, *Dual-electrode electrochemical detection for poly(dimethylsiloxane)-fabricated capillary electrophoresis microchips*. Anal Chem, 2000. **72**(14): p. 3196-202.

139. Pollack, M.G., R.B. Fair, and A.D. Shenderov, *Electrowetting-based actuation of liquid droplets for microfluidic applications*. Applied Physics Letters, 2000. **77**(11): p. 1725.
140. Vilkner, T., D. Janasek, and A. Manz, *Micro total analysis systems. Recent developments*. Anal Chem, 2004. **76**(12): p. 3373-85.
141. Siegel, A.C., et al., *Microsolidics: Fabrication of Three-Dimensional Metallic Microstructures in Poly(dimethylsiloxane)*. Advanced Materials, 2007. **19**(5): p. 727-733.
142. Im, S.H., E.S. Cho, and S.J. Kwon, *ITO Wet Etch Properties by Various Moving Modes of Substrate in an In-Line Wet Etch/Cleaning System*. Molecular Crystals and Liquid Crystals, 2009. **513**(1): p. 114-121.
143. Jacobs, J.W.M., et al., *Microstructural and electrochemical aspects of wet etching ITO films*. Proceedings of the Third Symposium on Thin Film Transistor Technologies, ed. Y. Kuo. Vol. 96. 1997. 158-173.
144. Leem, D.-S., T. Lee, and T.-Y. Seong, *Enhancement of the light output of GaN-based light-emitting diodes with surface-patterned ITO electrodes by maskless wet-etching*. Solid-State Electronics, 2007. **51**(5): p. 793-796.
145. Bertran, E., *RF sputtering deposition of Ag/ITO coatings at room temperature*. Solid State Ionics, 2003. **165**(1-4): p. 139-148.
146. Jang, S., et al., *Comparison of E-beam and Sputter-Deposited ITO Films for 1.55 $\mu$ m Metal–Semiconductor–Metal Photodetector Applications*. Journal of The Electrochemical Society, 2007. **154**(5): p. H336.

147. Jo, Y.J., C.H. Hong, and J.S. Kwak, *Improved electrical and optical properties of ITO thin films by using electron beam irradiation and their application to UV-LED as highly transparent p-type electrodes*. *Current Applied Physics*, 2011. **11**(4): p. S143-S146.
148. Moore, E., D. O'Connell, and P. Galvin, *Surface characterisation of indium-tin oxide thin electrode films for use as a conducting substrate in DNA sensor development*. *Thin Solid Films*, 2006. **515**(4): p. 2612-2617.
149. Pan, Y.Q. and L.X. Hang, *Effects of Vacuum Annealing and Oxygen Ion Beam Bombarding on the Electrical and Optical Properties of ITO Films Deposited by E-beam Evaporation*, in *6th International Symposium on Advanced Optical Manufacturing and Testing Technologies: Optoelectronic Materials and Devices for Sensing, Imaging, and Solar Energy*, Y. Jiang, J. Yu, and Z. Wang, Editors. 2012.
150. Wittenburg, N. and R. Baumeister, *Thermal avoidance in Caenorhabditis elegans: An approach to the study of nociception*. *Proceedings of the National Academy of Sciences of the United States of America*, 1999. **96**(18): p. 10477-10482.
151. Boxshall, K., et al., *Simple surface treatments to modify protein adsorption and cell attachment properties within a poly(dimethylsiloxane) micro-bioreactor*. *Surface and Interface Analysis*, 2006. **38**(4): p. 198-201.
152. Wu, M.H., *Simple poly(dimethylsiloxane) surface modification to control cell adhesion*. *Surface and Interface Analysis*, 2009. **41**(1): p. 11-16.

153. Wu, Z.G. and K. Hjort, *Surface modification of PDMS by gradient-induced migration of embedded Pluronic*. Lab on a Chip, 2009. **9**(11): p. 1500-1503.
154. Nonet, M.L., et al., *Synaptic transmission deficits in Caenorhabditis elegans synaptobrevin mutants*. J Neurosci, 1998. **18**(1): p. 70-80.
155. Krajniak, J., et al., *C.L.I.P.-continuous live imaging platform for direct observation of C. elegans physiological processes*. Lab Chip, 2013.
156. Jeong, D.W., C.Y. Lee, and S.Y. Lee, *Measurement of Fluid Temperature Across Microscale Gap Using Two-Color Ratiometric Laser-Induced Fluorescence Technique in Combination With Confocal Microscopy*. Journal of Heat Transfer, 2009. **131**(9): p. 091601.
157. Avery, L. and H.R. Horvitz, *Effects of starvation and neuroactive drugs on feeding in Caenorhabditis elegans*. J Exp Zool, 1990. **253**(3): p. 263-70.
158. Avery, L. and H.R. Horvitz, *Pharyngeal pumping continues after laser killing of the pharyngeal nervous system of C. elegans*. Neuron, 1989. **3**(4): p. 473-85.
159. Edwards, S.L., et al., *A novel molecular solution for ultraviolet light detection in Caenorhabditis elegans*. PLoS Biol, 2008. **6**(8): p. e198.
160. Jones, K.T. and K. Ashrafi, *Caenorhabditis elegans as an emerging model for studying the basic biology of obesity*. Dis Model Mech, 2009. **2**(5-6): p. 224-9.
161. Mak, H.Y., *Lipid droplets as fat storage organelles in Caenorhabditis elegans: Thematic Review Series: Lipid Droplet Synthesis and Metabolism: from Yeast to Man*. J Lipid Res, 2012. **53**(1): p. 28-33.
162. Mullaney, B.C. and K. Ashrafi, *C. elegans fat storage and metabolic regulation*. Biochim Biophys Acta, 2009. **1791**(6): p. 474-8.

163. Zhang, S.B.O., et al., *Genetic and dietary regulation of lipid droplet expansion in Caenorhabditis elegans*. Proceedings of the National Academy of Sciences of the United States of America, 2010. **107**(10): p. 4640-4645.
164. Xu, N.Y., et al., *The FATP1-DGAT2 complex facilitates lipid droplet expansion at the ER-lipid droplet interface*. Journal of Cell Biology, 2012. **198**(5): p. 895-911.
165. Hsu, A.L., C.T. Murphy, and C. Kenyon, *Regulation of aging and age-related disease by DAF-16 and heat-shock factor*. Science, 2003. **300**(5622): p. 1142-5.
166. Kimura, K.D., et al., *daf-2, an insulin receptor-like gene that regulates longevity and diapause in Caenorhabditis elegans*. Science, 1997. **277**(5328): p. 942-946.
167. Larsen, P.L., P.S. Albert, and D.L. Riddle, *Genes that regulate both development and longevity in Caenorhabditis elegans*. Genetics, 1995. **139**(4): p. 1567-1583.
168. Lin, K., et al., *daf-16: An HNF-3/forkhead family member that can function to double the life-span of Caenorhabditis elegans*. Science, 1997. **278**(5341): p. 1319-1322.
169. Ogg, S., et al., *The Fork head transcription factor DAF-16 transduces insulin-like metabolic and longevity signals in C. elegans*. Nature, 1997. **389**(6654): p. 994-9.
170. Ewbank, J.J., et al., *Structural and functional conservation of the Caenorhabditis elegans timing gene clk-1*. Science, 1997. **275**(5302): p. 980-3.
171. Lakowski, B. and S. Hekimi, *Determination of life-span in Caenorhabditis elegans by four clock genes*. Science, 1996. **272**(5264): p. 1010-3.

172. Taub, J., et al., *A cytosolic catalase is needed to extend adult lifespan in C-elegans daf-C and clk-1 mutants (Retracted Article. See, vol 421, pg 764, 2003).* Nature, 1999. **399**(6732): p. 162-166.
173. Wong, A., P. Boutis, and S. Hekimi, *Mutations in the clk-1 gene of Caenorhabditis elegans affect developmental and behavioral timing.* Genetics, 1995. **139**(3): p. 1247-59.
174. Antebi, A., et al., *daf-12 encodes a nuclear receptor that regulates the dauer diapause and developmental age in C-elegans.* Genes & Development, 2000. **14**(12): p. 1512-1527.
175. Berry, L.W., B. Westlund, and T. Schedl, *Germ-line tumor formation caused by activation of glp-1, a Caenorhabditis elegans member of the Notch family of receptors.* Development, 1997. **124**(4): p. 925-36.
176. Gerisch, B., et al., *A hormonal signaling pathway influencing C. elegans metabolism, reproductive development, and life span.* Dev Cell, 2001. **1**(6): p. 841-51.
177. Hsin, H. and C. Kenyon, *Signals from the reproductive system regulate the lifespan of C. elegans.* Nature, 1999. **399**(6734): p. 362-6.
178. Syntichaki, P., K. Troulinaki, and N. Tavernarakis, *eIF4E function in somatic cells modulates ageing in Caenorhabditis elegans.* Nature, 2007. **445**(7130): p. 922-6.
179. Houthoofd, K., et al., *Life extension via dietary restriction is independent of the Ins/IGF-1 signalling pathway in Caenorhabditis elegans.* Experimental Gerontology, 2003. **38**(9): p. 947-954.

180. Aitlhadj, L. and S.R. Sturzenbaum, *The use of FUdR can cause prolonged longevity in mutant nematodes*. Mech Ageing Dev, 2010. **131**(5): p. 364-5.
181. Davies, S.K., A.M. Leroi, and J.G. Bundy, *Fluorodeoxyuridine affects the identification of metabolic responses to daf-2 status in Caenorhabditis elegans*. Mech Ageing Dev, 2012. **133**(1): p. 46-9.
182. Van Raamsdonk, J.M. and S. Hekimi, *FUdR causes a twofold increase in the lifespan of the mitochondrial mutant gas-1*. Mech Ageing Dev, 2011. **132**(10): p. 519-21.
183. Greer, E.L., et al., *An AMPK-FOXO pathway mediates longevity induced by a novel method of dietary restriction in C. elegans*. Curr Biol, 2007. **17**(19): p. 1646-56.
184. Bishop, N.A. and L. Guarente, *Two neurons mediate diet-restriction-induced longevity in C. elegans*. Nature, 2007. **447**(7144): p. 545-9.
185. Klass, M.R., *Aging in the nematode Caenorhabditis elegans: major biological and environmental factors influencing life span*. Mech Ageing Dev, 1977. **6**(6): p. 413-29.
186. Panowski, S.H., et al., *PHA-4/Foxa mediates diet-restriction-induced longevity of C. elegans*. Nature, 2007. **447**(7144): p. 550-5.
187. Chalasani, S.H., et al., *Neuropeptide feedback modifies odor-evoked dynamics in Caenorhabditis elegans olfactory neurons*. Nat Neurosci, 2010. **13**(5): p. 615-21.
188. Harris, G., et al., *Dissecting the serotonergic food signal stimulating sensory-mediated aversive behavior in C. elegans*. PLoS One, 2011. **6**(7): p. e21897.

189. Kodama, E., et al., *Insulin-like signaling and the neural circuit for integrative behavior in C. elegans*. Genes Dev, 2006. **20**(21): p. 2955-60.
190. Lin, C.H., et al., *Insulin signaling plays a dual role in Caenorhabditis elegans memory acquisition and memory retrieval*. J Neurosci, 2010. **30**(23): p. 8001-11.
191. Tomioka, M., et al., *The insulin/PI 3-kinase pathway regulates salt chemotaxis learning in Caenorhabditis elegans*. Neuron, 2006. **51**(5): p. 613-25.